# IMPROVING THE PERFORMANCE OF AN UNDER-DAMPED MASS SPRING DAMPER SYSTEM THROUGH SWITCHED PARAMETERS

By

Amer Lafi Allafi

#### A THESIS

Submitted to
Michigan State University
in partial fulfillment of the requirements
for the degree of

Mechanical Engineering - Master of Science

2014

#### **ABSTRACT**

# IMPROVING THE PERFORMANCE OF AN UNDER-DAMPED MASS SPRING DAMPER SYSTEM THROUGH SWITCHED PARAMETERS

By

#### Amer Lafi Allafi

In this thesis we propose to improve the performance of the standard single degree-of-freedom under-damped mass-spring-damper (MSD) system using variable structure control. Two controllers are proposed: both of them switch the parameters of the system between their nominal values and their negative values. This approach results in a hybrid system comprised of the nominal system, which is asymptotically stable, and an unstable system. The first controller is based on switched stiffness whereas the second controllers is based on switched stiffness and damping. For both controllers, the parameters are switched based on the location of the system in its configuration space. A phase portrait analysis indicates that the resulting hybrid systems are asymptotically stable although they switch between an asymptotically stable and an unstable system. A comparison of the step response of the hybrid systems with that of the original underdamped system indicates that the switched systems have better performance in terms of rise time, settling time, and reduced or no overshoot. Different designs of the switching logic have been investigated and they provide clues on how the switching logic can be designed to achieve the maximum improvement in performance.

#### **ACKNOWLEDGMENTS**

I would like to express my sincere gratitude to my advisor Dr. Ranjan Mukherjee for his patience, motivation, vast knowledge, and guidance throughout this work. I would like to thank the other members of my committee, Dr. Hassan K. Khalil, and Dr. Jongeun Choi for the assistance they provided. I would also like to thank my family: my parents Lafi Allafi and Hessa Almuzaini, and my wife Najla Aleid, for supporting me spiritually throughout my life. Finally, I would like to thanks the Saudi Arabia Cultural Mission for the financial support during my Master program.

### TABLE OF CONTENTS

LIST OF FIGU	JRES	vi
Chapter 1 Intro	duction	1
Chapter 2 Mass	s-Spring-Damper System with Switched Stiffness and Damping	4
2.1. Mass-S	Spring-Damper System with Switched Stiffness	4
	Stability Characteristics of the Individual Systems	
	Behavior of the First System ( $\alpha = +1$ )	
	Behavior of the Second System ( $\alpha = -1$ )	
	Different Cases of the VSS with Switched Stiffness	
	-Spring-Damper System with Switched Stiffness and Damping	
	Stability Characteristics of the Individual Systems	
	Behavior of the First System ( $\alpha = +1$ )	
	Behavior of the Second System ( $\alpha = -1$ )	
	Different Cases of the VSS with Switched Stiffness	
Chapter 3 Varia	able Structure System with Switched Stiffness	13
	Portrait	
3.2. Case A		13
	Stability	
3.2.2.	Performance – Response to Step Input	20
	Performance – Speed of Convergence	
	$\beta: \lambda \leq \mu_1 < 0$	
	Stability	
	Performance – Response to Step Input	
	Performance – Speed of Convergence	
	ision	
Chapter 4 Vari	able Structure System with Switched Stiffness and Damping	51
4.1. Phase	Portrait	51
4.2. Case A	$\lambda: \mu_1 < \lambda < 0.$	53
4.2.1.	Stability	53
4.2.2.	Performance – Response to Step Input	58
	Performance – Speed of Convergence	
	$\beta: \lambda \leq \mu_1 < 0$	
	Stability	
	Performance – Response to Step Input	
	Performance – Speed of Convergence	
	asion	
Chapter 5 Cone	clusion	90

REFERENCES	Ω	٠,	1
REFERENCES	.ソ	' Z	_

### LIST OF FIGURES

Figure 2.1.	Phase portrait for $\alpha = +1$ and $\zeta < 1$	6
Figure 2.2.	Phase portrait for $\alpha = -1$	8
Figure 2.3.	Phase portrait for $\alpha = +1$ and $\zeta < 1$	11
Figure 2.4.	Phase portrait for $\alpha = -1$	12
Figure 3.1.	Phase portrait of the Variable Structure System (VSS) for $\alpha = +1$	14
Figure 3.2.	Phase portrait of the Variable Structure System (VSS) for $\alpha = -1$	14
Figure 3.3.	Phase portrait of the Variable Structure System (VSS) for $\lambda > \mu_1$ is the union of the phase portrait in Figs.3.1 and 3.2	15
Figure 3.4.	Convergence of VSS trajectories to the origin for $\zeta < 1$ and $\mu_1 < \lambda < 0$	20
Figure 3.5.	Comparison of the settling times of the VSS and the original system	24
Figure 3.6.	Comparison of the settling times of the VSS and the original system	25
Figure 3.7.	Comparison of the settling times of the VSS and the original system	27
Figure 3.8.	Comparison between the settling time of the VSS and the original system	29
Figure 3.9.	Phase portrait of the Variable Structure System (VSS) for $\alpha = +1$	31
Figure 3.10.	Phase portrait of the Variable Structure System (VSS) for $\alpha = -1$	31
Figure 3.11.	Phase portrait of the Variable Structure System (VSS) for $\lambda > \mu_1$	32
Figure 3.12.	Step response in the phase plane of the Variable Structure System (VSS) for $\lambda < \mu_1$	36
Figure 3.13.	Step response of the Variable Structure System (VSS) for $\lambda < \mu_{1}$	37
Figure 3.14.	Comparison of the rise times of the VSS and original system	41
Figure 3.15.	Comparison of the percentage of overshoots of the VSS and original system	42

Figure 3.16.	Comparison of the settling time of the VSS and original system	43
Figure 3.17.	Step response in the Phase plane for the Variable Structure System (VSS) for $\lambda < \mu_1$	45
Figure 3.18.	Step response for the Variable Structure System (VSS) for $\lambda < \mu_{1}$	45
Figure 3.19.	The rise time for VSS and original system	47
Figure 3.20.	The percentage of overshoot for VSS and original system	48
Figure 3.21.	The settling times of VSS and original system.	49
Figure 4.1.	Phase portrait of the Variable Structure System (VSS) for $\alpha = +1$	52
Figure 4.2.	Phase portrait of the Variable Structure System (VSS) for $\alpha = -1$	52
Figure 4.3.	Phase portrait of the Variable Structure System (VSS) for $\lambda > \mu_1$ is the union of the phase portrait in Figs.4.1 and 4.2	53
Figure 4.4.	Convergence of VSS trajectories to the origin for $\zeta < 1$ and $\mu_1 < \lambda < 0$	58
Figure 4.5.	Comparison of the settling times of the VSS and the original system	62
Figure 4.6.	Comparison of the settling times of the VSS and the original system	64
Figure 4.7.	Comparison of the settling times of the VSS and the original system	66
Figure 4.8.	Phase portrait of the Variable Structure System (VSS) for $\alpha = +1$	68
Figure 4.9.	Phase portrait of the Variable Structure System (VSS) for $\alpha = -1$	68
Figure 4.10.	Phase portrait of the Variable Structure System (VSS) for $\lambda > \mu_1$	69
Figure 4.11.	Phase portrait of the Variable Structure System	70
Figure 4.12.	The percentage of the contraction in energy of the VSS between points A and C	74
Figure 4.13.	Step response in the phase plane of the Variable Structure System (VSS) for $\lambda < \mu_1$	76
Figure 4.14.	Step response of the Variable Structure System (VSS) for $\lambda < \mu_{1}$	77
Figure 4.15.	Comparison of the rise times of the VSS and original system	80

Figure 4.16.	Comparison of the percentage of overshoots of the VSS and original system.	81
Figure 4.17.	Comparison of the settling time of the VSS and original system	82
Figure 4.18.	Step response in the Phase plane for the Variable Structure System (VSS) for $\lambda < \mu_1$	84
Figure 4.19.	Step response for the Variable Structure System (VSS) for $~\lambda < \mu_1$	84
Figure 4.20.	The rise time for VSS and original system	87
Figure 4.21.	The percentage of overshoot for VSS and original system	87
Figure 4.22.	The settling times of VSS and original system	88

## Chapter 1

## Introduction

The single degree-of-freedom mass-spring-damper (MSD) system describes the dynamics of many real physical systems. The behavior of the MSD is well understood and therefore controllers are also designed to make the closed-loop dynamics of many physical systems emulate the dynamics of the MSD. The behavior of the MSD is largely dependent on the damping ratio  $\zeta$ : a small damping ratio results in fast response (small rise time) but a large overshoot and a large settling time; on the other hand, a large damping ratio results in sluggish response (large rise and settling times) but no overshoot. While emulating the dynamics of the MSD system, it is common to choose the damping ratio to lie in the range  $0.5 < \zeta < 0.8$  since smaller values of  $\zeta$  result in large overshoots and larger values of  $\zeta$  result in sluggish response [1]. To improve the performance of the MSD and have fast response with no overshoot, we investigate the stability and the performance of two hybrid MSD systems. The first system uses switched stiffness; the stiffness of this system is switched between its nominal value and its negative value. The second system uses switched stiffness and damping coefficients; the stiffness and damping coefficients are switched between their nominal values and their negative values. In both hybrid systems, switching is based on the location of the system in its configuration space.

Each hybrid system, namely, the MSD with switched stiffness and the MSD with switched stiffness and damping, can be described by a differential equation with a discontinues forcing function, where the forcing function can be viewed as a sliding mode controller [2-5]. Sliding mode control (SMC) is typically used for robust stabilization of dynamical systems in the presence of uncertainties but here it is used for a completely different purpose, namely, to improve the performance of the system. The improvement in performance is achieved by switching between the original system, which is asymptotically stable, and the system with negative stiffness, which is unstable.

The idea of using switched stiffness for performance improvement has been investigated by several researchers [6-9]. In all of these studies, the stiffness of a mass-spring system is switched between two positive values; this approach results in a hybrid system comprised of two stable subsystems. In this work, the stiffness of the MSD system is switched between a positive value and a negative value; the resulting hybrid system is comprised of two sub-systems that are asymptotically stable and unstable, respectively. The improvement in performance using negative stiffness has also been investigated [10-12]; in most of these studies, negative stiffness has been incorporated in the design for improved vibration isolation. These studies are different from our study since the stiffness is not switched.

The idea of varying the damping coefficient for performance improvement has also been investigated [14-15]. In these studies, the stiffness and the damping coefficients are varied with respect to time. The results have been applied to different application problems such as improved vibration isolation in high-speed rotors. In our work, switching of the stiffness and the damping parameters is based on the location of the system in its configuration space. Also, the stiffness and damping coefficients are switched between a constant negative value and a positive value.

This thesis is organized as follows. The dynamics of the hybrid MSD system and the stability characteristics of the individual subsystems are presented in Chapter 2. The stability characteristics and performance of the MSD with switched stiffness is analyzed in Chapter 3. The time response of the hybrid system is then compared to that of the original system. Chapter 4 repeats the analysis for the MSD with switched stiffness and damping. Chapter 5 contains concluding remarks.

## Chapter 2

## Mass-Spring-Damper System with Switched

## Stiffness and Damping

### 2.1. Mass-Spring-Damper System with Switched Stiffness

We consider the following mass-spring-damper system with switched stiffness:

$$m\ddot{x} + c\dot{x} + \alpha kx = 0 \tag{2.1}$$

where m, c, and k are the mass damping coefficient, and stiffness, respectively,  $\alpha$  switches between  $\pm 1$  according to the logic:

$$\alpha = \begin{cases} +1 & if \quad (S > 0 \text{ and } x \ge 0) \text{ or } (S < 0 \text{ and } x \le 0) \\ -1 & if \quad S \times 0 \end{cases}$$
 (2.2)

and S is defined by the relation:

$$S = x_2 - \lambda x_1, \qquad \lambda < 0 \tag{2.3}$$

The unforced system in (2.1) can be viewed as the following forced system:

$$m\ddot{x} + c\dot{x} + kx = F \tag{2.4}$$

where, the forcing function F is defined as:

$$F = \begin{cases} 0 & \text{if } (S > 0 \text{ and } x \ge 0) \text{ or } (S < 0 \text{ and } x \le 0) \\ 2kx & \text{if } Sx < 0 \end{cases}$$
 (2.5)

Equation (2.1) can be rewritten as:

$$\ddot{x} = -\frac{c}{m}\dot{x} - \alpha \frac{k}{m}x\tag{2.6}$$

The variable structure system (VSS) in Eq.(2.6) is comprised of two linear systems: one where  $\alpha = 1$ , and the other where  $\alpha = -1$ . We will study the behavior of these two individual systems with the objective of investigating the stability and performance of the variable structure system for different values of m, c, and, k.

#### 2.1.1. Stability Characteristics of the Individual Systems

To investigate the stability characteristics of the VSS in Eq.(2.6) we need to first investigate the stability properties of the individual systems. To this end we define the states  $x_1 = x$ , and  $x_2 = \dot{x}$ . Then, the state space equations are:

$$\dot{x}_1 = x_2 \tag{2.7}$$

$$\dot{x}_2 = -\frac{c}{m}x_2 - \alpha \frac{k}{m}x_1 \tag{2.8}$$

If we define  $\omega_n^2 = k/m$  and  $\zeta = c/2m\omega_n$  the state space equation can be rewritten as

$$\dot{x}_1 = x_2$$

$$\dot{x}_2 = -\alpha \omega_n^2 x_1 - 2\zeta \omega_n x_2$$
(2.9)

## 2.1.2. Behavior of the First System $(\alpha=+1)$

For the first system, where  $\alpha = +1$ , we have

$$\begin{bmatrix} \dot{x}_1 \\ \dot{x}_2 \end{bmatrix} = \begin{bmatrix} A_1 \end{bmatrix} \begin{bmatrix} x_1 \\ x_2 \end{bmatrix}, \qquad A_1 \triangleq \begin{bmatrix} 0 & 1 \\ -\omega_n^2 & -2\zeta\omega_n \end{bmatrix}$$
 (2.10)

The eigenvalues of  $A_1$  are:

$$\sigma_1$$
,  $\sigma_2 = \omega_n \left[ -\zeta \pm \sqrt{\zeta^2 - 1} \, \right] < 0$ 

The original system is under-damped, i.e.  $\zeta < 1$ . Therefore, the eigenvalues are complex and are given by:

$$\sigma_1 = \omega_n \left[ -\zeta + i\sqrt{1 - \zeta^2} \right] \tag{2.11}$$

$$\sigma_2 = \omega_n \left[ -\zeta - i\sqrt{1 - \zeta^2} \right] \tag{2.12}$$

and the origin is a stable focus. [13]. The eigenvectors corresponding to the eigenvalues in Eqs.(2.11) and (2.12) are described by the equations:

$$\chi_2 = \sigma_1 \chi_1 \tag{2.13}$$

$$\chi_2 = \sigma_2 \chi_1 \tag{2.14}$$

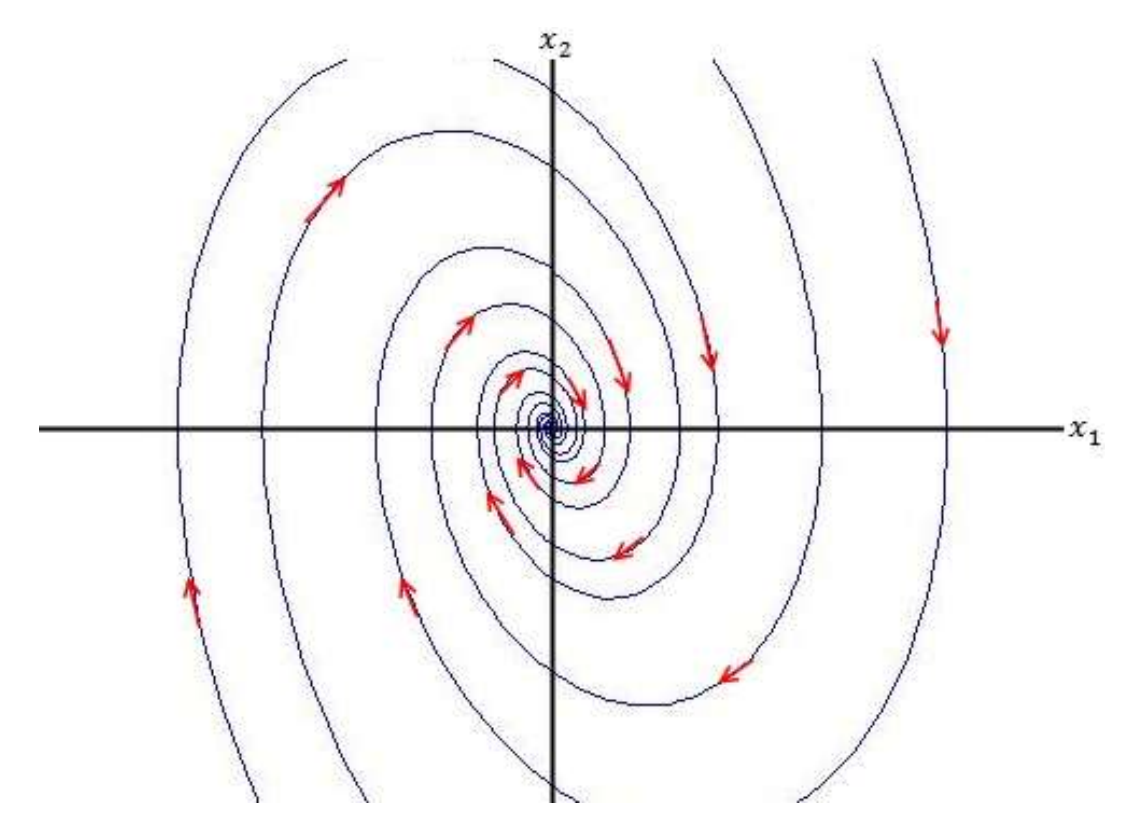


Figure 2.1. Phase portrait for  $\alpha = +1$  and  $\zeta < 1$ 

and the phase portrait of the system is shown in Fig.2.1.

### 2.1.3. Behavior of the Second System ( $\alpha = -1$ )

For the second system, when  $\alpha = -1$ , we have

$$\begin{bmatrix} \dot{x}_1 \\ \dot{x}_2 \end{bmatrix} = \begin{bmatrix} A_2 \end{bmatrix} \begin{bmatrix} x_1 \\ x_2 \end{bmatrix}, \qquad A_2 \triangleq \begin{bmatrix} 0 & 1 \\ \omega_n^2 & -2\zeta\omega_n \end{bmatrix}$$
 (2.15)

The eigenvalues of  $A_2$  are:

$$\mu_1 = \omega_n \left[ -\zeta - \sqrt{\zeta^2 + 1} \right] < 0 \tag{2.16}$$

$$\mu_2 = \omega_n \left[ -\zeta + \sqrt{\zeta^2 + 1} \right] > 0 \tag{2.17}$$

Therefore, the origin is a saddle [13]. The stable and unstable eigenvectors corresponding to the eigenvalues in Eqs.(2.16) and (2.17) are described by the equations:

$$x_2 = \mu_1 x_1 \tag{2.18}$$

$$x_2 = \mu_2 x_1 \tag{2.19}$$

and the phase portrait of the system is shown in Fig.2.2.

#### 2.1.4. Different Cases of the VSS with Switched Stiffness

The VSS with switched stiffness has the same behavior as that of the first system when (S > 0) and  $x \ge 0$  or (S < 0) and  $x \le 0$ , and that of the second system when  $Sx_1 < 0$  – see Eqs.(2.2) and (2.6). Since the first system (where  $\alpha = +1$ ) can be only under-damped ( $\zeta < 1$ ), we study of the VSS Switched Stiffness and we carry out our investigating separately for  $\lambda > \mu_1$  and  $\lambda \le \mu_1$  in Chapter 3.

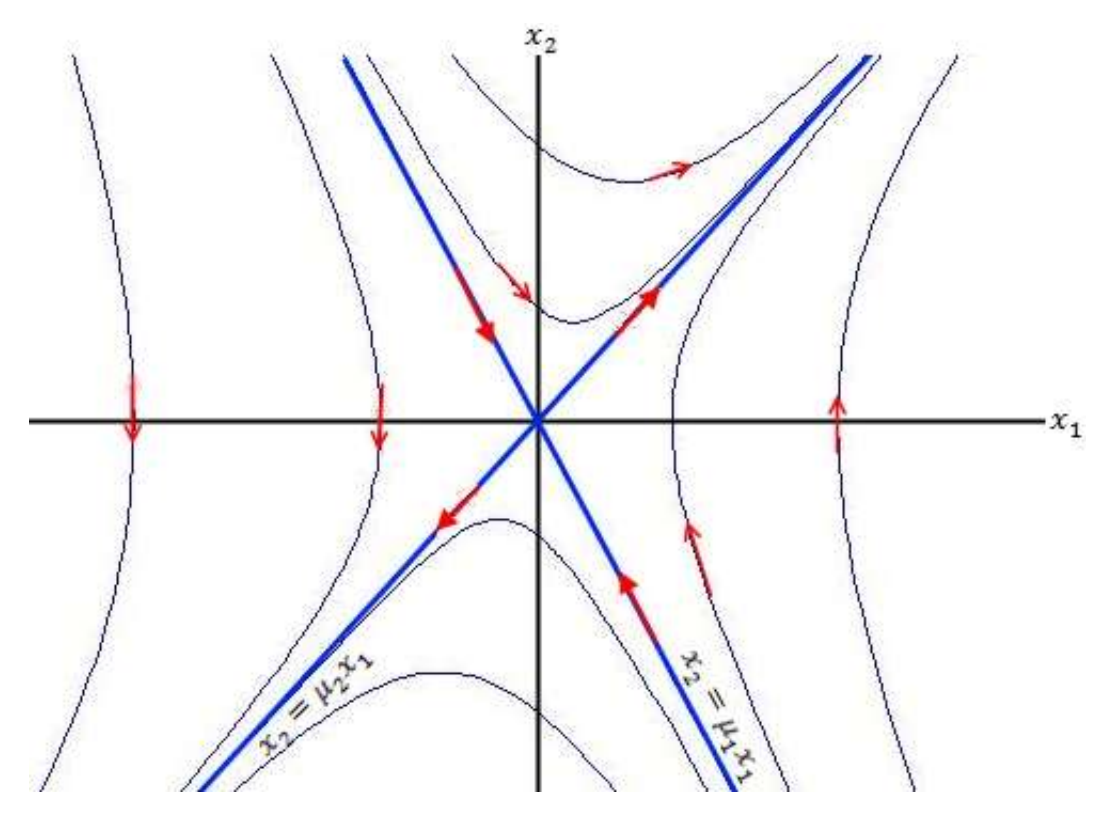


Figure 2.2. Phase portrait for  $\alpha = -1$ 

## 2.2. Mass-Spring-Damper System with Switched Stiffness and Damping

Consider the following mass-spring-damper system with switched stiffness:

$$m\ddot{x} + \alpha c \dot{x} + \alpha k x = 0 \tag{2.20}$$

where m, c, and k are the mass damping coefficient, and stiffness, respectively,  $\alpha$  switches between  $\pm 1$  according to the logic:

$$\alpha = \begin{cases} +1 & if \quad (S > 0 \text{ and } x \ge 0) \text{ or } (S < 0 \text{ and } x \le 0) \\ -1 & if \quad S \text{ } x < 0 \end{cases}$$
 (2.21)

and S is defined by the relation:

$$S = x_2 - \lambda x_1, \qquad \lambda < 0 \tag{2.22}$$

The unforced system in (2.20) can be viewed as the following forced system:

$$m\ddot{x} + c\dot{x} + kx = F \tag{2.23}$$

where, the forcing function F is defined as:

$$F = \begin{cases} 0 & \text{if } (S > 0 \text{ and } x \ge 0) \text{ or } (S < 0 \text{ and } x \le 0) \\ 2kx + 2c\dot{x} & \text{if } Sx < 0 \end{cases}$$
 (2.24)

Equation (2.20) can be rewritten as:

$$\ddot{x} = -\alpha \frac{c}{m} \dot{x} - \alpha \frac{k}{m} x \tag{2.25}$$

The variable structure system (VSS) in Eq.(2.25) is comprised of two linear systems: one where  $\alpha = 1$ , and the other where  $\alpha = -1$ . We will study the behavior of these two individual systems with the objective of investigating the stability and performance of the variable structure system for different values of m, c, and, k.

#### 2.2.1. Stability Characteristics of the Individual Systems

To investigate the stability characteristics of the VSS in Eq.(2.25) we need to first investigate the stability properties of the individual systems. To this end we define the states  $x_1 = x$ , and  $x_2 = \dot{x}$ . Then, the state space equations are:

$$\dot{x}_1 = x_2 \tag{2.26}$$

$$\dot{x}_2 = -\alpha \frac{c}{m} x_2 - \alpha \frac{k}{m} x_1 \tag{2.27}$$

If we define  $\omega_n^2 = k/m$  and  $\zeta = c/2m\omega_n$  the state space equation can be rewritten as

$$\dot{x}_1 = x_2$$

$$\dot{x}_2 = -\alpha \omega_n^2 x_1 - 2\alpha \zeta \omega_n x_2 \tag{2.28}$$

### 2.2.2. Behavior of the First System ( $\alpha = +1$ )

For the first system, where  $\alpha = +1$ , we have

$$\begin{bmatrix} \dot{x}_1 \\ \dot{x}_2 \end{bmatrix} = \begin{bmatrix} A_1 \end{bmatrix} \begin{bmatrix} x_1 \\ x_2 \end{bmatrix}, \qquad A_1 \triangleq \begin{bmatrix} 0 & 1 \\ -\omega_n^2 & -2\zeta\omega_n \end{bmatrix}$$
 (2.29)

The eigenvalues of  $A_1$  are:

$$\sigma_1, \sigma_2 = \omega_n \left[ -\zeta \pm \sqrt{\zeta^2 - 1} \right] < 0$$

The original system is under-damped, i.e.  $\zeta < 1$ . Therefore, The eigenvalues are complex and are given by:

$$\sigma_1 = \omega_n \left[ -\zeta + i\sqrt{1 - \zeta^2} \right] \tag{2.30}$$

$$\sigma_2 = \omega_n \left[ -\zeta - i\sqrt{1 - \zeta^2} \right] \tag{2.31}$$

and the origin is a stable focus [13]. The eigenvectors corresponding to the eigenvalues in Eqs.(2.30) and (2.31) are described by the equations

$$x_2 = \sigma_1 x_1 \tag{2.32}$$

$$\chi_2 = \sigma_2 \chi_1 \tag{2.33}$$

and the phase portrait of the system is shown in Fig.2.3.

## 2.2.3. Behavior of the Second System $(\alpha = -1)$

For the second system, when  $\alpha = -1$ , we have

$$\begin{bmatrix} \dot{x}_1 \\ \dot{x}_2 \end{bmatrix} = \begin{bmatrix} A_2 \end{bmatrix} \begin{bmatrix} x_1 \\ x_2 \end{bmatrix}, \qquad A_2 \triangleq \begin{bmatrix} 0 & 1 \\ \omega_n^2 & 2\zeta\omega_n \end{bmatrix}$$
 (2.34)

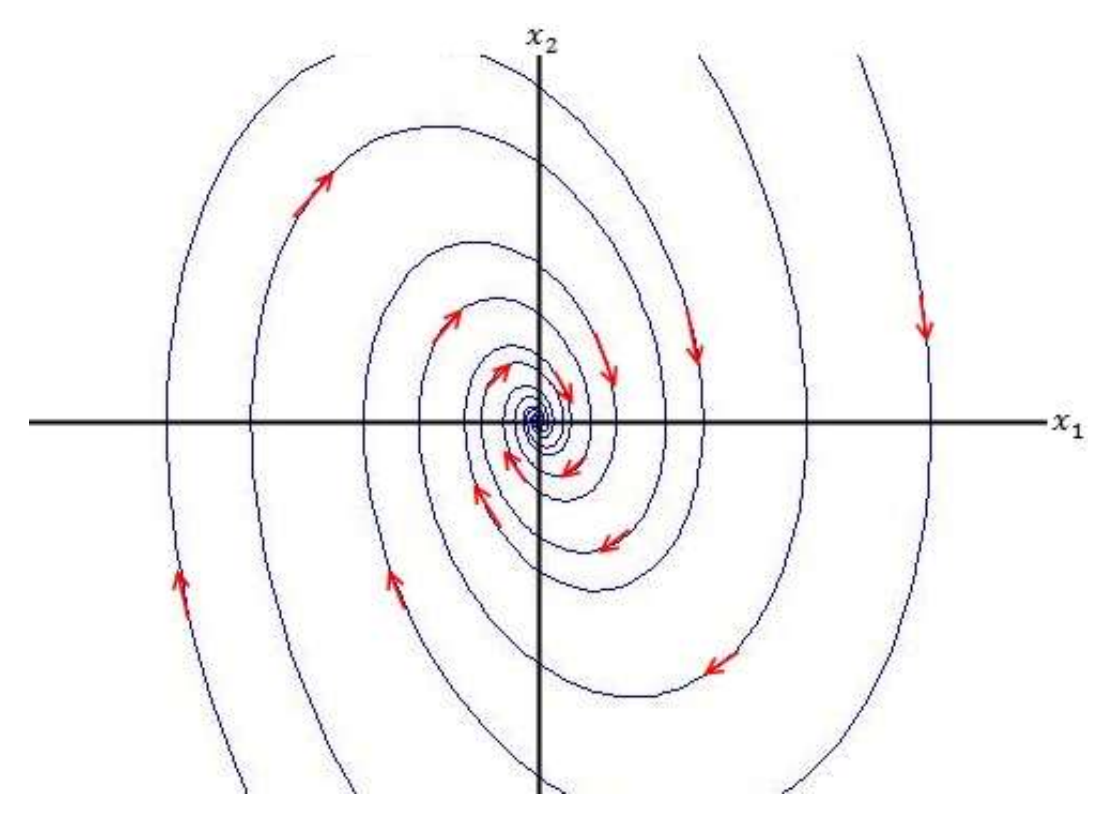


Figure 2.3. Phase portrait for  $\alpha = +1$  and  $\zeta < 1$ 

The eigenvalues of A<sub>2</sub> are:

$$\mu_1 = \omega_n \left[ \zeta - \sqrt{\zeta^2 + 1} \right] < 0 \tag{2.35}$$

$$\mu_2 = \omega_n \left[ \zeta + \sqrt{\zeta^2 + 1} \right] > 0 \tag{2.36}$$

Therefore, the origin is a saddle [13]. The stable and unstable eigenvectors, corresponding to the eigenvalues in Eqs.(2.35) and (2.36), are described by the equations

$$x_2 = \mu_1 x_1 \tag{2.37}$$

$$x_2 = \mu_2 x_1 \tag{2.38}$$

and the phase portrait of the system is shown in Fig.2.4.

### 2.2.4. Different Cases of the VSS with Switched Stiffness and Damping

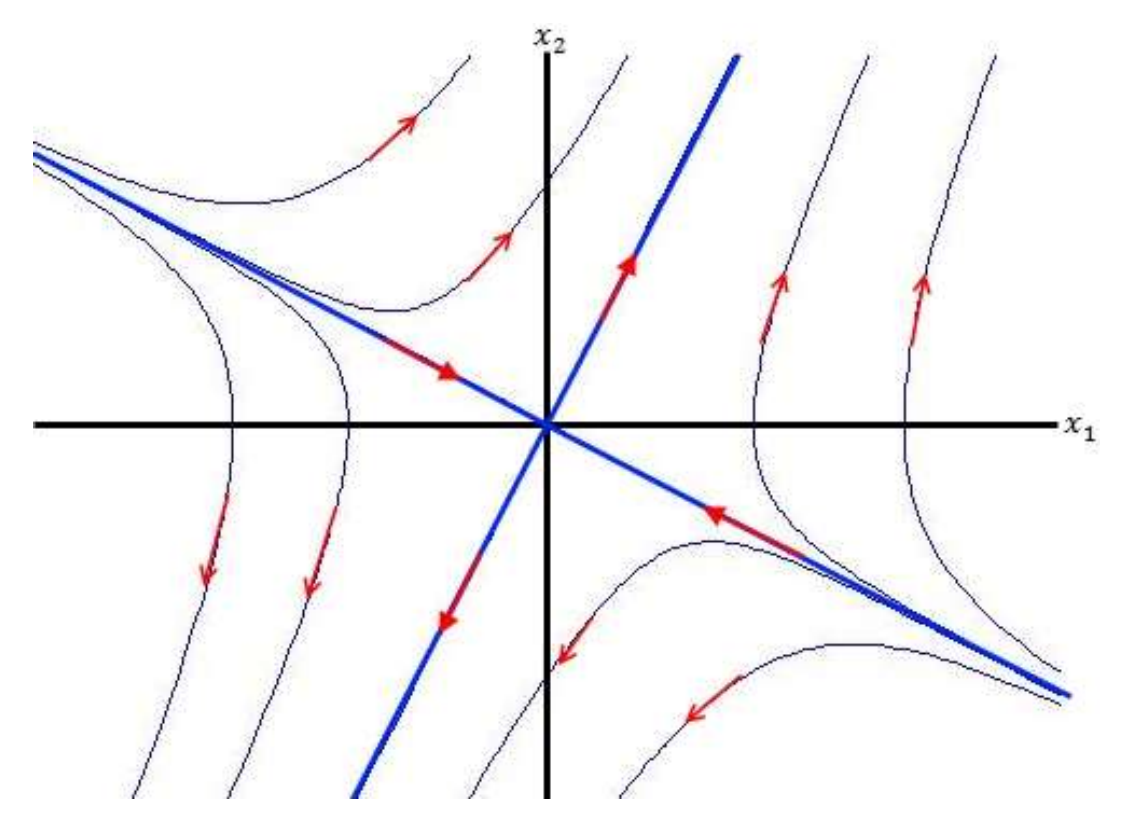


Figure 2.4. Phase portrait for  $\alpha = -1$ 

The VSS with switched stiffness and damping has the same behavior as that of the first system when  $(S > 0 \text{ and } x \ge 0)$  or  $(S < 0 \text{ and } x \le 0)$ , and that of the second system when  $Sx_1 < 0$  – see Eq.(2.21). Since the first system (where  $\alpha = +1$ ) can be only under-damped ( $\zeta < 1$ ), we study of the VSS Switched Stiffness and Damping and we carry out our investigating separately for  $\lambda > \mu_1$  and  $\lambda \le \mu_1$  in Chapter 4.

## Chapter 3

## Variable Structure System with Switched

## Stiffness

#### 3.1. Phase Portrait

In this chapter, we investigate the behavior of the VSS with switched stiffness. The phase portrait of the VSS is the union of the phase portrait of the first system  $(\alpha = +1)$  in the region  $(S > 0 \text{ and } x \ge 0)$  or  $(S < 0 \text{ and } x \le 0)$ , and the phase portrait of the second system  $(\alpha = -1)$  in the region  $Sx_1 < 0$ . The phase portrait of the first system  $(\alpha = +1)$  in the region (S > 0) and (S < 0) or (S < 0) and (S < 0) is shown in Fig.3.1 and the phase portrait of the second system  $(\alpha = -1)$  in the region (S < 0) is shown in Fig.3.2. The union of these phase portraits is shown in Fig.3.3.

For the phase portrait in Fig.3.3, the slope of the line S=0 or  $x_2=\lambda\,x_1$  is shown to be greater than the slope of the line  $x_2=\mu_1x_1$ , i.e.,  $\lambda>\mu_1$ . This is not necessarily true always, and therefore we need to additionally investigate the case where  $\lambda\leq\mu_1$ . These two cases, namely,  $(\mu_1<\lambda<0)$ , and  $(\lambda\leq\mu_1<0)$ , are investigated in sections 3.2 and 3.3.

## 3.2. Case A: $\mu_1 < \lambda < 0$

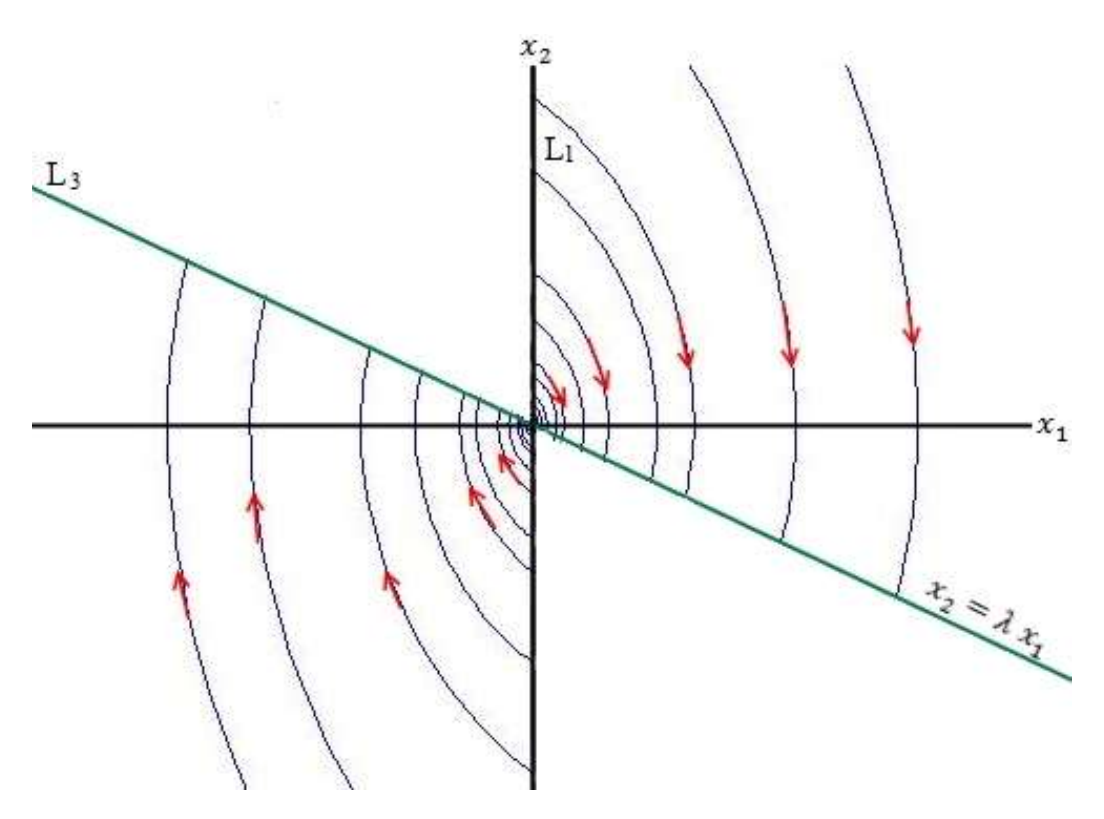


Figure 3.1. Phase portrait of the Variable Structure System (VSS) for  $\alpha = +1$ 

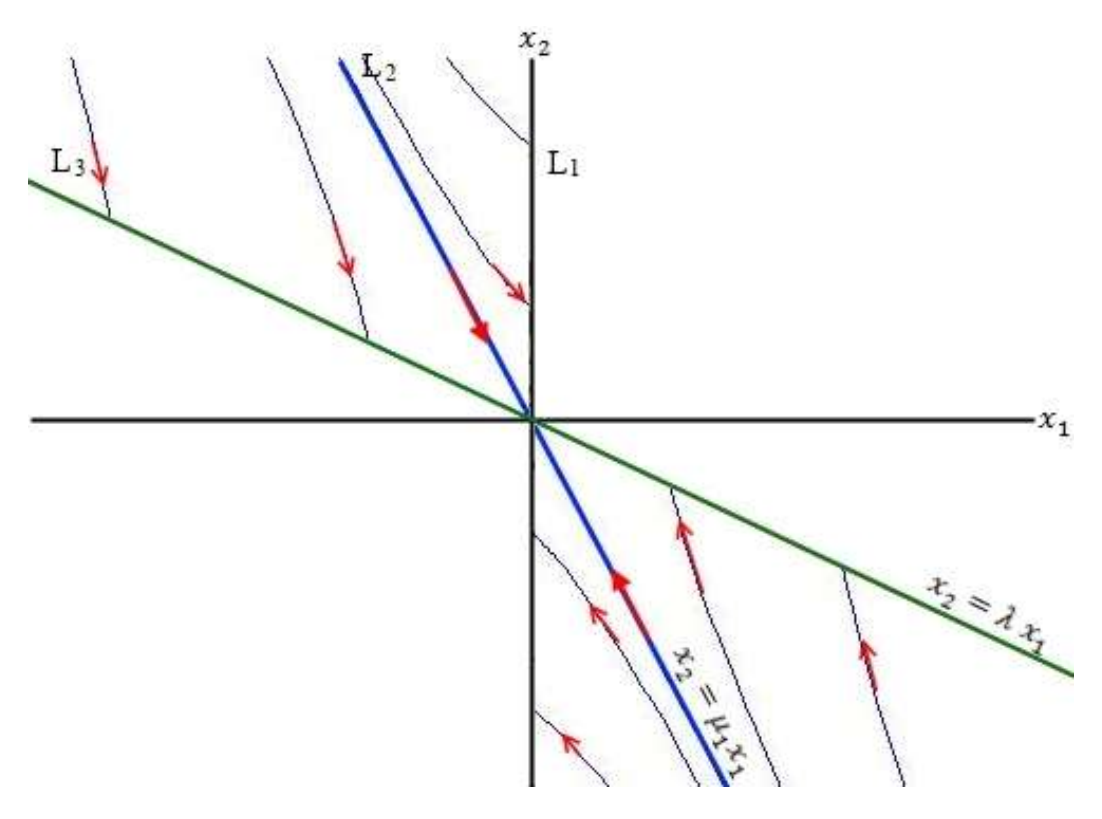


Figure 3.2. Phase portrait of the Variable Structure System (VSS) for  $\alpha = -1$ 

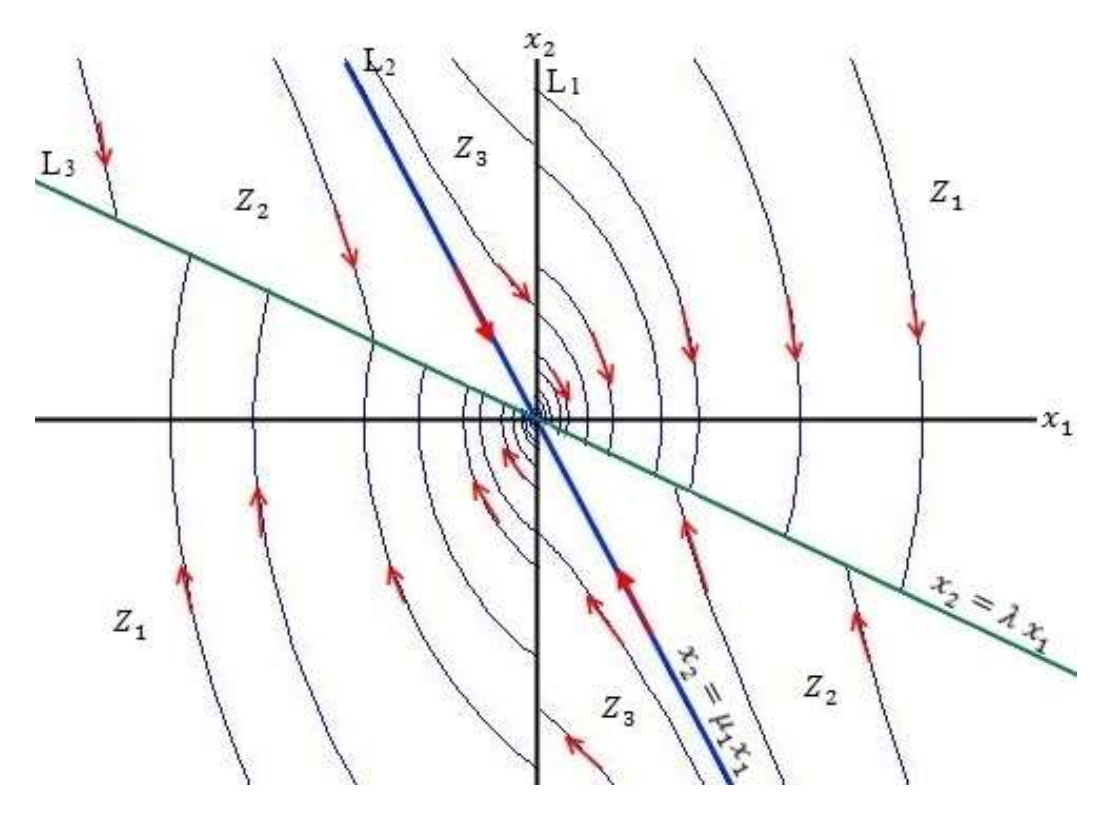


Figure 3.3. Phase portrait of the Variable Structure System (VSS) for  $\lambda > \mu_1$  is the union of the phase portrait in Figs.3.1 and 3.2

### **3.2.1. Stability**

The VSS is a hybrid system that switches between an asymptotically stable system, the phase portrait of which is shown in Fig.3.1, and an unstable system whose phase portrait is shown in Fig.3.2. The union of these phase portraits is shown in Fig.3.3. To investigate the stability of the equilibrium of the VSS, the phase plane is divided into three zones, namely:

$$\begin{split} Z_1 &= \{x \in R^2 | Sx_1 > 0\} \\ Z_2 &= \{x \in R^2 | (x_2 - \mu_1 x_1)(x_2 - \lambda x_1) < 0\} \\ Z_3 &= \{x \in R^2 | x_1(x_2 - \mu_1 x_1) < 0\} \end{split}$$

The three zones are separated by the following three lines:

$$L_1$$
:  $x_1 = 0$ 

L<sub>2</sub>: 
$$x_2 = \mu_1 x_1$$

$$L_3: x_2 = \lambda x_1$$

We investigate the system trajectories in these zones and on these lines next.

To study the behavior of the trajectories on  $L_1$ , we investigate the direction of the vector field on  $L_1$ . For  $x_2 > 0$  (and  $x_1 = 0$ ), we have the following equations and vector field:

$$\dot{x}_1 = x_2 > 0$$

$$\dot{x}_2 = -\frac{c}{m}x_2 < 0$$

Therefore, the trajectories enter  $Z_1$ . For  $x_2 < 0$  (and  $x_1 = 0$ ), we have the following equations and vector field:

$$\dot{x}_1 = x_2 < 0$$

$$\dot{x}_2 = -\frac{c}{m}x_2$$

Therefore, all trajectories on  $L_1$  will enter  $Z_1$ .

The line L<sub>2</sub> is the stable eigenvector of the second system where  $\alpha = -1$  – see Eqs.(2.16) and (2.18). On L<sub>2</sub> we have  $x_2 = \dot{x}_1 = \mu_1 x_1 \rightarrow x_1(t) = x_1(0) e^{\mu_1 t}$ ,  $\mu_1 < 0$ . Therefore, all trajectories on L<sub>2</sub> converge to the origin.

The boundaries of  $Z_1$  are  $L_1$  and  $L_3$ . We have already shown that trajectories on  $L_1$  enter  $Z_1$ . We now show all trajectories in  $Z_1$  reach  $L_3$  in finite time. To show this we consider the equation of motion of the system for  $\alpha = 1$ , given by Eq.(2.9):

$$\dot{x}_2 = \ddot{x}_1 = -2\zeta \omega_n \dot{x}_1 - \omega_n^2 x_1$$

The general form of the solution of this differential equation is

$$x_1(t) = e^{-\zeta \omega_n t} [A \cos \omega_d t + B \sin \omega_d t]$$
 (3.1)

and 
$$x_{2}(t) = -\zeta \omega_{n} e^{-\zeta \omega_{n} t} [A \cos \omega_{d} t + B \sin \omega_{d} t]$$
$$+ e^{-\zeta \omega_{n} t} [-A \omega_{d} \sin \omega_{d} t + B \omega_{d} \cos \omega_{d} t]$$
(3.2)

where  $\omega_d = \omega_n \sqrt{1 - \zeta^2}$ 

Substitution of the initial conditions  $x_1(0) = x_{10}$ , and  $x_2(0) = x_{20}$  into Eqs.(3.1) and (3.2), where  $(x_{10}, x_{20})$  lies in  $Z_1$ , we get:

$$A = x_{10}, \qquad B = \frac{x_{20} + \zeta \omega_n x_{10}}{\omega_n \sqrt{1 - \zeta^2}}$$
 (3.3)

To find the time when trajectory in  $Z_1$  reaches  $L_3$ , we substitute Eqs.(3.1) and (3.2) into the equation of  $L_3$ , namely:

$$x_2(t) = \lambda x_1(t)$$

This gives:

$$-\zeta \omega_n e^{-\zeta \omega_n t} [A \cos \omega_d t + B \sin \omega_d t] + \omega_d e^{-\zeta \omega t} [-A \sin \omega_d t + B \cos \omega_d t]$$

$$= \lambda e^{-\zeta \omega_n t_1} [A \cos \omega_d t + B \sin \omega_d t]$$

$$\Rightarrow \tan \omega_d t = \frac{\lambda A - \omega_d B + \zeta \omega_n A}{-\zeta \omega_n B - \omega_d A - \lambda B}$$
(3.4)

Substitution of the values of A and B from Eq.(3.3) into Eq.(3.4) gives

$$\tan \omega_{d} t = \frac{\lambda x_{10} - x_{20} - \zeta \omega_{n} x_{10} + \zeta \omega_{n} x_{10}}{-\frac{\zeta x_{20} + \zeta^{2} \omega_{n} x_{10}}{\sqrt{1 - \zeta^{2}}} - \frac{\omega_{n} (1 - \zeta^{2}) x_{10}}{\sqrt{1 - \zeta^{2}}} - \lambda \left(\frac{x_{20} + \zeta \omega_{n} x_{10}}{\omega_{n} \sqrt{1 - \zeta^{2}}}\right)}$$

$$\Rightarrow t = \frac{1}{\omega_{d}} \tan^{-1} \left[ \frac{(\lambda x_{10} - x_{20}) \sqrt{1 - \zeta^{2}}}{-\zeta x_{20} - \omega_{n} x_{10} - \lambda \left(\frac{x_{20} + \zeta \omega_{n} x_{10}}{\omega_{n}}\right)} \right]$$
(3.5)

This expression implies that all trajectories in  $Z_1$  reaches  $L_3$  at finite time.

The boundaries of  $Z_2$  are  $L_2$  and  $L_3$ . Furthermore, the trajectories in  $Z_2$  cannot cross  $L_2$  since  $L_2$  represents a trajectory itself, and trajectories cannot cross each other. We now show all

trajectories in  $Z_2$  reach  $L_3$  in finite time. To show this we consider the equation of motion of the system for  $\alpha = -1$ , given by Eq.(2.9):

$$\dot{x}_2 = \ddot{x}_1 = -2\zeta\omega_n\dot{x}_1 + \omega_n^2x_1$$

The general form of the solution of this differential equation is

$$x_1(t) = D e^{\omega_n t(-\zeta - \sqrt{1 + \zeta^2})} + E e^{\omega_n t(-\zeta + \sqrt{1 + \zeta^2})}$$
(3.6)

and

$$x_2(t) = \omega_n \left(-\zeta - \sqrt{1+\zeta^2}\right) D e^{\omega_n t \left(-\zeta - \sqrt{1+\zeta^2}\right)}$$

$$+\omega_n \left(-\zeta + \sqrt{1+\zeta^2}\right) E \, e^{\omega_n t \left(-\zeta + \sqrt{1+\zeta^2}\right)} \tag{3.7}$$

Substitution of the initial conditions  $x_1(0) = x_{10}$ , and  $x_2(0) = x_{20}$  into Eqs.(3.6) and (3.7), where  $(x_{10}, x_{20})$  lies in  $Z_2$  we get:

$$D = x_{10} - \frac{x_{20} + \omega_n x_{10} (\zeta + \sqrt{1 + \zeta^2})}{2\omega_n \sqrt{1 + \zeta^2}}, \qquad E = \frac{x_{20} + \omega_n x_{10} (\zeta + \sqrt{1 + \zeta^2})}{2\omega_n \sqrt{1 + \zeta^2}}$$
(3.8)

To find the time when trajectory in  $Z_2$  reaches  $L_3$ , we substitute Eqs.(3.6), and (3.7) into the equation of  $L_3$ , namely:

$$x_2(t) = \lambda x_1(t)$$

This gives:

$$\omega_{n}\left(-\zeta - \sqrt{1+\zeta^{2}}\right) D e^{\omega_{n}t\left(-\zeta - \sqrt{1+\zeta^{2}}\right)} + \omega_{n}\left(-\zeta + \sqrt{1+\zeta^{2}}\right) E e^{\omega_{n}t\left(-\zeta + \sqrt{1+\zeta^{2}}\right)}$$

$$= \lambda \left(D e^{\omega_{n}t\left(-\zeta - \sqrt{1+\zeta^{2}}\right)} + E e^{\omega_{n}t\left(-\zeta + \sqrt{1+\zeta^{2}}\right)}\right)$$

$$e^{\omega_{n}t(2\sqrt{1+\zeta^{2}})} = \frac{D\left[\lambda - \omega_{n}\left(-\zeta - \sqrt{1+\zeta^{2}}\right)\right]}{E\left[\omega_{n}\left(-\zeta + \sqrt{1+\zeta^{2}}\right) - \lambda\right]}$$
(3.9)

Substitution of the values of D and E from Eq.(48)into Eq.(3.9) gives:

$$e^{\omega_n t(2\sqrt{1+\zeta^2})} = \frac{-\left(x_{20} + \omega_n x_{10}(\zeta - \sqrt{1+\zeta^2})\right) \left[\lambda - \omega_n(-\zeta - \sqrt{1+\zeta^2})\right]}{\left(x_{20} + \omega_n x_{10}(\zeta + \sqrt{1+\zeta^2})\right) \left[\omega_n(-\zeta + \sqrt{1+\zeta^2}) - \lambda\right]}$$

$$\Rightarrow t = \frac{1}{2\omega_n\sqrt{1+\zeta^2}} \ln\left[\frac{Q_1}{Q_2}\right] \tag{3.10}$$

where  $Q_1$  and  $Q_2$ , which necessarily have the same sign, are

$$Q_1 = -\left(x_{20} + \omega_n x_{10} \left(\zeta - \sqrt{1 + \zeta^2}\right)\right) \left[\lambda - \omega_n \left(-\zeta - \sqrt{1 + \zeta^2}\right)\right]$$

$$Q_2 = \left(x_{20} + \omega_n x_{10} \left(\zeta + \sqrt{1 + \zeta^2}\right)\right) \left[\omega_n \left(-\zeta + \sqrt{1 + \zeta^2}\right) - \lambda\right]$$

This expression implies that all trajectories in  $\mathbb{Z}_2$  reaches  $\mathbb{L}_3$  at finite time.

The line L<sub>3</sub> is a sliding surface since all trajectories in  $Z_1$  and  $Z_2$  approach L<sub>3</sub> – see Fig.3.3. On L<sub>3</sub> we have  $x_2 = \dot{x}_1 = \lambda x_1 \rightarrow x_1(t) = x_1(0) e^{\lambda t}$ . Therefore, all trajectories on L<sub>3</sub> converge to the origin.

The boundaries of  $Z_3$  are  $L_1$  and  $L_2$ . Furthermore, the trajectories in  $Z_3$  cannot cross  $L_2$  since  $L_2$  represent a trajectory itself and trajectories cannot cross each other. Moreover, the trajectories on  $L_1$  enter  $Z_1$ . We now show all trajectories in  $Z_3$  reach  $L_1$  in finite time. The general form of the solution of the differential equation is described by Eqs.(3.6), and (3.7). To find the time when trajectory in  $Z_3$  reaches  $L_1$ , we substitute Eq. (3.6) into the equation of  $L_1$ , namely:

$$x_1 = 0$$

This gives:

$$D e^{\omega_n t(-\zeta - \sqrt{1 + \zeta^2})} + E e^{\omega_n t(-\zeta + \sqrt{1 + \zeta^2})} = 0$$

$$e^{\omega_n t(2\sqrt{1 + \zeta^2})} = -\frac{D}{E}$$
(3.11)

Substitution of the values of D and E from Eq.(3.8) into Eq.(3.11) gives

$$e^{\omega_n t(2\sqrt{1+\zeta^2})} = \frac{Q_3}{Q_4}$$

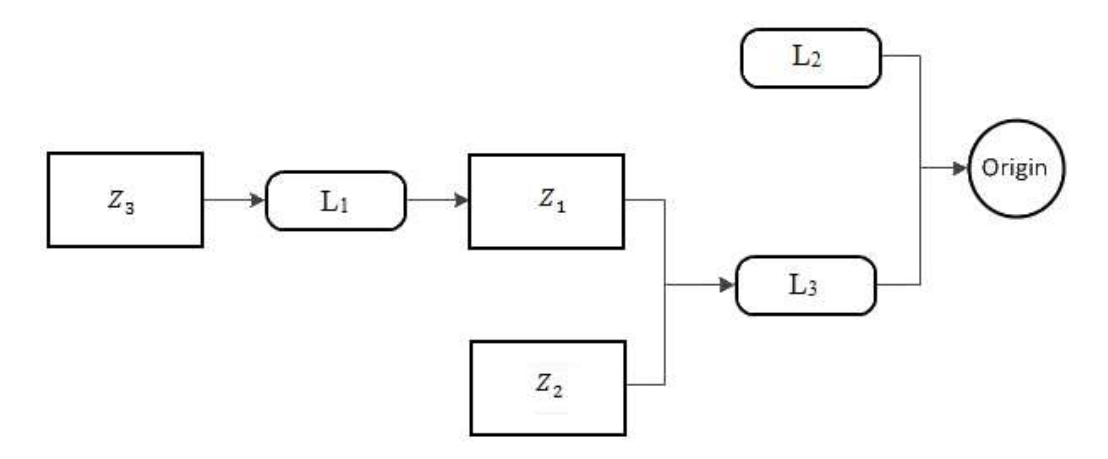


Figure 3.4. Convergence of VSS trajectories to the origin for  $\zeta < 1$  and  $\mu_1 < \lambda < 0$ 

$$\Rightarrow t = \frac{1}{2\omega_n \sqrt{1+\zeta^2}} \ln \left[ \frac{Q_3}{Q_4} \right] \tag{3.12}$$

where  $Q_3$  and  $Q_4$ , which necessarily have the same sign, are

$$Q_3 = \left[ x_{20} + \omega_n x_{10} \left( \zeta - \sqrt{1 + \zeta^2} \right) \right]$$

$$Q_4 = \left[ x_{20} + \omega_n x_{10} \left( \zeta + \sqrt{1 + \zeta^2} \right) \right]$$

This expression implies that the trajectories in  $Z_3$  reaches  $L_1$  at finite time.

The VSS is a hybrid system that switches between an asymptotically stable system and unstable system. However, from the above discussion it is clear that the origin of the VSS is asymptotically stable. The trajectories of the VSS converge to the origin through  $L_2$  or  $L_3$  – see Fig.3.4.

### 3.2.2. Performance – Response to Step Input

To investigate the performance of the VSS, we will study the response of the VSS to a step input and compare its performance with that of the original system for the same step input.

For the original system, the response to a step input would be described by the following equation and initial conditions:

$$m\ddot{x} + c\dot{x} + kx = u = k, \quad x(0) = 0, \dot{x}(0) = 0$$
 (3.13)

We choose a step input of variable k such that the steady state value of x is unity. On change of variable y = (x - 1) and  $\dot{y} = \dot{x}$ , we get the unforced system:

$$\ddot{y} = -\frac{c}{m}\dot{y} - \frac{k}{m}y, \quad y(0) = -1, \quad \dot{y}(0) = 0$$
 (3.14)

To obtain the same VSS as in Eqs.(2.2) and (2.6), we redefine F in Eq.(2.5) as follows:

$$F = k + \begin{cases} 0 & \text{if } (S > 0 \text{ and } x \ge 1) \text{ or } (S < 0 \text{ and } x \le 1) \\ 2k(x-1) & \text{if } S(x-1) < 0 \end{cases}$$
(3.15)

Substitution of the values of Eq.(55) into Eq.(1) and change of variables y = (x - 1) and  $\dot{y} =$  $\dot{x}$ , we get:

$$\ddot{y} = -\frac{c}{m}\dot{y} - \alpha \frac{k}{m}y, \quad y(0) = -1, \quad \dot{y}(0) = 0$$
 (3.16)

where 
$$\alpha = \begin{cases} +1 & \text{if } (S > 0 \text{ and } y \ge 0) \text{ or } (S < 0 \text{ and } y \le 0) \\ -1 & \text{if } Sy < 0 \end{cases}$$

Note that Eqs.(3.14) and (3.16) are very similar and have the same initial conditions. Also, note that Eq.(3.16) is identical to Eq.(2.6); therefore, the analysis presented in the section 3.2.1 is applicable.

The phase portrait of the VSS in Eq.(3.16) has been studied in section 3.2.1. From this study we know that no trajectories of the VSS will undergo a phase change of more than  $2\pi$ , and therefore, the VSS will not exhibit oscillations for a step input. Consequently, the rise time and percentage overshoot of the system are not relevant. In the absence of oscillations, we investigate the performance of the VSS using the metric of settling time (the time required for the response curve to reach and stay within 2% of the final value) [1]. To this end, we first consider the time needed by the VSS to reach the sliding surface L<sub>3</sub>, given by Eq.(3.5), which is now rewritten using variables y and  $\dot{y}$ . If  $y_0$  and  $\dot{y}_0$  donate the values of y(0) and  $\dot{y}(0)$  respectively, the time needed to reach L<sub>3</sub> is given by :

$$t = \frac{1}{\omega_d} \tan^{-1} \left[ \frac{(\lambda y_0 - \dot{y}_0) \sqrt{1 - \zeta^2}}{-\zeta \dot{y}_0 - \omega_n y_0 - \lambda \left( \frac{\dot{y}_0 + \zeta \omega_n y_0}{\omega_n} \right)} \right]$$

Substitution of the values of  $y_0 = -1$  and  $\dot{y}_0 = 0$ , gives:

$$t_1 = \frac{1}{\omega_d} \tan^{-1} \left[ \frac{-\lambda \sqrt{1 - \zeta^2}}{\omega_n + \lambda \zeta} \right]$$
 (3.17)

we substitute the values of  $y_0 = -1$ ,  $\dot{y}_0 = 0$ , and  $t_1$  described by Eq.(3.16) into Eqs.(3.1) and (3.2), with variables  $x_1$  and  $x_2$  replaced by y and  $\dot{y}$  respectively. This gives the values of y and  $\dot{y}$  when the VSS reaches the sliding surface L<sub>3</sub>:

$$y_s = e^{-\zeta \omega_n t_1} \left[ -\cos \omega_d t_1 - \frac{\zeta}{\sqrt{1 - \zeta^2}} \sin \omega_d t_1 \right]$$
 (3.18)

$$\dot{y}_{s} = -\zeta \omega_{n} e^{-\zeta \omega_{n} t_{1}} \left[ -\cos \omega_{d} t_{1} - \frac{\zeta}{\sqrt{1 - \zeta^{2}}} \sin \omega_{d} t_{1} \right]$$

$$+ e^{-\zeta \omega_{n} t_{1}} \left[ \omega_{d} \sin \omega_{d} t_{1} - \frac{\zeta}{\sqrt{1 - \zeta^{2}}} \omega_{d} \cos \omega_{d} t_{1} \right]$$
(3.19)

where  $\omega_d = \omega_n \sqrt{1 - \zeta^2}$ 

To find the time needed for the trajectories on  $L_3$  to enter the region  $|y| \le 0.02$ , we consider the dynamics on  $L_3$ , namely:

$$y(t) = y_s e^{\lambda t}, \qquad \lambda < 0 \tag{3.20}$$

Substitution of y(t) = -0.02 yields

$$e^{\lambda t} = \frac{-0.02}{y_s} \quad \Rightarrow t_2 = \frac{1}{\lambda} \ln \left( \frac{-0.02}{y_s} \right) \tag{3.21}$$

The settling time of the VSS is given by:

$$t_s = t_1 + t_2 = \frac{1}{\omega_d} \tan^{-1} \left[ \frac{-\lambda \sqrt{1 - \zeta^2}}{\omega_n + \lambda \zeta} \right] + \frac{1}{\lambda} \ln \left( \frac{-0.02}{y_s} \right)$$
(3.22)

where  $y_s$  is defined by Eq.(3.18). For proper comparison of the performance, we nondimensionalize time using the variable  $\tau = \omega_n t$ . Concurrently, we define  $\lambda = \kappa \mu_1$  where  $\kappa$ ,  $0 < \kappa < 1$ , is a constant. The nondimensional settling time is now given by the following equation:

$$\tau_s = \tau_1 + \tau_2 \tag{3.23}$$

where

$$\tau_1 = \frac{1}{\sqrt{1 - \zeta^2}} \tan^{-1} \frac{\kappa \left[ \zeta + \sqrt{\zeta^2 + 1} \right] \sqrt{1 - \zeta^2}}{1 - \zeta \kappa \left[ \zeta + \sqrt{\zeta^2 + 1} \right]}$$
(3.24)

$$\tau_2 = \frac{-1}{\kappa \left[\zeta + \sqrt{\zeta^2 + 1}\right]} \ln\left(\frac{-0.02}{y_s}\right) \tag{3.25}$$

and where

$$y_s = e^{-\zeta \tau_1} \left[ -\cos \tau_1 \sqrt{1 - \zeta^2} - \frac{\zeta}{\sqrt{1 - \zeta^2}} \sin \tau_1 \sqrt{1 - \zeta^2} \right]$$
 (3.26)

Figure 3.5 shows a comparison of the settling time of the VSS for different value of  $\kappa$  ( $\kappa=0.1,\kappa=0.3,\kappa=0.5,\kappa=0.9$ ) and the original system. The settling time for the original system shows several discontinuities in the settling time; this is due to the sensitivity of the settling time to changes in  $\zeta$  [Ogata, 2009]. For  $\kappa=0.1$ , the VSS has better performance than that of the original system only when  $\zeta<0.11$ . For  $\kappa=0.3$ , the performance is better for a larger range of  $\zeta$ , namely  $\zeta<0.39$ . As we increase  $\kappa$ , the performance is better for a larger range of  $\zeta$ : for  $\kappa=0.9$  the performance is better for  $\zeta<0.79$ . The settling time of the original system can be reduced by increasing the value of  $\zeta$  but for most  $\zeta$  values, a VSS can be found ( $\kappa$  can be chosen) that has better performance in terms of the settling time. For

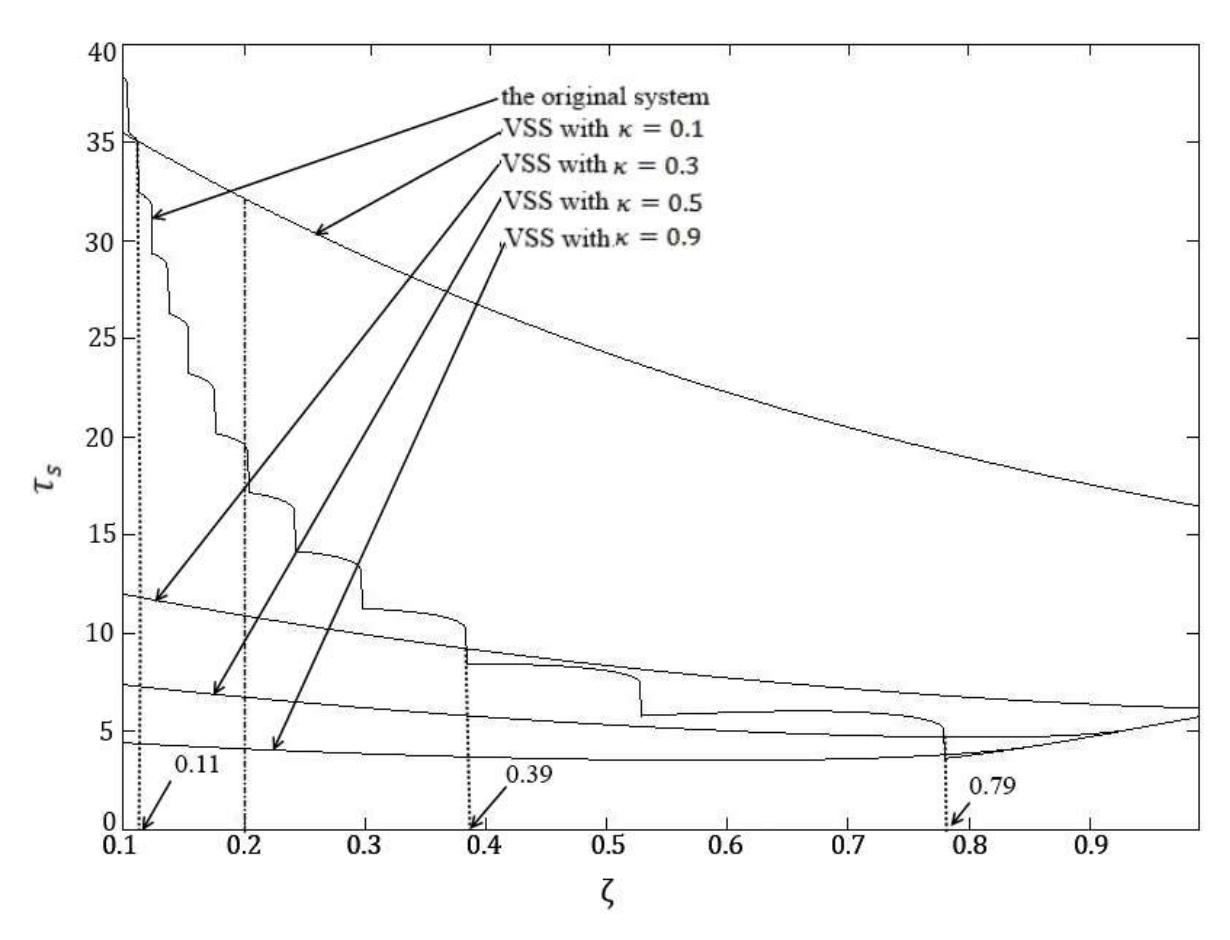


Figure 3.5. Comparison of the settling times of the VSS and the original system.

example, for  $\zeta=0.2$ , the settling time for the original system is  $\tau_s=19.55$ , whereas it is equal to 32.13, 10.87, 6.72, and 4.0 for VSS with  $\kappa=0.1,0.3,0.5$ , and 0.9 respectively. It is clear that the VSS improves the settling time for  $\zeta=0.2$  by 44.4% when  $\kappa=0.3$ , by 65,6% when  $\kappa=0.5$ , and by 79.1% when  $\kappa=0.9$ . The best performance is achieved by the VSS when  $\kappa\to 1$  or  $\lambda\to \mu_1$ . However, the maximum value of  $\kappa$  can be chosen is less than unity (0.95, for example) because of the finite time needed to switching of  $\alpha$  from +1 to -1. If  $\kappa\approx 1$  the area of  $Z_2$  in Fig.3.3 is almost zero and there will be no switching in this zone and the switching will be in  $Z_3$ . Figure 3.5 also indicates that there is no difference in the settling time of the original system and the VSS with  $\kappa=0.9$  for  $\zeta\geq 0.9$ . This is because the trajectories of the VSS enters the region  $|y|\leq 0.02$  before it reaches the sliding surface  $L_3$ . This implies that the

VSS has no advantage over the original system when the system is under-damped and has values of  $\zeta$  close to unity.

It is important to note that  $\mu_1 = \mu_1(\zeta)$  and  $\mu_1$  decreases as  $\zeta$  increases. If  $\lambda = \kappa \mu_1$  but  $\lambda$  is constant, we have a situation where  $\kappa$  decreases as  $\zeta$  increases. Since the performance is better (settling time is smaller) for larger values of  $\kappa$ , a constant value of  $\lambda$  results in poorer performance for large values of  $\zeta$ . This is shown with the help of Fig.3.6. Note  $\zeta$  and  $\mu_1$  are plotted along x-axis in the figure and it can be seen that the settling time  $\tau_s$  for VSS increases as  $\zeta$  increases.

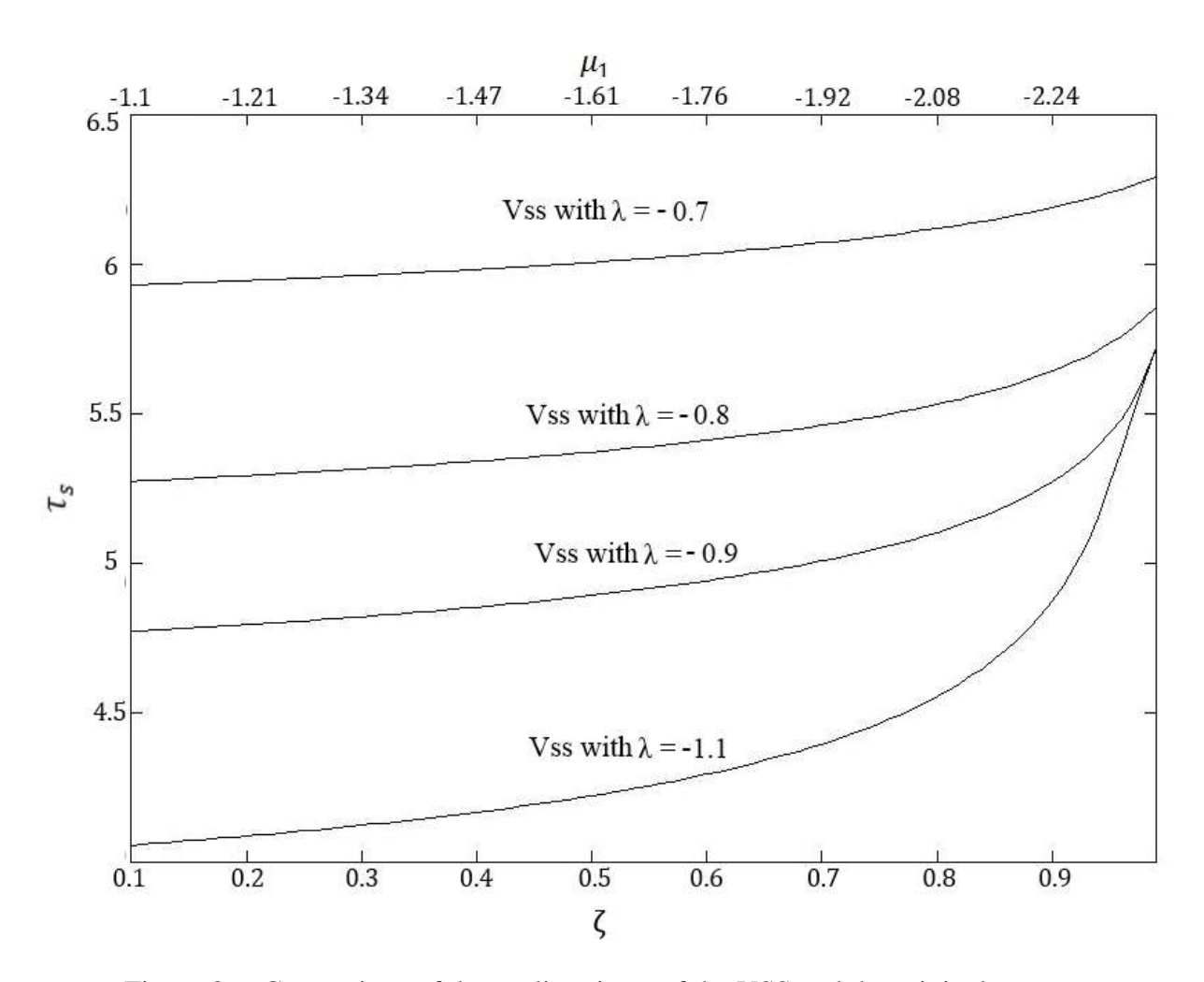


Figure 3.6. Comparison of the settling times of the VSS and the original system.

In this section, we investigated the performance of the VSS with switched stiffness for a step input for different values of sliding surface slope  $\lambda$ . The VSS has smaller settling time than that of the original mass-spring-damper system for a range of  $\zeta$  values. For higher values of  $\lambda$  the settling time of the VSS decreases and the best performance is achieved when  $\lambda \to \mu_1$ .

#### **3.2.3.** Performance – Speed of Convergence

In last section, we investigated the performance of the VSS for a step input. This problem was recast as an initial value problem with the initial conditions at (-1,0) in the phase plane. Since (-1,0) lies in  $Z_1$ , we now compare the performance of the VSS with switched stiffness and the original system for arbitrary initial conditions in  $\mathbb{Z}_2$  and  $\mathbb{Z}_3$ . For an initial conditions in  $\mathbb{Z}_2$  (see Fig.3.3), the time needed by the VSS to reaches the sliding surface  $\mathbb{L}_3$  ( $x_2 =$  $\lambda x_1$ ) has been studied in section 3.2.1, and was described by Eq.(3.10). The values of  $x_1$  and  $x_2$  when the VSS reaches the sliding surface L<sub>3</sub> has been studied in section 3.2.1, and was described by Eq.(3.6), and (3.7). The time needed for the trajectories on L<sub>3</sub> to enter the region  $|x_1| \le 0.02$  has been studied in section 3.2.1, and was described by Eq.(3.21). Using these relations, the settling time of the VSS can be shown to be:

$$\tau_s = \tau_1 + \tau_2 \tag{3.27}$$

where 
$$\tau_1 = \omega_n t_1 = \frac{1}{2\sqrt{1-\zeta^2}}$$

$$\ln \left[ \frac{[-x_{20} - x_{10}(\zeta - \sqrt{1 + \zeta^2})][(\zeta + \sqrt{1 + \zeta^2}) - \kappa(\zeta + \sqrt{1 + \zeta^2})]}{[x_{20} + x_{10}(\zeta + \sqrt{1 + \zeta^2})][(-\zeta + \sqrt{1 + \zeta^2}) + \kappa(\zeta + \sqrt{1 + \zeta^2})]} \right]$$
(3.28)

$$\tau_2 = \omega_n t_2 = \frac{-1}{\left[\zeta + \sqrt{\zeta^2 + 1}\right]} \ln\left(\frac{-0.02}{x_{1s}}\right)$$
 (3.29)

where 
$$x_{1s} = D e^{\tau_1(-\zeta - \sqrt{1 + \zeta^2})} + E e^{\tau_1(-\zeta + \sqrt{1 + \zeta^2})}$$
 (3.30)  
and 
$$D = x_{10} - \frac{x_{20} + x_{10}(\zeta + \sqrt{1 + \zeta^2})}{2\sqrt{1 + \zeta^2}}, \qquad E = \frac{x_{20} + x_{10}(\zeta + \sqrt{1 + \zeta^2})}{2\sqrt{1 + \zeta^2}}$$

where  $x_{10}$  and  $x_{20}$  are the initials conditions in  $Z_2$ . Figure 3.7 shows a comparison of the settling time of the VSS for different value of  $\kappa$  ( $\kappa=0.1, \kappa=0.3, \kappa=0.5, \kappa=0.9$ ) and the original system for initial conditions in  $Z_2$ . The initial conditions were arbitrarily chosen as  $x_{10}=-1$ , and  $x_{20}=-0.95\,\mu_1$ . For  $\kappa=0.1$ , the VSS has better performance than that of the original system only when  $\zeta<0.18$ . For  $\kappa=0.3$ , the performance is better for a larger range of  $\zeta$ , namely  $\zeta<0.68$ . As we increase  $\kappa$ , the performance is better for a larger range of  $\zeta$ : for  $\kappa=0.5$  and 0.9, the performance is better for all value of  $\zeta$ . The settling time of the original

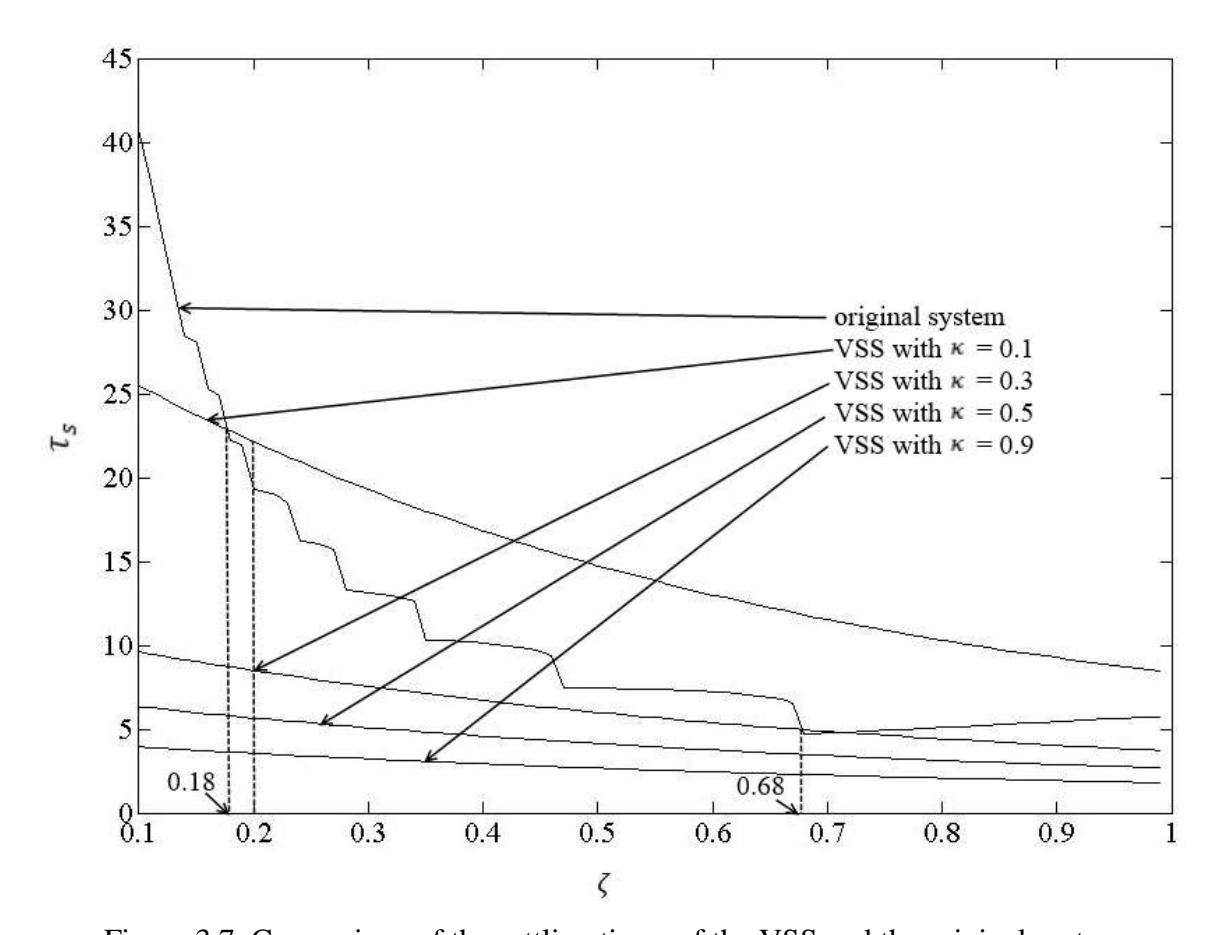


Figure 3.7. Comparison of the settling times of the VSS and the original system

system can be reduced by increasing the value of  $\zeta$  but for most  $\zeta$  values, a VSS can be found ( $\kappa$  can be chosen) that has better performance in terms of the settling time. For example, for  $\zeta=0.2$ , the settling time for the original system is  $\tau_s=19.29$ , whereas it is equal to 22.13, 8.48, 5.59, and 3.55 for VSS with  $\kappa=0.1,0.3,0.5$ , and 0.9 respectively. It is clear that the VSS improves the settling time for  $\zeta=0.2$  by 56% when  $\kappa=0.3$ , by 70.66% when  $\kappa=0.5$ , and by 81.58% when  $\kappa=0.9$ . The best performance is achieved by the VSS when  $\kappa\to 1$  or  $\lambda\to\mu_1$ .

For an initial conditions in  $Z_3$  (see Fig.3.3), the time needed by the VSS to reaches  $L_1$  has been studied in section 3.2.1, and was described by Eq.(3.12). The values of  $x_1$  and  $x_2$  when the VSS reach the sliding surface  $L_1$  ( $x_1 = 0$ ) has been studied in section 3.2.1, and was described by Eq.(3.6), and (3.7). The time needed by the VSS to reaches the sliding surface  $L_3$  ( $x_2 = \lambda x_1$ ) has been studied in section 3.2.1, and was described by Eq.(3.5). The values of  $x_1$  and  $x_2$  when the VSS reach the sliding surface  $L_3$  has been studied in section 3.2.1, and was described by Eq.(3.1) and (3.2). The time needed for the trajectories on  $L_3$  to enter the region  $|x_1| \le 0.02$  has been studied in section 3.2.1, and was described by Eq.(3.21). Using these relations, the settling time of the VSS can be shown to be:

$$\tau_s = \tau_1 + \tau_2 + \tau_3 \tag{3.31}$$

where

$$\tau_1 = \omega_n t_1 = \frac{1}{2\sqrt{1+\zeta^2}} \ln \left[ \frac{\left[ x_{20} + x_{10} \left( \zeta - \sqrt{1+\zeta^2} \right) \right]}{\left[ x_{20} + x_{10} \left( \zeta + \sqrt{1+\zeta^2} \right) \right]} \right]$$
(3.32)

$$\tau_2 = \omega_n t_2 = \frac{1}{\sqrt{1 - \zeta^2}} \tan^{-1} \left[ \frac{\sqrt{1 - \zeta^2}}{\zeta - \kappa (\zeta + \sqrt{1 + \zeta^2})} \right]$$
 (3.33)

$$\tau_3 = \omega_n t_3 = \frac{-1}{\kappa \left[\zeta + \sqrt{\zeta^2 + 1}\right]} \ln \left(\frac{0.02}{x_{1s}}\right)$$
 (3.34)

and 
$$x_{1s} = e^{-\zeta \omega_n \tau_2} \left[ \frac{x_{2l1}}{\sqrt{1 - \zeta^2}} \sin \sqrt{1 - \zeta^2} \tau_2 \right]$$
 (3.35)

where 
$$x_{2l1} = \left(-\zeta - \sqrt{1 + \zeta^2}\right) D e^{\tau_1 \left(-\zeta - \sqrt{1 + \zeta^2}\right)} + \left(-\zeta + \sqrt{1 + \zeta^2}\right) E e^{\tau_1 \left(-\zeta + \sqrt{1 + \zeta^2}\right)}$$
 (3.36)

where 
$$D = x_{10} - \frac{x_{20} + \omega_n x_{10} (\zeta + \sqrt{1 + \zeta^2})}{2\omega_n \sqrt{1 + \zeta^2}}, \qquad E = \frac{x_{20} + \omega_n x_{10} (\zeta + \sqrt{1 + \zeta^2})}{2\omega_n \sqrt{1 + \zeta^2}}$$

where  $x_{10}$  and  $x_{20}$  are the initials conditions in  $Z_3$ . Figure 3.8 shows a comparison of the settling time of the VSS for different value of  $\kappa$  ( $\kappa = 0.1, \kappa = 0.3, \kappa = 0.5, \kappa = 0.9$ ) and the original system for initial conditions in  $Z_3$ . The initial conditions were arbitrarily chosen as  $x_{10} = -1$ , and  $x_{20} = -1.1 \,\mu_1$ . For  $\kappa = 0.1$ , the VSS has better performance than that of the original

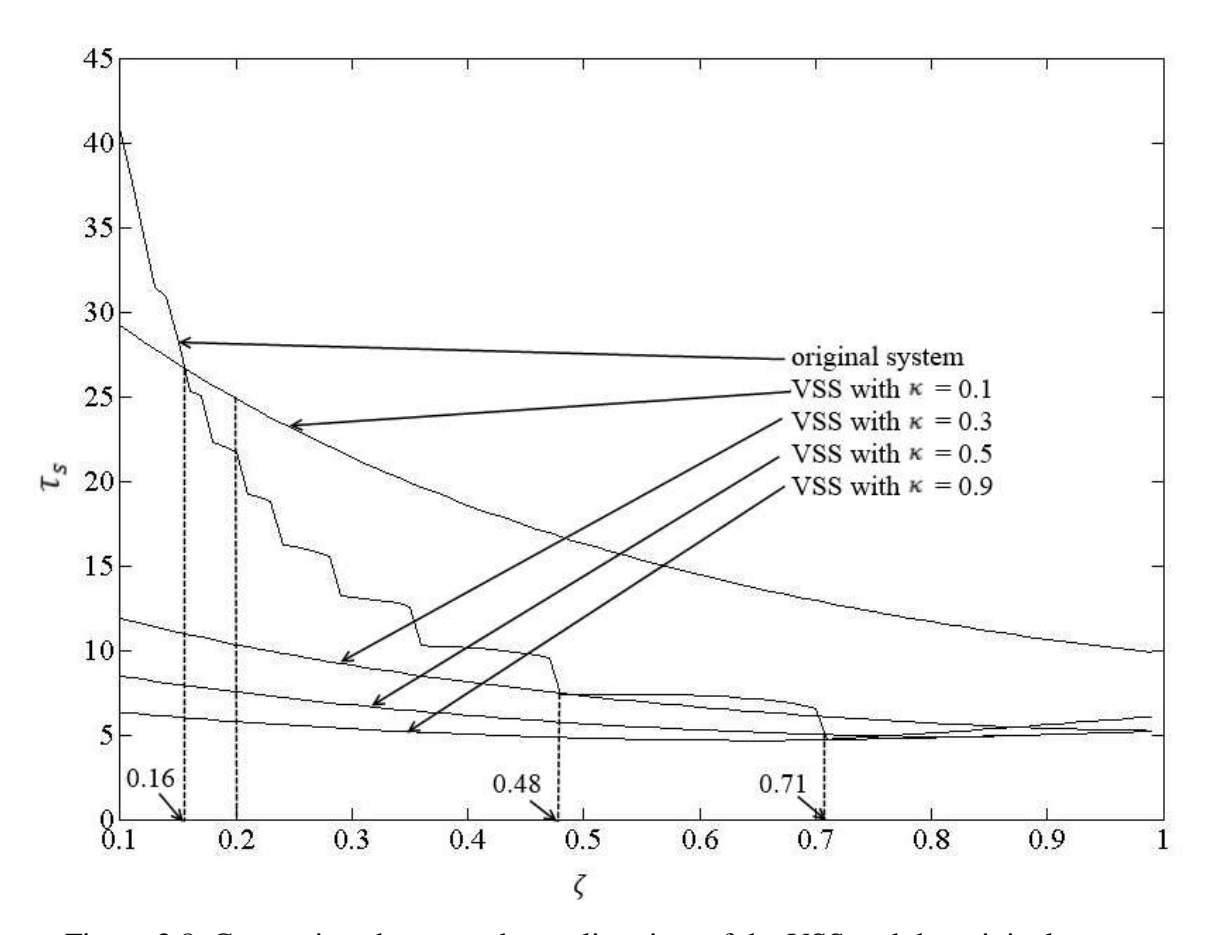


Figure 3.8. Comparison between the settling time of the VSS and the original system

system only when  $\zeta < 0.16$ . For  $\kappa = 0.3$ , the performance is better for a larger range of  $\zeta$ , namely  $\zeta < 0.48$ . For  $\kappa = 0.5$ , the performance is better for a larger range of  $\zeta$ , namely  $\zeta < 0.71$ . As we increase  $\kappa$ , the performance is better for a larger range of  $\zeta$ : for  $\kappa = 0.9$ , the performance is better for all value of  $\zeta$ . The settling time of the original system can be reduced by increasing the value of  $\zeta$  but for most  $\zeta$  values, a VSS can be found ( $\kappa$  can be chosen) that has better performance in terms of the settling time. For example, for  $\zeta = 0.2$ , the settling time for the original system is  $\tau_s = 21.67$ , whereas it is equal to 24.87, 10.32, 7.51, and 5.78 for VSS with  $\kappa = 0.1$ , 0.3, 0.5, and 0.9 respectively. It is clear that the VSS improves the settling time for  $\zeta = 0.2$  by 52.34% when  $\kappa = 0.3$ , by 65.31% when  $\kappa = 0.5$ , and by 73.33% when  $\kappa = 0.9$ . The best performance is achieved by the VSS when  $\kappa \to 1$  or  $\lambda \to \mu_1$ .

In this section, we investigated the performance of the VSS with switched stiffness for arbitrary initial conditions in  $Z_2$  and  $Z_3$ , and for different values of sliding surface slope  $\lambda$ . The VSS has a smaller settling time than that of the original mass-spring-damper system for a range of  $\zeta$  values. For higher value of  $\lambda$  the settling time of the VSS decreases and with the best performance is achieved by the VSS when  $\lambda \to \mu_1$ .

### 3.3. Case B: $\lambda \le \mu_1 < 0$

### **3.3.1.** Stability

The VSS is a hybrid system that switches between an asymptotically stable system, the phase portrait of which is shown in Fig.3.9, and an unstable system whose phase portrait is shown in Fig.3.10. The union of these phase portraits is shown in Fig.3.11. To investigate the stability of the equilibrium of the VSS, the phase plane is divided into two zones, namely:

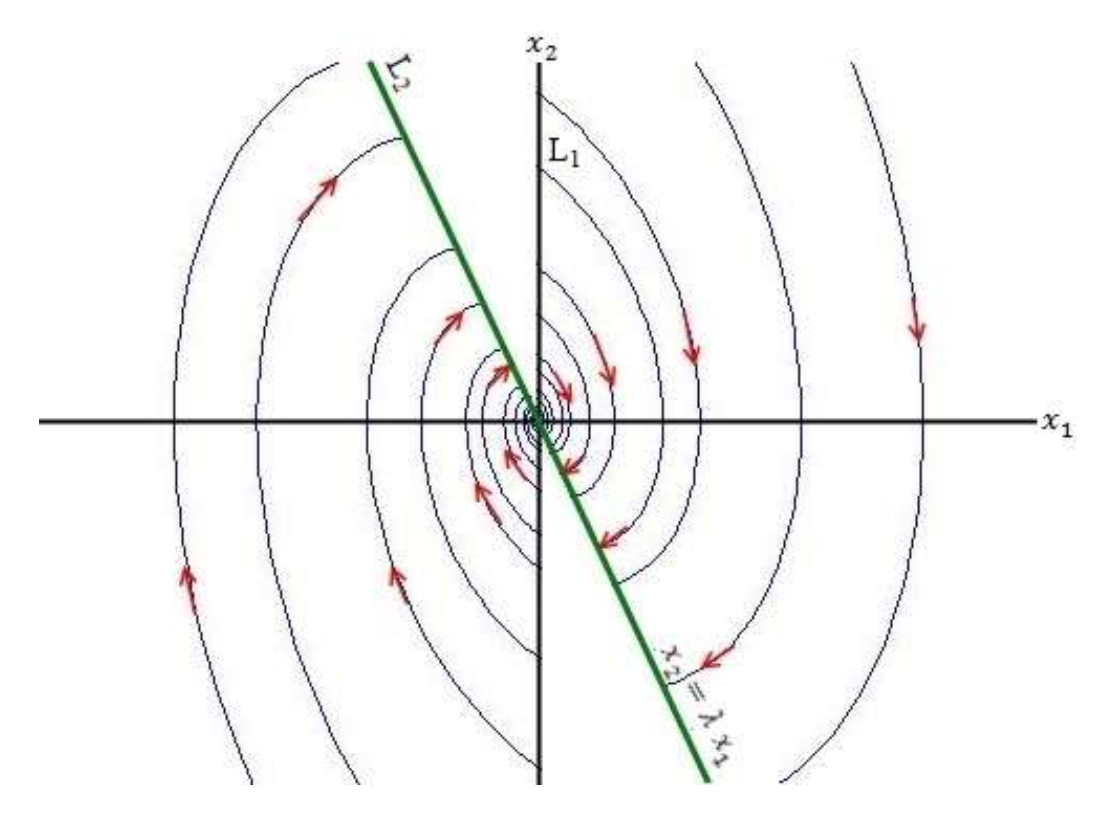


Figure 3.9. Phase portrait of the Variable Structure System (VSS) for  $\alpha=+1$ 

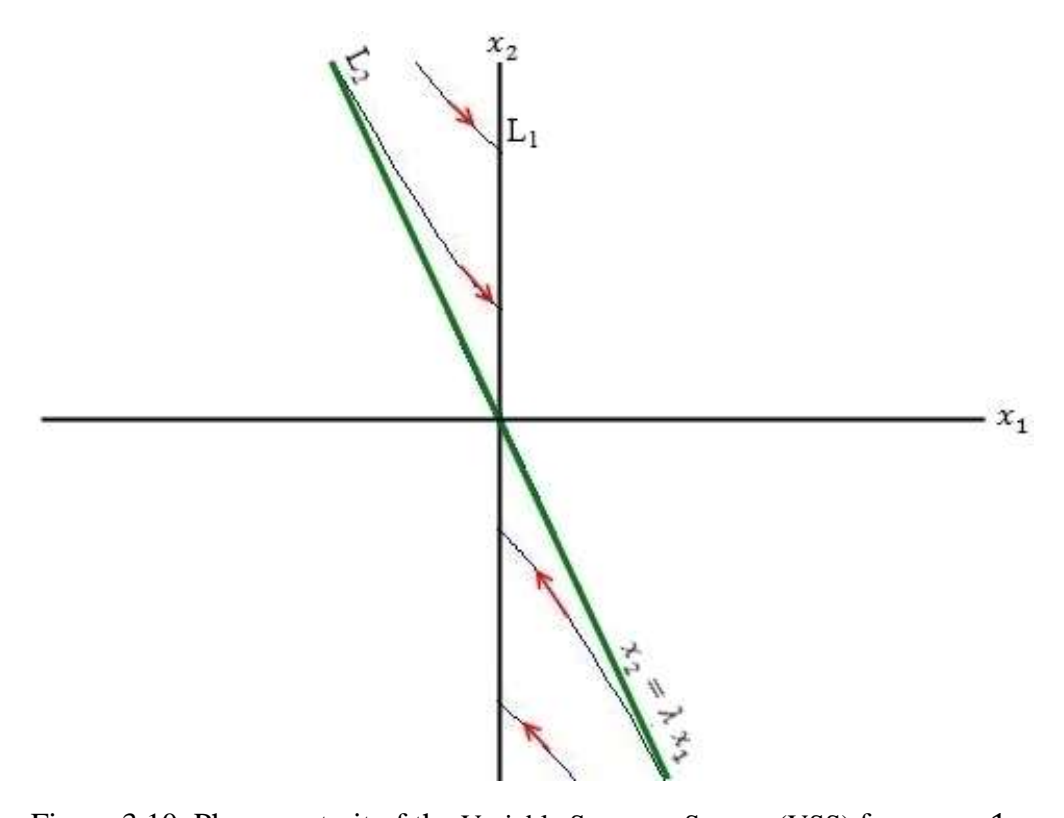


Figure 3.10. Phase portrait of the Variable Structure System (VSS) for  $\alpha=-1$ 

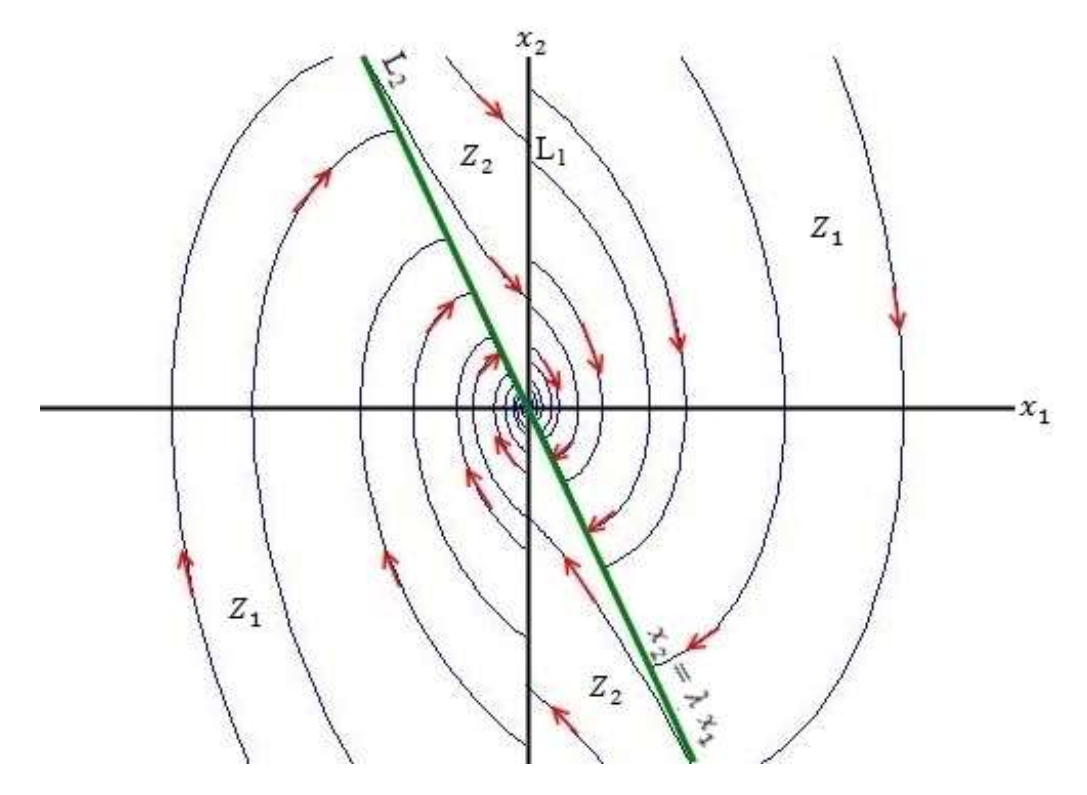


Figure 3.11. Phase portrait of the Variable Structure System (VSS) for  $\lambda > \mu_1$ 

$$Z_1 = \{ x \in R^2 | Sx_1 > 0 \}$$

$$Z_2 = \{x \in R^2 | x_1(x_2 - \lambda \, x_1) < 0\}$$

The two zones are separated by the following two lines:

$$L_1: x_1 = 0$$

$$L_2: x_2 = \lambda x_1$$

We investigate the system trajectories in these zones and on these lines next.

To study the behavior of the trajectories on  $L_1$ , we investigate the direction of the vector field on  $L_1$ . For  $x_2 > 0$  (and  $x_1 = 0$ ), we have the following equations and vector field:

$$\dot{x}_1 = x_2 > 0$$

$$\dot{x}_2 = -\frac{c}{m}x_2 < 0$$

Therefore, the trajectories enter  $Z_1$ . For  $x_2 < 0$  (and  $x_1 = 0$ ), we have the following equations and vector field:

$$\dot{x}_1 = x_2 < 0$$

$$\dot{x}_2 = -\frac{c}{m}x_2 > 0$$

Therefore, all trajectories on  $L_1$  will enter  $Z_1$ .

The boundaries of  $Z_1$  are  $L_1$  and  $L_2$ . We have already shown that trajectories on  $L_1$  enter  $Z_1$ . We now show all trajectories in  $Z_1$  reaches  $L_2$  in finite time. The time when the trajectory in  $Z_1$  reaches  $L_2$  has been studied in section 3.2.1, and was described by Eq.(3.5). For convenience, it is provided below:

$$t = \frac{1}{\omega_d} \tan^{-1} \left[ \frac{(\lambda x_{10} - x_{20}) \sqrt{1 - \zeta^2}}{-\zeta x_{20} - \omega_n x_{10} - \lambda \left( \frac{x_{20} + \zeta \omega_n x_{10}}{\omega_n} \right)} \right]$$

This expression implies that all trajectories in  $Z_1$  reaches  $L_2$  at finite time.

The boundaries of  $Z_2$  are  $L_2$  and  $L_1$ . We have already shown that the trajectories on  $L_1$  enter  $Z_1$ . We now show that all trajectories in  $Z_2$  reaches  $L_1$  in finite time. The time when a trajectory in  $Z_2$  reaches  $L_1$  has been studied in section 3.2.1, and was described by Eq.(3.12). For convenience, it is provided below:

$$t = \frac{1}{2\omega_n \sqrt{1+\zeta^2}} \ln \left[ \frac{\left[ x_{20} + \omega_n x_{10} \left( \zeta - \sqrt{1+\zeta^2} \right) \right]}{\left[ x_{20} + \omega_n x_{10} \left( \zeta + \sqrt{1+\zeta^2} \right) \right]} \right]$$

This expression implies that all trajectories in  $\mathbb{Z}_2$  reaches  $\mathbb{L}_1$  at finite time.

From the above discussion it is clear that the trajectories of the VSS move alternately between zones  $Z_1$  and  $Z_2$  by crossing lines  $L_2$  and  $L_1$ . We now show that all these trajectories

converge to the origin. We consider the Lyapunov Function candidate given below, which is equal to the total energy of the mass-spring-damper:

$$V = \frac{1}{2} k x_1^2 + \frac{1}{2} m x_2^2 \tag{3.37}$$

The derivative of V with respect to time gives:

$$\dot{V} = k x_1 \dot{x}_1 + m x_2 \dot{x}_2 \tag{3.38}$$

In  $Z_1$ , where  $\alpha = 1$ , we have

$$\dot{V} = k x_1 x_2 + m x_2 \dot{x}_2 
= k x_1 x_2 - c x_2^2 - k x_1 x_2 
= -c x_2^2 \le 0$$
(3.39)

In  $Z_2$ , where  $\alpha = -1$ , we have

$$\dot{V} = k x_1 x_2 + m x_2 \dot{x}_2$$

$$= k x_1 x_2 - c x_2^2 + k x_1 x_2$$

$$= 2 k x_1 x_2 - c x_2^2$$

In  $Z_2$ ,  $x_2 < \lambda x_1$  when  $x_1 > 0$ , and  $x_2 > \lambda x_1$  when  $x_1 < 0$ . Therefore

where 
$$\dot{V} < 2 k \lambda x_1^2 - c x_2^2$$
 where  $\lambda < 0$   
 $\dot{V} < 0$  for all  $(x_1, x_2) \neq (0, 0)$  (3.40)

From the above discussion, we have  $\dot{V} \leq 0$  in the entire domain. It is negative definite in  $Z_2$  but negative semidefinite in  $Z_1$ . Using LaSalle's theorem [Khalil, 2009], we can show that in  $Z_1$ 

$$\dot{V} \equiv 0 \ \Rightarrow \ x_2 \equiv 0 \ \Rightarrow \ \dot{x}_2 \ \equiv 0 \Rightarrow \ x_1 \equiv 0$$

Furthermore,  $V \to \infty$  as  $x \to \infty$ . Therefore, the origin of the VSS is globally asymptotically stable.

### 3.3.2. Performance – Response to Step Input

To investigate the performance of the VSS, we will study the response of the VSS to a step input and compare its performance with that of the original system for the same step input.

For the original system, the response to a step input has been studied in section 3.2.1, and was described in Eq.(3.14). For convenience, it is provided below:

$$\ddot{y} = -\frac{c}{m}\dot{y} - \frac{k}{m}y, \quad y(0) = -1, \quad \dot{y}(0) = 0$$
 (3.41)

The response of the VSS to the same step input was described in Eq.(3.16). For convenience, it is provided below:

$$\ddot{y} = -\frac{c}{m}\dot{y} - \alpha \frac{k}{m}y, \quad y(0) = -1, \quad \dot{y}(0) = 0$$
 (3.42)

where 
$$\alpha = \begin{cases} +1 & \text{if } (S > 0 \text{ and } y \ge 0) \text{ or } (S < 0 \text{ and } y \le 0) \\ -1 & \text{if } Sy < 0 \end{cases}$$

Note that Eqs.(3.41) and (3.42) are very similar and have the same initial conditions. Also, note that Eq.(3.42) is identical to Eq.(2.6); therefore, all the analysis presented in section 3.3.1 will be applicable.

The phase portrait of the VSS in Eq. (3.42) has been studied in section 3.3.1. From this study we know that the trajectories of the system will spiral to the origin. Unlike the previous case, it is not possible to claim that the phase change of the trajectories will be less than  $2\pi$ . In other words, a step input will result in oscillation, similar to the original system. Therefore, the performance of the original system and the VSS can be compared by on the basis of:

- (a) the rise time  $t_r$  (the time required for the response to reach the final value for the first time) [Ogata, 2009],
- (b) the maximum percentage of overshoot  $M_p$  (the maximum peak value of the response of the VSS measured from the final value) [Ogata, 2009], and

#### (c) the settling time.

The rise time and the maximum percentage of overshoot can be calculated analytically but the same is not true for the settling time. To calculate the rise time and the maximum percentage of overshoot, we define three points A, B, and C on the phase portrait of the VSS, shown in Fig 3.12. These points are also shown in Fig.3.13, which is a plot of the time response of the VSS to the step input. Consider the time needed by the VSS to reach point A; this has been studied in section 3.2.1, and was described by Eq.(3.5). Using variables y and  $\dot{y}$  we can write it as follows:

$$t_A = \frac{1}{\omega_d} \tan^{-1} \left[ \frac{(\lambda y_0 - \dot{y}_0) \sqrt{1 - \zeta^2}}{-\zeta \dot{y}_0 - \omega_n y_0 - \lambda \left( \frac{\dot{y}_0 + \zeta \omega_n y_0}{\omega_n} \right)} \right] = \frac{1}{\omega_d} \tan^{-1} \left[ \frac{-\lambda \sqrt{1 - \zeta^2}}{\omega_n + \lambda \zeta} \right]$$
(3.43)

where  $y_0 = -1$  and  $\dot{y}_0 = 0$  are the initial conditions. The values of y and  $\dot{y}$  at A has been

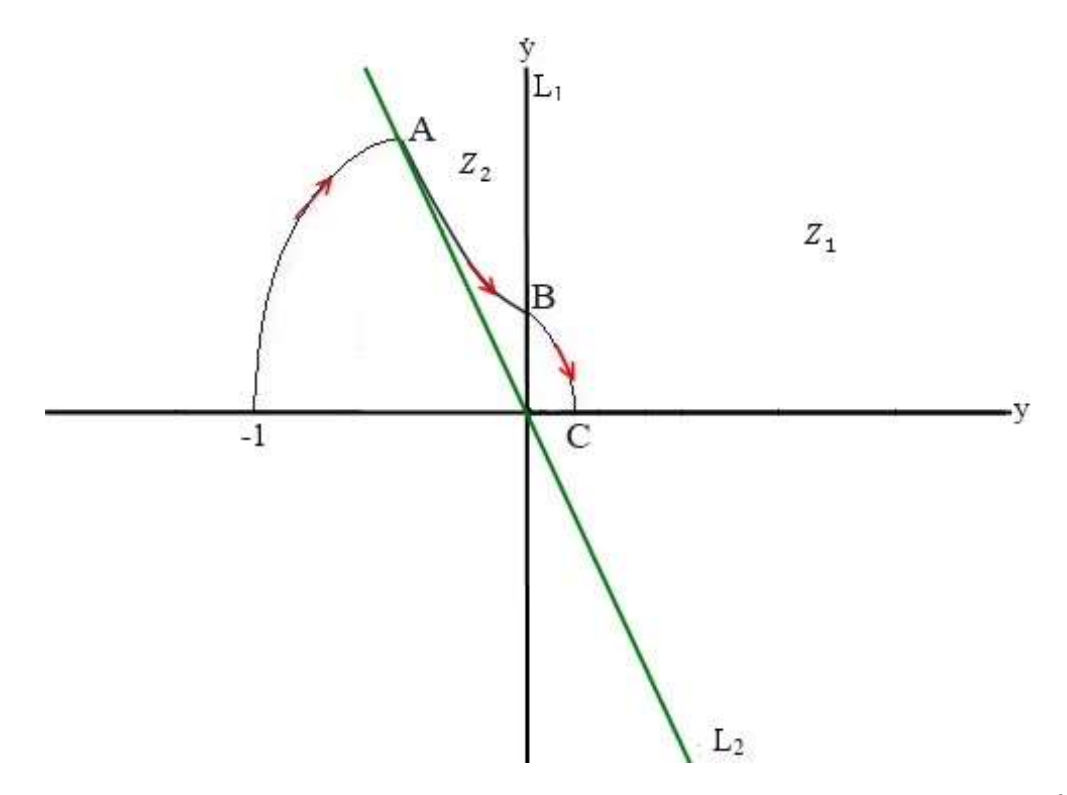


Figure 3.12. Step response in the phase plane of the Variable Structure System (VSS) for  $\lambda < \mu_1$ 

studied in section 3.2.1, and was described by Eq.(3.1), and (3.2). For convenience, it is provided below:

$$y_A = e^{-\zeta \omega_n t_A} [A \cos \omega_d t_A + B \sin \omega_d t_A]$$
 (3.44)

$$\dot{y}_A = -\zeta \omega_n e^{-\zeta \omega_n t_A} [A \cos \omega_d t_A + B \sin \omega_d t_A]$$

$$+ e^{-\zeta \omega_n t_A} [-A \omega_d \sin \omega_d t_A + B \omega_d \cos \omega_d t_A]$$
 (3.45)

where

$$\omega_d=\;\omega_n\,\sqrt{1-\zeta^2}$$
,  $A=\;-1$  ,  $B=-rac{\zeta}{\sqrt{1-\zeta^2}}$ 

The time needed for the VSS to move from point A to point B has been studied in section 3.2.1, and was described by Eq.(3.12), For convenience, it is provided below:

$$t_{AB} = \frac{1}{2\omega_n \sqrt{1+\zeta^2}} \ln \left[ \frac{\left[ \dot{y}_A + \omega_n y_A \left( \zeta - \sqrt{1+\zeta^2} \right) \right]}{\left[ \dot{y}_A + \omega_n y_A \left( \zeta + \sqrt{1+\zeta^2} \right) \right]} \right]$$
(3.46)

where  $y_A$ , and  $\dot{y}_A$  are the initial conditions and given by Eqs.(3.44) and (3.45). The values of y

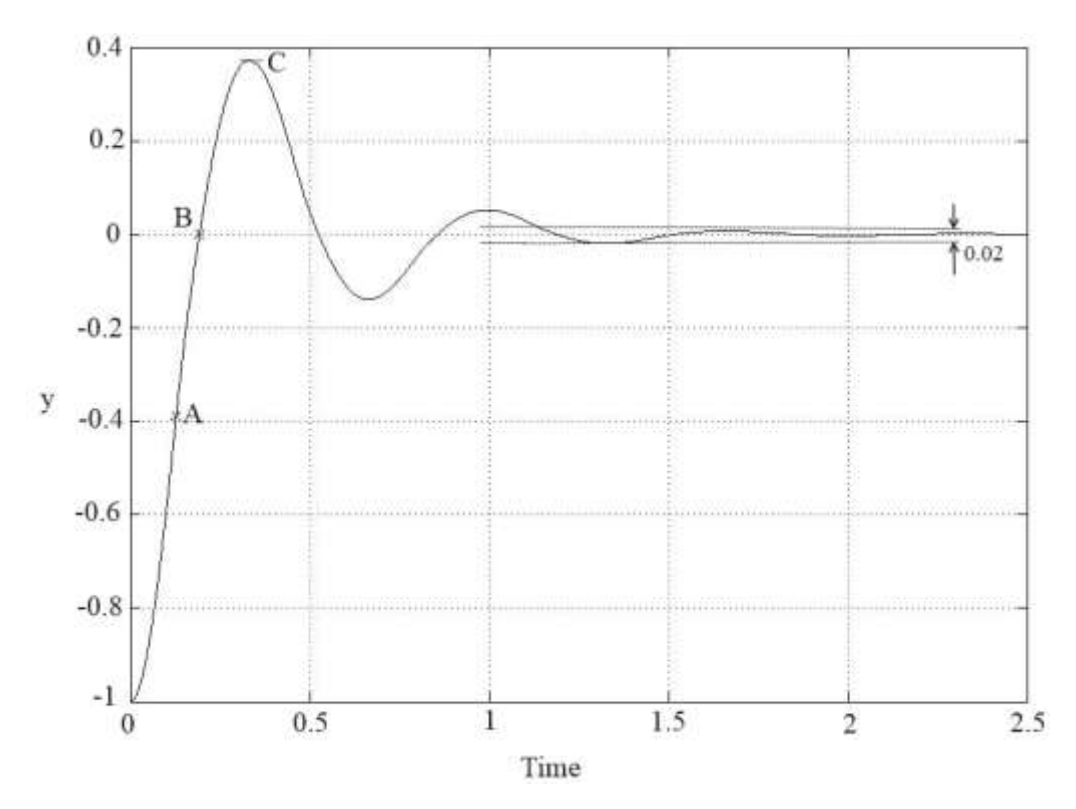


Figure 3.13. Step response of the Variable Structure System (VSS) for  $\lambda < \mu_1$ 

and  $\dot{y}$  at B has been studied in section 3.2.1, and was described by Eq.(3.4) and (3.7). For convenience, it is provided below:

$$y_B = 0 ag{3.47}$$

$$\dot{y}_{B} = \omega_{n} \left( -\zeta - \sqrt{1 + \zeta^{2}} \right) D e^{\omega_{n} t_{AB} \left( -\zeta - \sqrt{1 + \zeta^{2}} \right)}$$

$$+ \omega_{n} \left( -\zeta + \sqrt{1 + \zeta^{2}} \right) E e^{\omega_{n} t_{AB} \left( -\zeta + \sqrt{1 + \zeta^{2}} \right)}$$
(3.48)

where

$$D = y_A - \frac{\dot{y}_A + \omega_n y_A \left(\zeta + \sqrt{1 + \zeta^2}\right)}{2\omega_n \sqrt{1 + \zeta^2}}, \qquad E = \frac{\dot{y}_A + \omega_n y_A \left(\zeta + \sqrt{1 + \zeta^2}\right)}{2\omega_n \sqrt{1 + \zeta^2}}$$

To find the time needed for the VSS to move from point B to point C, we substitute Eq.(3.2) into the equation of y-axis where point C lie on this axis, namely:

$$\dot{y}=0$$

This gives:

$$-\zeta \omega_n e^{-\zeta \omega_n t} [A \cos \omega_d t + B \sin \omega_d t]$$

$$+ e^{-\zeta \omega_n t} [-A \omega_d \sin \omega_d t + B \omega_d \cos \omega_d t] = 0$$

$$\Rightarrow \tan \omega_d t = \frac{-\zeta \omega_n A + B \omega_d}{\zeta \omega_n B + \omega_d A}$$
(3.49)

Substitution of the values of A and B from Eq.(3.3) into Eq.(3.49) gives:

$$\Rightarrow \tan \omega_d t = \frac{\sqrt{1 - \zeta^2}}{\zeta}$$

$$\Rightarrow t_{BC} = \frac{1}{\omega_d} \tan^{-1} \left[ \frac{\sqrt{1 - \zeta^2}}{\zeta} \right]$$
(3.50)

Substitution of the value of  $t_{BC}$  from Eq.(3.50) into Eqs.(3.1) and (3.2) gives the values of y and  $\dot{y}$  at C, namely:

$$y_C = e^{-\zeta \omega_n t_{BC}} \left[ \frac{\dot{y}_B}{\omega_n \sqrt{1 - \zeta^2}} \sin \omega_n \sqrt{1 - \zeta^2} t_{BC} \right]$$
 (3.51)

$$\dot{y}_C = 0 \tag{3.52}$$

The rise time of the VSS can now be calculated as follows:

$$t_r = t_A + t_{AB}$$

$$= \frac{1}{2\omega_n\sqrt{1+\zeta^2}} \ln \left[ \frac{\left[ \dot{y}_A + \omega_n y_A \left( \zeta - \sqrt{1+\zeta^2} \right) \right]}{\left[ \dot{y}_A + \omega_n y_A \left( \zeta + \sqrt{1+\zeta^2} \right) \right]} \right] + \frac{1}{\omega_d} \tan^{-1} \left[ \frac{-\lambda\sqrt{1-\zeta^2}}{\omega_n + \lambda\zeta} \right]$$
(3.53)

where  $y_A$ , and  $\dot{y}_A$  are defined by Eqs.(3.44) and (3.45) respectively. The maximum percent overshoot of the VSS depend on  $t_{BC}$  and is given by:

$$M_p = e^{-\zeta \omega_n t_{BC}} \left[ \frac{\dot{y}_B}{\omega_n \sqrt{1 - \zeta^2}} \sin \omega_n \sqrt{1 - \zeta^2} t_{BC} \right] \times 100$$

$$= e^{\left(\frac{-\zeta}{\sqrt{1 - \zeta^2}} \tan^{-1} \left[\frac{\sqrt{1 - \zeta^2}}{\zeta}\right]\right)} \left[\frac{\dot{y}_B}{\omega_n}\right] \times 100$$
(3.54)

where  $\dot{y}_B$  is defined by Eq.(3.48). For proper comparison of the performance, we nondimensionalize the time using the variable  $\tau = \omega_n t$ . Concurrently, we define  $\lambda = \rho \mu_1$  where  $\rho \geq 1$  is a constant. The nondimensional rise time and the maximum percentage overshoot are given by the following equations respectively:

$$\tau_r = \omega_n t_r = \frac{1}{\sqrt{1 - \zeta^2}} \tan^{-1} \left[ \frac{\rho \left[ \zeta + \sqrt{\zeta^2 + 1} \right] \sqrt{1 - \zeta^2}}{1 - \zeta \rho \left[ \zeta + \sqrt{\zeta^2 + 1} \right]} \right]$$

$$+ \frac{1}{2\sqrt{1 + \zeta^2}} \ln \left[ \frac{\left[ \dot{y}_A + y_A \left( \zeta - \sqrt{1 + \zeta^2} \right) \right]}{\left[ \dot{y}_A + y_A \left( \zeta + \sqrt{1 + \zeta^2} \right) \right]} \right]$$
(3.55)

$$M_p = e^{\frac{-\zeta}{\sqrt{1-\zeta^2}} \tan^{-1} \frac{\sqrt{1-\zeta^2}}{\zeta}} \dot{y}_B \times 100$$
 (3.56)

where 
$$y_A = e^{-\zeta \tau_A} \left[ A \cos \sqrt{1 - \zeta^2} \tau_A + B \sin \sqrt{1 - \zeta^2} \tau_A \right]$$
 (3.57)  

$$\dot{y}_A = -\zeta e^{-\zeta \tau_A} \left[ A \cos \sqrt{1 - \zeta^2} \tau_A + B \sin \sqrt{1 - \zeta^2}_d \tau_A \right]$$

$$+ \sqrt{1 - \zeta^2} e^{-\zeta \tau_A} \left[ -A \sin \sqrt{1 - \zeta^2} \tau_A + B \cos \sqrt{1 - \zeta^2} \tau_A \right]$$

(3.58)

$$\dot{y}_B = \left(-\zeta - \sqrt{1 + \zeta^2}\right) D e^{\tau_{AB}\left(-\zeta - \sqrt{1 + \zeta^2}\right)}$$

$$+ \left(-\zeta + \sqrt{1 + \zeta^2}\right) E e^{\tau_{AB}\left(-\zeta + \sqrt{1 + \zeta^2}\right)}$$
(3.59)

$$\tau_A = \frac{1}{\sqrt{1 - \zeta^2}} \tan^{-1} \left[ \frac{\rho \left[ \zeta + \sqrt{\zeta^2 + 1} \right] \sqrt{1 - \zeta^2}}{1 - \zeta \rho \left[ \zeta + \sqrt{\zeta^2 + 1} \right]} \right]$$
(3.60)

$$\tau_{AB} = \frac{1}{2\sqrt{1+\zeta^2}} \ln \left[ \frac{\left[ \dot{y}_A + y_A \left( \zeta - \sqrt{1+\zeta^2} \right) \right]}{\left[ \dot{y}_A + y_A \left( \zeta + \sqrt{1+\zeta^2} \right) \right]} \right]$$
(3.61)

$$A = -1$$
,  $B = -\frac{\zeta}{\sqrt{1-\zeta^2}}$ 

$$D = y_A - \frac{\dot{y}_A + y_A(\zeta + \sqrt{1 + \zeta^2})}{2\sqrt{1 + \zeta^2}}, \qquad E = \frac{\dot{y}_A + y_A(\zeta + \sqrt{1 + \zeta^2})}{2\sqrt{1 + \zeta^2}}$$

The settling time for the VSS is the time needed for the VSS trajectory to enter the region  $|y| \le 0.02$ . This cannot be calculate analytically because the VSS may enter the region  $|y| \le 0.02$  in  $Z_1$  or in  $Z_2$ . Therefore, we calculate the settling time numerically.

Figure 3.14 shows a comparison of the rise times of the VSS for different values of  $\rho$  ( $\rho=1.1, \rho=1.5, \rho=2, \rho=5$ ) and the original system. It is clear that the original system has smaller rise time than the VSS. For example, for  $\zeta=0.2$ , the rise time for the original system is  $\tau_r=1.2$ , whereas it is equal to 2.5, 1.97, 1.87, and 1.81 for the VSS with  $\rho=1.1, 1.5, 2$ , and 5 respectively. It is clear that the rise time for the VSS increases for  $\zeta=0.2$  by 106.9% when  $\rho=1.1$ , by 63.9% when  $\rho=1.5$ , by 55% when  $\rho=2$ , and by 50.2% when  $\rho=5$ . As  $\rho\to\infty$  or  $\lambda\to\infty$  the rise time of the VSS tend to be equal to that of the original system.

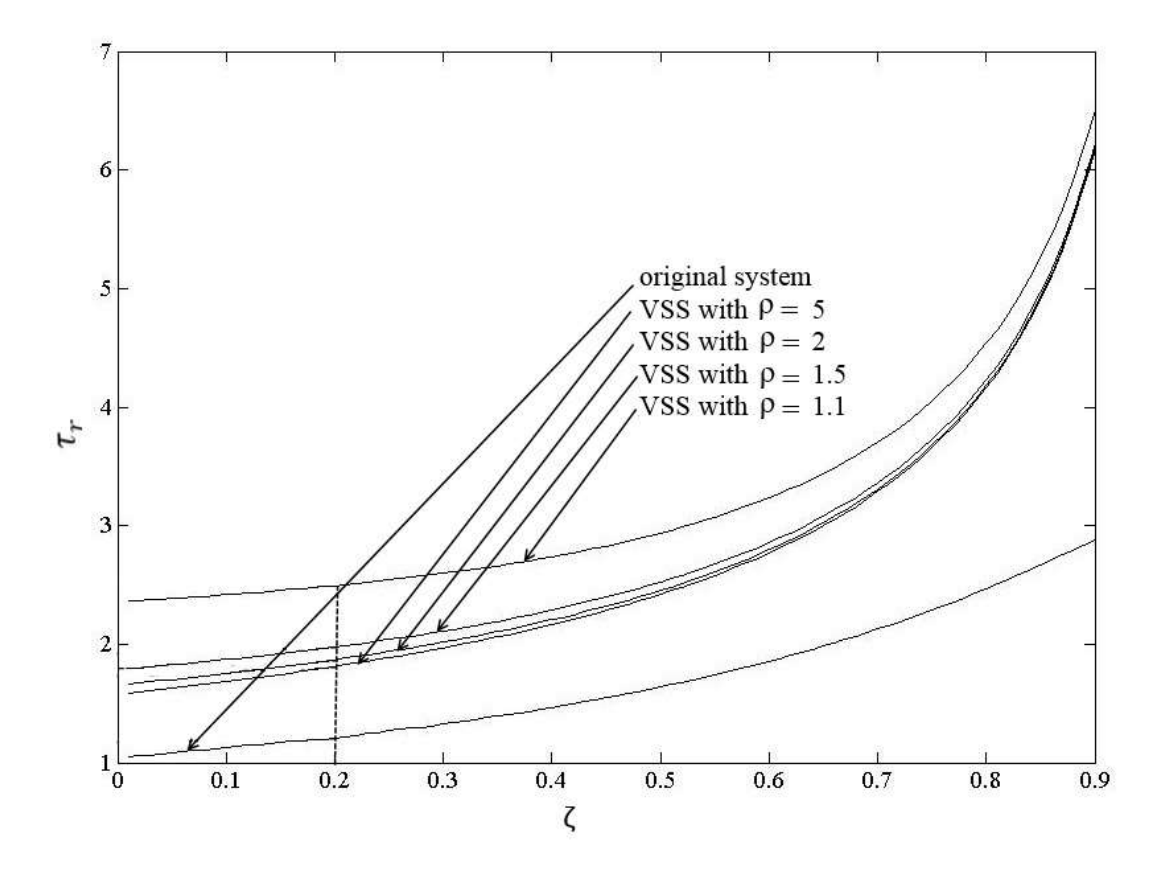


Figure 3.14. Comparison of the rise times of the VSS and original system

Figure 3.15 shows a comparison of the maximum percentage of overshoots of the VSS for different values of  $(\rho=1.1,\,\rho=1.5,\,\rho=2,\,\rho=5)$  and the original system. It is clear that the VSS has lower percentage of overshoot than the original system. For example, for  $\zeta=0.2$ , the percentage of overshoot for the original system is  $M_p=52.6\%$ , whereas it is equal to 15.67%, 34.04%, 42.43%, and 51.13% for VSS with  $\rho=1.1,1.5,2$ , and 5 respectively. It is clear that the VSS reduces the percentage of overshoot for  $\zeta=0.2$  by 70.23% when  $\rho=1.1$ , by 35.34% when  $\rho=1.5$ , by 19.4% when  $\rho=2$ , and by 2.88% when  $\rho=5$ . The best percentage of overshoot is achieved by the VSS when  $\rho\to1$  or  $\lambda\to\mu_1$ .

Figure 3.16 shows a comparison of the settling time of the VSS for different value of  $\rho$  ( $\rho$  = 1.1,  $\rho$  = 1.5,  $\rho$  = 2,  $\rho$  = 5) and the original system. It is clear that the VSS has better settling

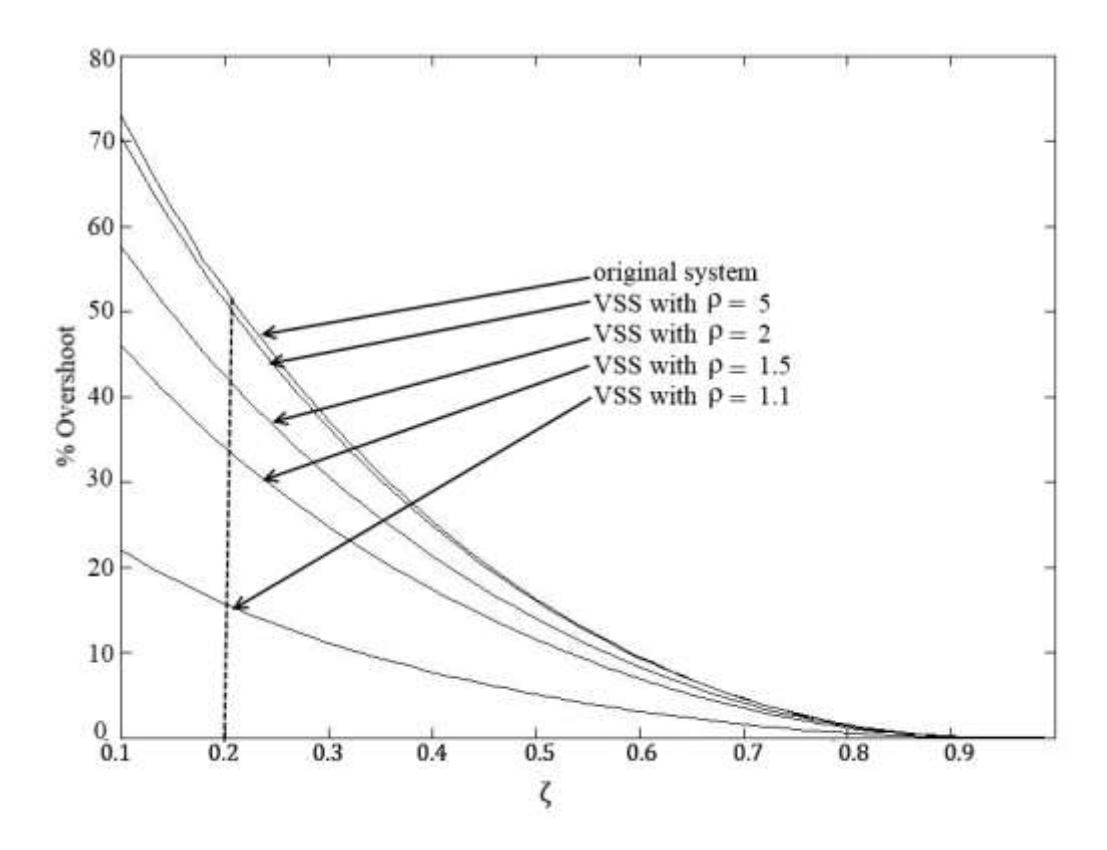


Figure 3.15. Comparison of the percentage of overshoots of the VSS and original system time than the original system. For example, for  $\zeta=0.2$ , the settling time for the original system is  $\tau_s=19.55$ , whereas it is equal to 8.43, 11.24, 14.03, and 17.08 for VSS with  $\rho=1.1$ , 1.5, 2, and 5 respectively. It is clear that the VSS reduces the settling time for  $\zeta=0.2$  by 56.97% when  $\rho=1.1$ , by 42.61% when  $\rho=1.5$ , by 28.36% when  $\rho=2$ , and by 12.83% when  $\rho=5$ . The best performance is achieved by the VSS when  $\rho\to1$  or  $\lambda\to\mu_1$ .

In this section, we investigated the performance of the VSS with switched stiffness for a step input for different values of sliding surface slope  $\lambda$ . The original system has a smaller rise time than the VSS. on the other hand, the VSS has a smaller maximum percentage of overshoot and a smaller settling time than that of the original system. Therefore, the VSS improves the performance of the mass-spring-damper system, the best performance achieved when  $\lambda \to \mu_1$ .

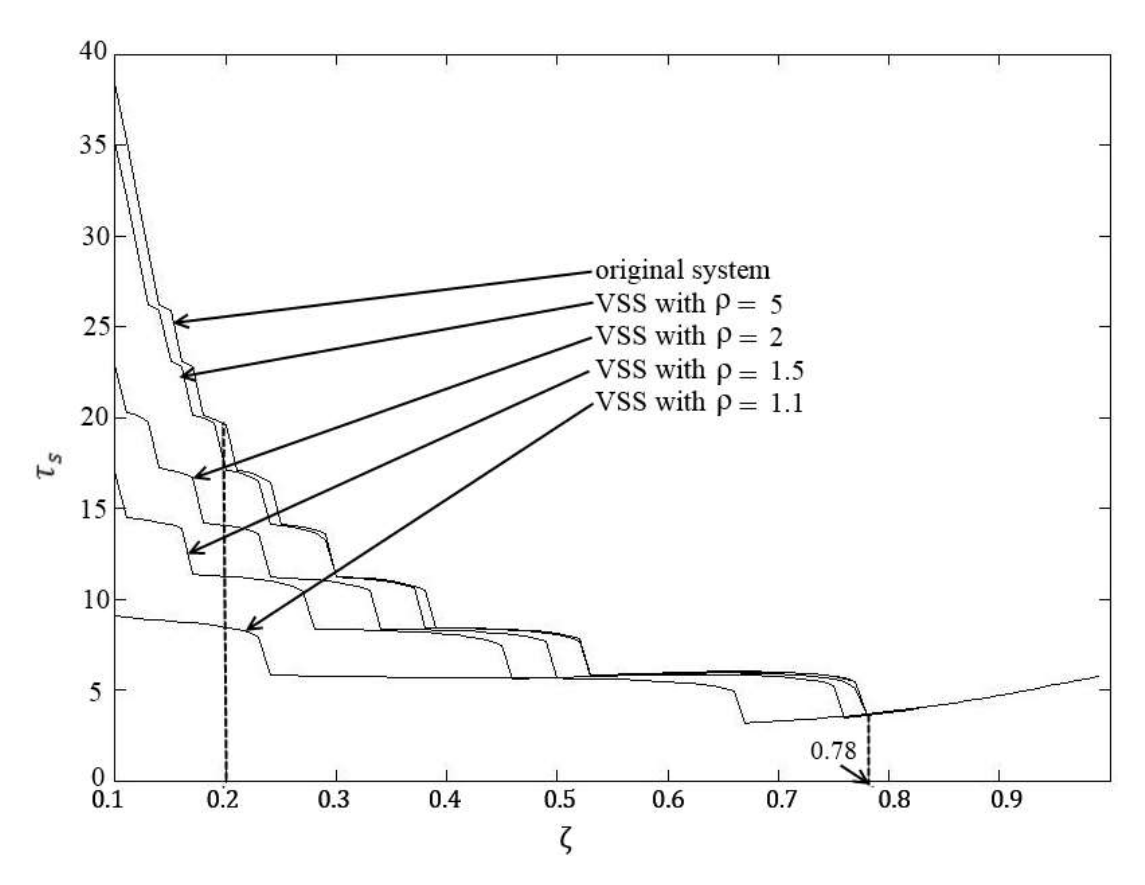


Figure 3.16. Comparison of the settling time of the VSS and original system

### 3.3.3. Performance – Speed of Convergence

In last section, we investigated the performance of the VSS for a step input. This problem was recast as an initial value problem with the initial conditions at (-1,0) in the phase plane. Since (-1,0) lies in  $Z_1$ , we now compare the performance of the VSS with switched stiffness and the original system for arbitrary initial conditions in  $Z_2$ . For initial conditions in  $Z_2$  (see Fig.3.17), the performance of the original system and the VSS can be compared by computing:

- (a) the rise time  $t_r$ ,
- (b) the maximum percentage of overshoot  $M_p$ ,
- (c) the settling time.

The rise time and the maximum percentage of overshoot can be calculated analytically but the same is not true for the settling time. To calculate the rise time and maximum percentage of overshoot, we define two points A and B on the phase portrait of the VSS, shown in Fig.3.17. These points are also shown in Fig.3.18, which is a plot of the time response of the VSS to the step input. Consider the time needed by the VSS to reach point B; this B has been studied in section 3.2.1, and was described by Eq.(3.12). The values of  $x_1$  and  $x_2$  at A has been studied in section 3.2.1, and was described by Eq.(3.6) and (3.7). To find the time needed for the VSS to move from point A to point B, we substitute Eq.(3.2) into the equation of y-axis where point B lies on this axis, namely:

$$x_2 = 0$$

This gives

$$-\zeta \omega_n e^{-\zeta \omega_n t} [A \cos \omega_d t + B \sin \omega_d t]$$

$$+ e^{-\zeta \omega_n t} [-A \omega_d \sin \omega_d t + B \omega_d \cos \omega_d t] = 0$$

$$\Rightarrow \tan \omega_d t = \frac{-\zeta \omega_n A + B \omega_d}{\zeta \omega_n B + \omega_d A}$$
(3.62)

Substitution of the values of A and B from Eq.(3.3) into Eq.(3.62) gives:

$$\Rightarrow \tan \omega_d t = \frac{\sqrt{1 - \zeta^2}}{\zeta}$$

$$\Rightarrow t_{AB} = \frac{1}{\omega_d} \tan^{-1} \left[ \frac{\sqrt{1 - \zeta^2}}{\zeta} \right]$$
(3.63)

Substitution of the value of  $t_{AB}$  into Eqs.(3.1), and (3.2) gives the values of  $x_1$  and  $x_2$  at B, namely:

$$x_{1B} = e^{-\zeta \omega_n t_{AB}} \left[ \frac{x_{2A}}{\omega_n \sqrt{1 - \zeta^2}} \sin \omega_n \sqrt{1 - \zeta^2} t_{AB} \right]$$
(3.64)

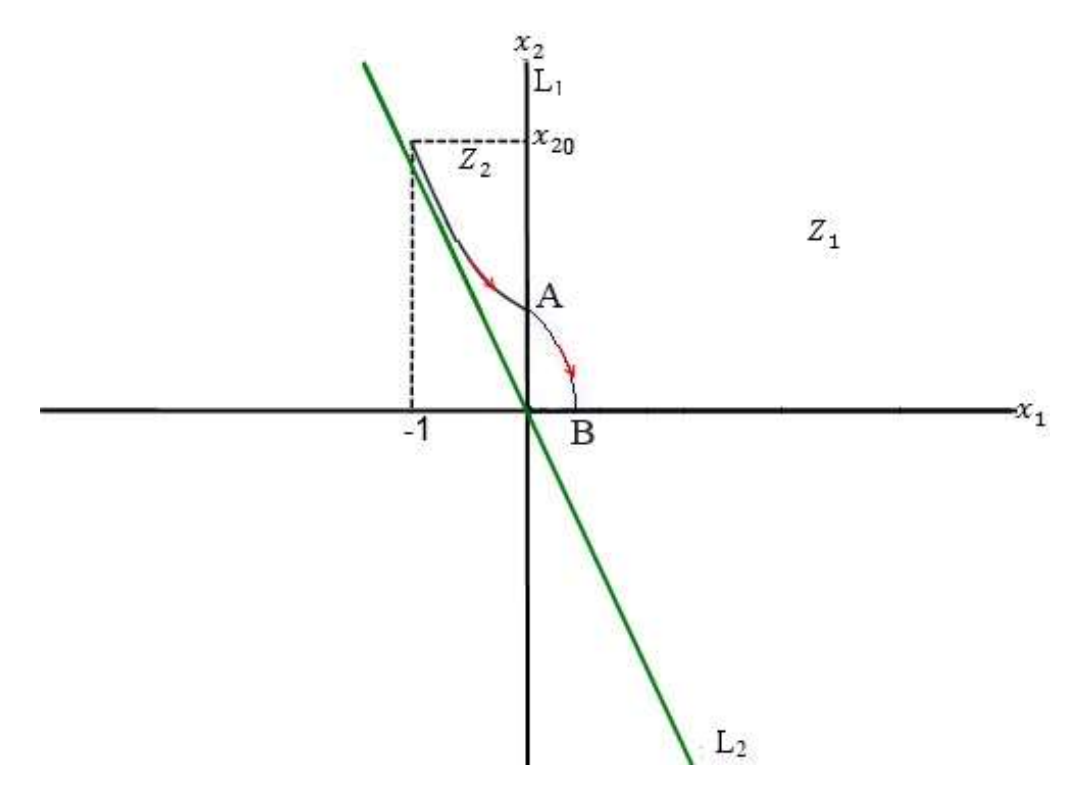


Figure 3.17. Step response in the Phase plane for the Variable Structure System (VSS) for  $~\lambda < \mu_{\,1}$ 

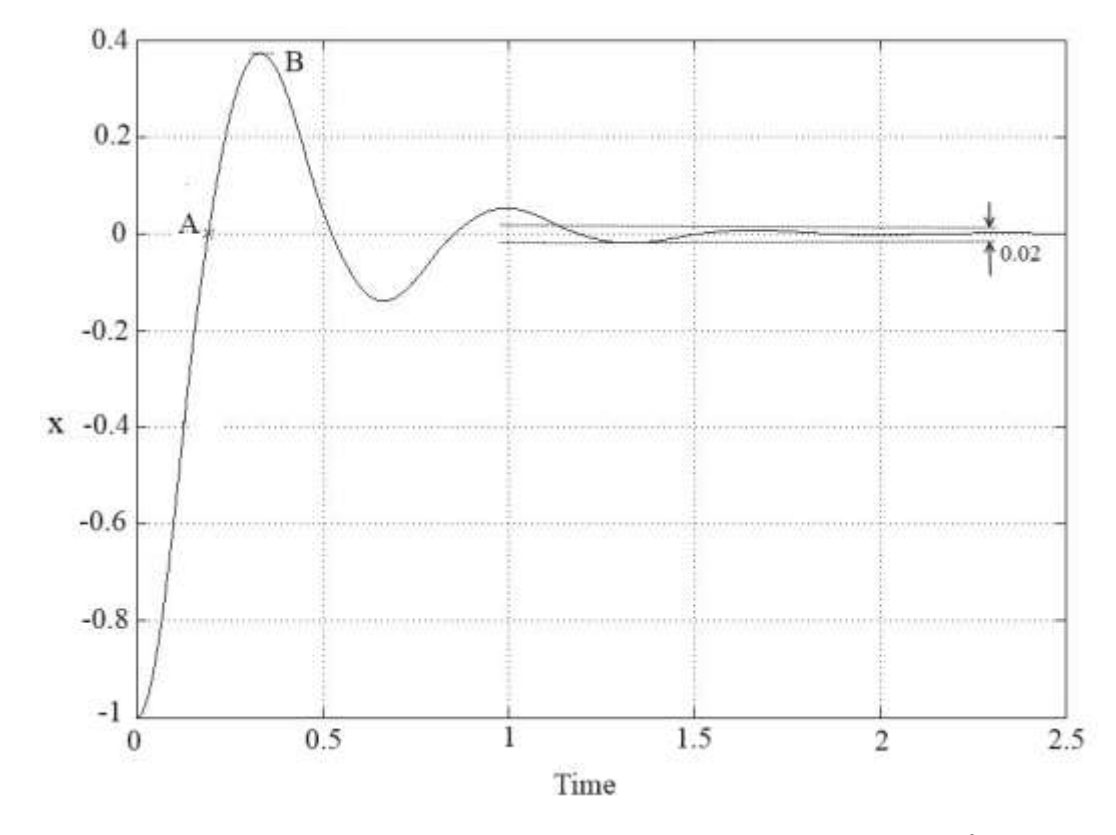


Figure 3.18. Step response for the Variable Structure System (VSS) for  $~\lambda < \mu_{\,1}$ 

$$x_{2B} = 0 (3.65)$$

The rise time of the VSS can now be calculated as follows:

$$t_r = t_A = \frac{1}{2\omega_n \sqrt{1+\zeta^2}} \ln \left[ \frac{\left[ x_{20} + \omega_n x_{10} \left( \zeta - \sqrt{1+\zeta^2} \right) \right]}{\left[ x_{20} + \omega_n x_{10} \left( \zeta + \sqrt{1+\zeta^2} \right) \right]} \right]$$
(3.66)

where  $x_{10}$ , and  $x_{20}$  are the initial conditions. The maximum percent overshoot of the VSS depend on  $t_{BC}$  and is given by:

$$M_p = e^{-\zeta \omega_n t_{AB}} \left[ \frac{x_{2A}}{\omega_n \sqrt{1 - \zeta^2}} \sin \omega_n \sqrt{1 - \zeta^2} t_{AB} \right] \times 100$$

$$= e^{\left(\frac{-\zeta}{\sqrt{1 - \zeta^2}} \tan^{-1} \left[\frac{\sqrt{1 - \zeta^2}}{\zeta}\right]\right)} \left[\frac{x_{2A}}{\omega_n}\right] \times 100$$
(3.67)

where  $x_{2A}$  is defined by Eq.(3.7). For proper comparison of the performance, we nondimensionalize the time using the variable  $\tau = \omega_n t$ . Concurrently, we define  $\lambda = \rho \mu_1$  where  $\rho \geq 1$  is a constant. The nondimensional rise time and the maximum percent overshoot are given by the following equations respectively:

$$\tau_r = \omega_n t_r = \frac{1}{2\sqrt{1+\zeta^2}} \ln \left[ \frac{\left[ x_{20} + x_{10} \left( \zeta - \sqrt{1+\zeta^2} \right) \right]}{\left[ x_{20} + x_{10} \left( \zeta + \sqrt{1+\zeta^2} \right) \right]} \right]$$
(3.68)

$$M_p = e^{\frac{-\zeta}{\sqrt{1-\zeta^2}} \tan^{-1} \frac{\sqrt{1-\zeta^2}}{\zeta}} x_{2A} \times 100$$
 (3.69)

where

$$x_{2A} = \left(-\zeta - \sqrt{1+\zeta^2}\right) D e^{\tau_A \left(-\zeta - \sqrt{1+\zeta^2}\right)} + \left(-\zeta + \sqrt{1+\zeta^2}\right) E e^{\tau_A \left(-\zeta + \sqrt{1+\zeta^2}\right)} \quad (3.70)$$

$$\tau_A = \frac{1}{2\sqrt{1+\zeta^2}} \ln \left[ \frac{\left[ x_{20} + x_{10} \left( \zeta - \sqrt{1+\zeta^2} \right) \right]}{\left[ x_{20} + x_{10} \left( \zeta + \sqrt{1+\zeta^2} \right) \right]} \right]$$
(3.71)

$$D = x_{10} - \frac{x_{20} + x_{10}(\zeta + \sqrt{1 + \zeta^2})}{2\sqrt{1 + \zeta^2}}, \qquad E = \frac{x_{20} + x_{10}(\zeta + \sqrt{1 + \zeta^2})}{2\sqrt{1 + \zeta^2}}$$

where  $x_{10}$  and  $x_{20}$  are the initials conditions in  $Z_2$ . The settling time of the VSS is the time needed for the VSS to enter the region  $|x_1| \le 0.02$ . There is no way to calculate the settling time analytically, because the VSS may enter the region  $|x_1| \le 0.02$  in  $Z_1$  or  $Z_2$ . Therefore we calculate the settling time numerically.

Figure 3.19 shows a comparison between the rise time of the VSS with  $\rho=1.1$  and the original system for initial conditions in  $Z_2$ . The initial conditions were arbitrarily chosen as  $x_{10}=-1$ , and  $x_{20}=2.88$ . It is clear that the original system has better rise time than the VSS. For example, for  $\zeta=0.2$ , the rise time for the original system is  $\tau_r=0.35$ , whereas it is equal to 0.39 for the VSS with  $\rho=1.1$ . It is clear that the VSS increases the rise time for  $\zeta=0.2$  by 9.8%. As  $\rho\to\infty$  or  $\lambda\to\infty$ , the rise time of the VSS tend to be equal to that of the original system.

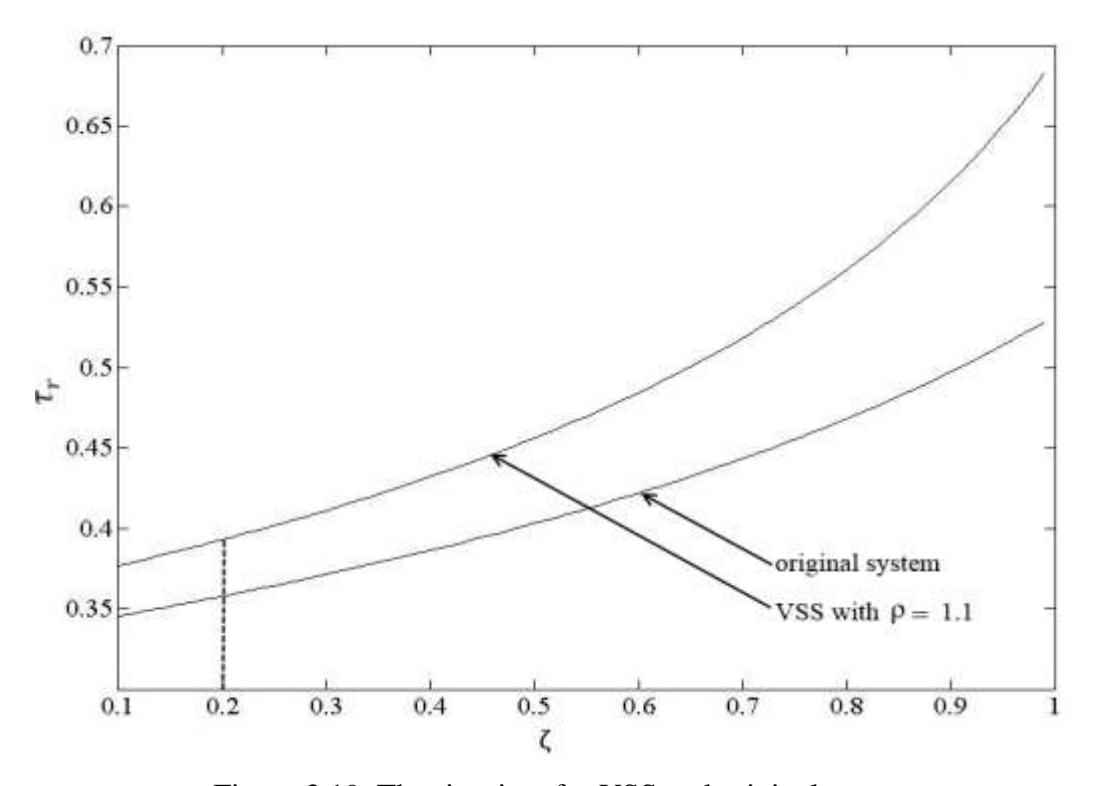


Figure 3.19. The rise time for VSS and original system

Figure 3.20 shows a comparison between the percentage of overshoot of the VSS with  $\rho=1.1$  and the original system for initial conditions in  $Z_2$ . The initial conditions were arbitrarily chosen as  $x_{10}=-1$ , and  $x_{20}=2.88$ . It is clear that the VSS has lower percentage of overshoot than the original system. For example, for  $\zeta=0.2$ , the percentage of overshoot for the original system is  $M_p=200.8\%$ , whereas it is equal to 173.2% for VSS with  $\rho=1.1$ . It is clear that the VSS reduces the percentage of overshoot for  $\zeta=0.2$  by 13.75% when  $\rho=1.1$ . The best percentage of overshoot is achieved by the VSS when  $\rho\to 1$  or  $\lambda\to\mu_1$ .

Figure 3.21 shows a comparison between the settling time of the VSS with  $\rho = 1.1$  and the original system for initial conditions in  $Z_2$ . The initial conditions were arbitrarily chosen as  $x_{10} = -1$ , and  $x_{20} = 2.88$ . It is clear that the VSS has lower settling time than the original system. For example, for  $\zeta = 0.2$ , the settling time for the original system is  $\tau_s = 24.69$ ,

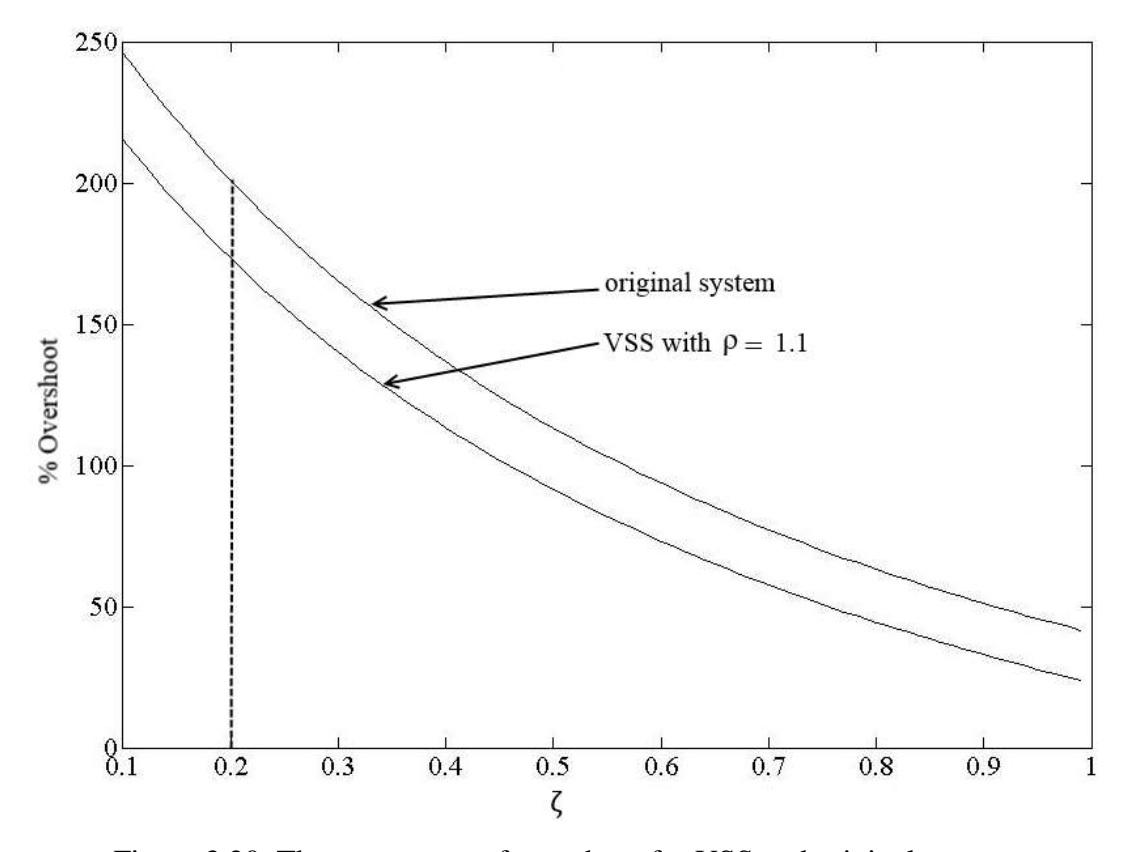


Figure 3.20. The percentage of overshoot for VSS and original system

whereas it is equal to 10.75, for the VSS. It is clear that the VSS reduces the settling time for  $\zeta=0.2$  by 56.45%. The best performance is achieved by the VSS when  $\rho\to 1$  or  $\lambda\to\mu_1$ .

In this section, we investigated the performance of the VSS with switched stiffness for arbitrary initial conditions in  $Z_2$ . The original system has a smaller rise time than the VSS. on the other hand, the VSS has a smaller maximum percentage of overshoot and a smaller settling time than that of the original system. Therefore, the VSS improves the performance of the mass-spring-damper system, with the best performance achieved when  $\lambda \to \mu_1$ .

### 3.4. Conclusion

In this Chapter, we investigated the behavior of the VSS with switched stiffness. For Case A ( $\mu_1 < \lambda < 0$ ), the VSS is asymptotically stable and no trajectories of the VSS undergo a

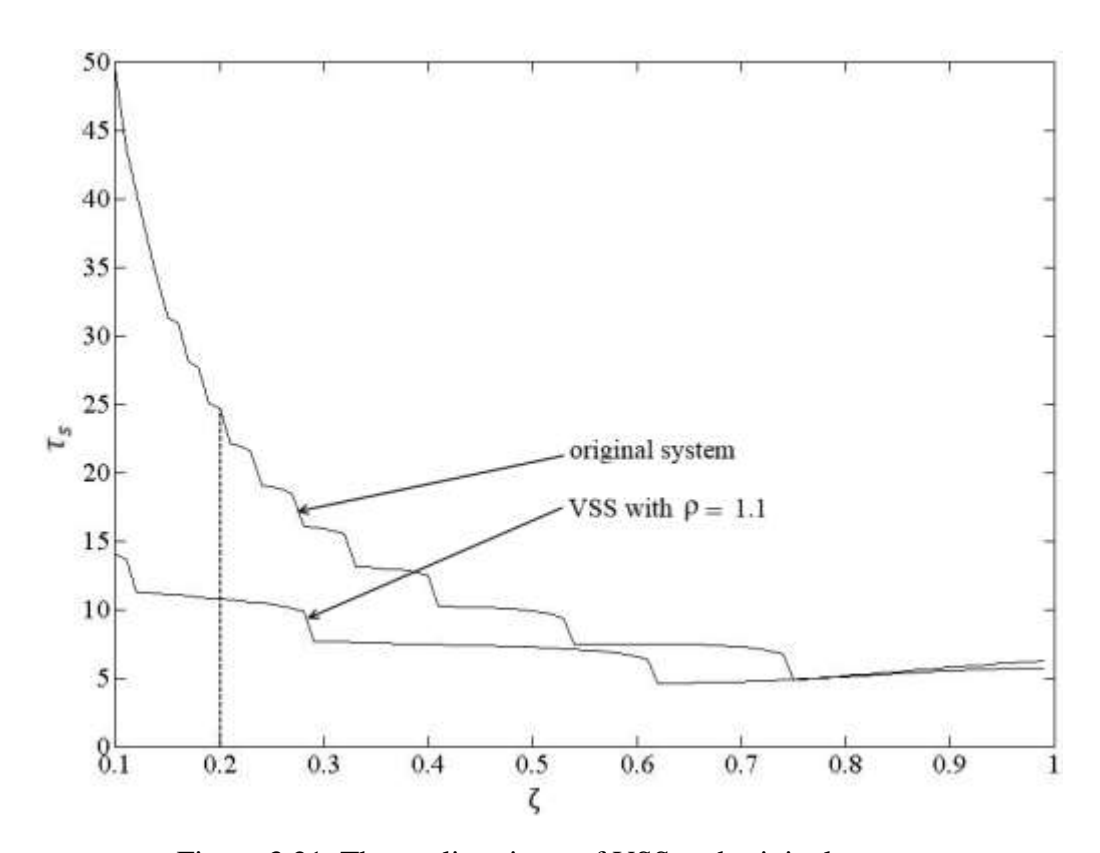


Figure 3.21. The settling times of VSS and original system

phase change of more than  $2\pi$ ; therefore, the VSS does not exhibit oscillations. Also, the VSS has a smaller settling time than that of the original system for a range of  $\zeta$  values. As we increase  $\lambda$ , the settling time of the VSS decreases for a larger range of  $\zeta$  values. Therefore, the VSS improve the performance for the mass-spring-damper system. For Case B ( $\lambda \leq \mu_1 < 0$ ), the VSS is asymptotically stable and the VSS exhibits oscillations. The original system has a smaller rise time than the VSS. on the other hand, the VSS has a smaller maximum percentage of overshoot and a smaller settling time than that of the original system. Therefore, the VSS will improve the performance of the mass-spring-damper system. For both cases, the best performance is achieved by the VSS when  $\lambda \to \mu_1$ .

# Chapter 4

# Variable Structure System with Switched

# Stiffness and Damping

#### 4.1. Phase Portrait

In this chapter, we investigate the behavior of the VSS with switched stiffness and damping. The phase portrait of the VSS is the union of the phase portrait of the first system  $(\alpha = +1)$  in the region  $(S > 0 \text{ and } x \ge 0)$  or  $(S < 0 \text{ and } x \le 0)$ , and the phase portrait of the second system  $(\alpha = -1)$  in the region  $Sx_1 < 0$ . The phase portrait of the first system  $(\alpha = +1)$  in the region  $(S > 0 \text{ and } x \ge 0)$  or  $(S < 0 \text{ and } x \le 0)$  is shown in Fig.4.1 and the phase portrait of the second system  $(\alpha = -1)$  in the region  $Sx_1 < 0$  is shown in Fig.4.2. The union of these phase portraits is shown in Fig.4.3.

For the phase portrait in Fig.4.3, the slope of the line S=0 or  $x_2=\lambda\,x_1$  is shown to be greater than the slope of the line  $x_2=\mu_1x_1$ , i.e.,  $\lambda>\mu_1$ . This is not necessarily true always, and therefore we need to additionally investigate the case where  $\lambda\leq\mu_1$ . These two cases, namely, ( $\mu_1<\lambda<0$ ), and ( $\lambda\leq\mu_1<0$ ), are investigated in sections 4.2 and 4.3.

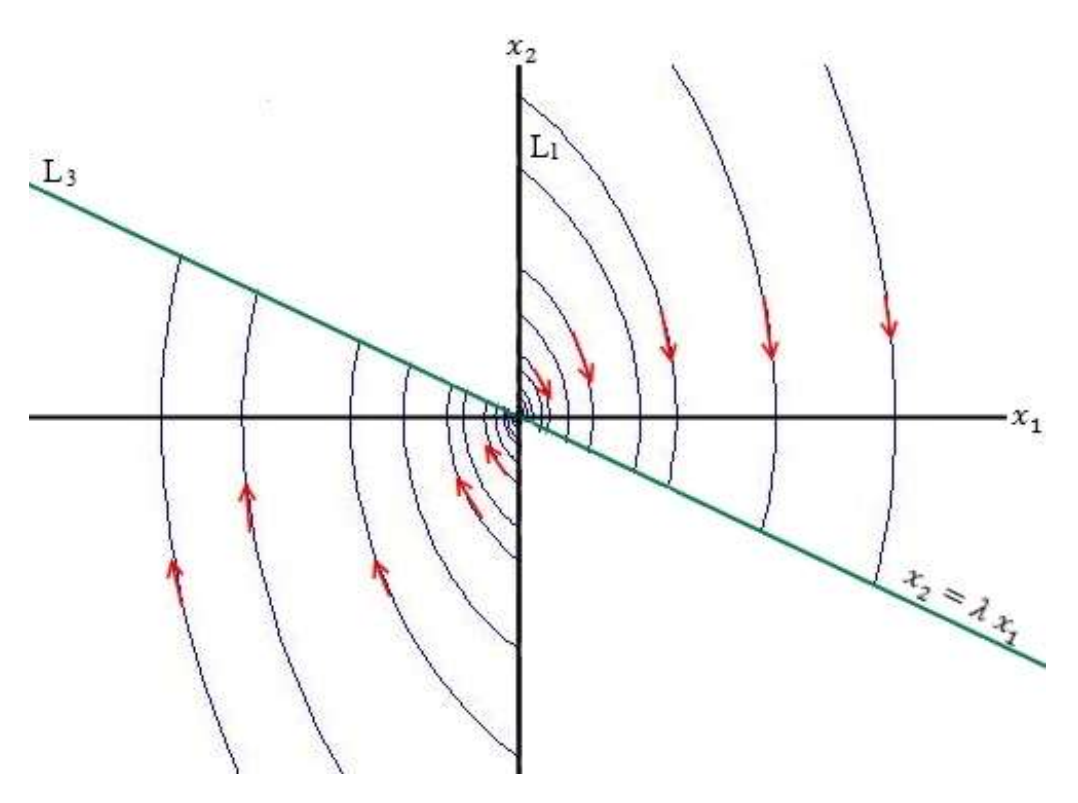


Figure 4.1. Phase portrait of the Variable Structure System (VSS) for  $\alpha = +1$ 

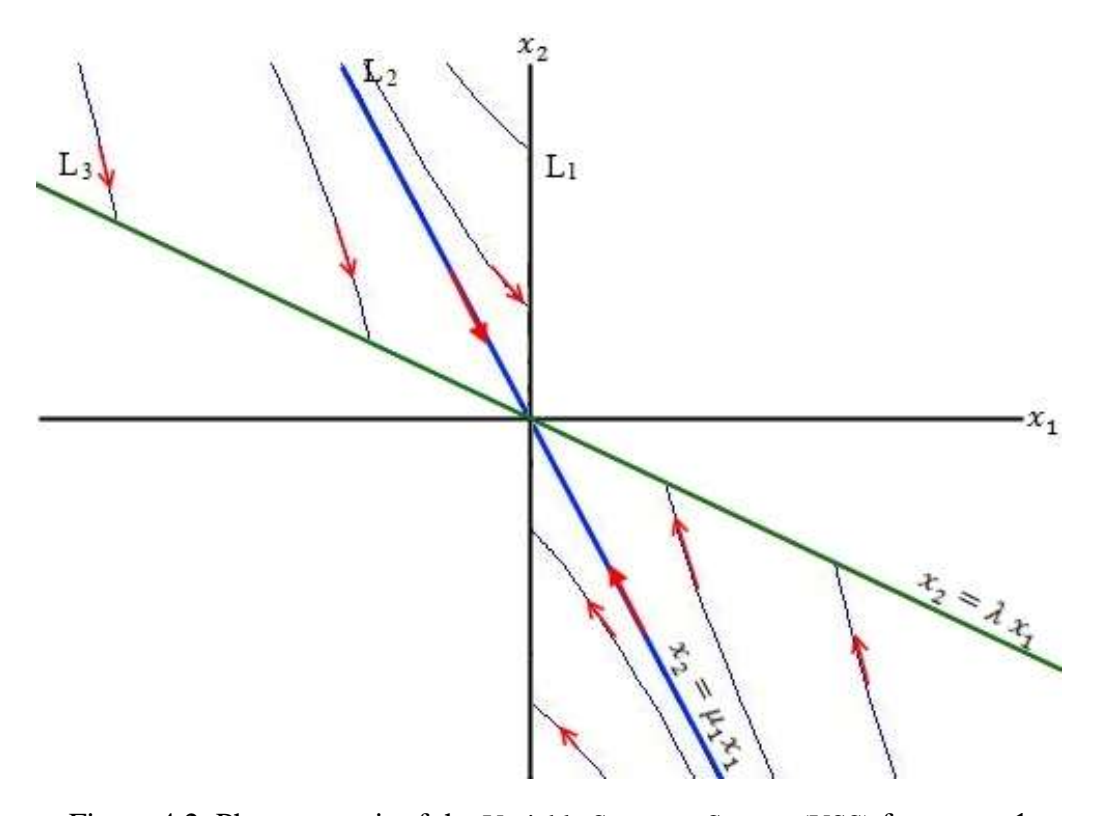


Figure 4.2. Phase portrait of the Variable Structure System (VSS) for  $\alpha = -1$ 

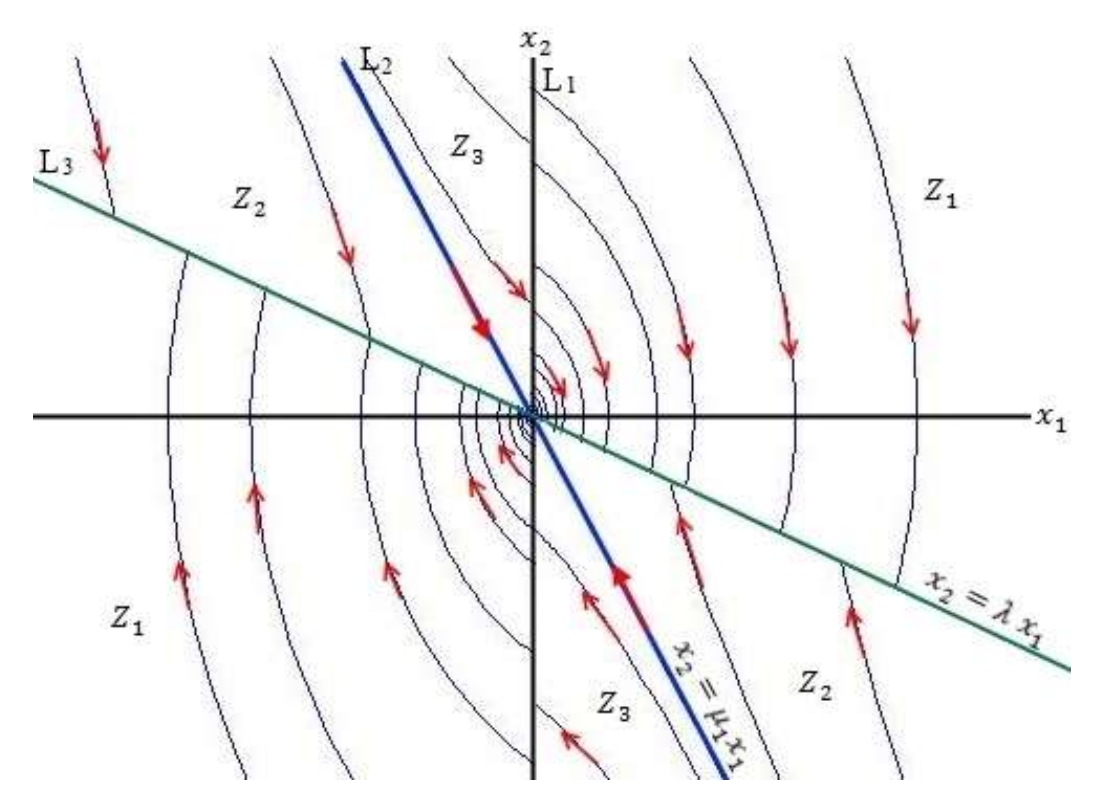


Figure 4.3. Phase portrait of the Variable Structure System (VSS) for  $\lambda > \mu_1$  is the union of the phase portrait in Figs.4.1 and 4.2

## 4.2. Case A: $\mu_1 < \lambda < 0$

## **4.2.1.** Stability

The VSS is a hybrid system that switches between an asymptotically stable system, the phase portrait of which is shown in Fig.4.1, and an unstable system whose phase portrait is shown in Fig.4.2. The union of these phase portraits is shown in Fig.4.3. To investigate the stability of the equilibrium of the VSS, the phase plane is divided into three zones, namely:

$$\begin{split} Z_1 &= \{x \in R^2 | Sx_1 > 0\} \\ Z_2 &= \{x \in R^2 | (x_2 - \mu_1 x_1)(x_2 - \lambda x_1) < 0\} \\ Z_3 &= \{x \in R^2 | x_1(x_2 - \mu_1 x_1) < 0\} \end{split}$$

The three zones are separated by the following three lines:

$$L_1: x_1 = 0$$

L<sub>2</sub>: 
$$x_2 = \mu_1 x_1$$

L<sub>3</sub>: 
$$x_2 = \lambda x_1$$

We investigate the system trajectories in these zones and on these lines next.

To study the behavior of the trajectories on  $L_1$ , we investigate the direction of the vector field on  $L_1$ . For  $x_2 > 0$  (and  $x_1 = 0$ ), we have the following equations and vector field:

$$\dot{x}_1 = x_2 > 0$$

$$\dot{x}_2 = -\frac{c}{m}x_2 < 0$$

Therefore, the trajectories enter  $Z_1$ . For  $x_2 < 0$  (and  $x_1 = 0$ ), we have the following equations and vector field:

$$\dot{x}_1 = x_2 < 0$$

$$\dot{x}_2 = -\frac{c}{m}x_2$$

Therefore, all trajectories on  $L_1$  will enter  $Z_1$ .

The line L<sub>2</sub> is the stable eigenvector of the second system where  $\alpha = -1$  – see Eqs.(2.35) and (2.37). On L<sub>2</sub> we have  $x_2 = \dot{x}_1 = \mu_1 x_1 \rightarrow x_1(t) = x_1(0) e^{\mu_1 t}$ ,  $\mu_1 < 0$ . Therefore, all trajectories on L<sub>2</sub> converge to the origin.

The boundaries of  $Z_1$  are  $L_1$  and  $L_3$ . We have already shown that trajectories on  $L_1$  enter  $Z_1$ . We now show all trajectories in  $Z_1$  reach  $L_3$  in finite time. To show this we consider the equation of motion of the system for  $\alpha = 1$ , given by Eq.(2.28):

$$\dot{x}_2 = \ddot{x}_1 = -2\zeta \omega_n \dot{x}_1 - \omega_n^2 x_1$$

The general form of the solution of this differential equation is:

$$x_1(t) = e^{-\zeta \omega_n t} [A \cos \omega_d t + B \sin \omega_d t]$$
(4.1)

(4.2)

and

$$x_2(t) = -\zeta \omega_n e^{-\zeta \omega_n t} [A \cos \omega_d t + B \sin \omega_d t]$$
$$+ e^{-\zeta \omega_n t} [-A \omega_d \sin \omega_d t + B \omega_d \cos \omega_d t]$$

where  $\omega_d = \omega_n \sqrt{1 - \zeta^2}$ 

Substitution of the initial conditions  $x_1(0) = x_{10}$ , and  $x_2(0) = x_{20}$  into Eqs.(4.1) and (4.2), where  $(x_{10}, x_{20})$  lies in  $Z_1$ , we get:

$$A = x_{10}, \qquad B = \frac{x_{20} + \zeta \omega_n x_{10}}{\omega_n \sqrt{1 - \zeta^2}} \tag{4.3}$$

To find the time when trajectory in  $Z_1$  reaches  $L_3$ , we substitute Eqs.(4.1) and (4.2) into the equation of  $L_3$ , namely:

$$x_2(t) = \lambda x_1(t)$$

This gives:

$$-\zeta \omega_n e^{-\zeta \omega_n t} [A \cos \omega_d t + B \sin \omega_d t] + \omega_d e^{-\zeta \omega_t} [-A \sin \omega_d t + B \cos \omega_d t]$$

$$= \lambda e^{-\zeta \omega_n t_1} [A \cos \omega_d t + B \sin \omega_d t]$$

$$\Rightarrow \tan \omega_d t = \frac{\lambda A - \omega_d B + \zeta \omega_n A}{-\zeta \omega_n B - \omega_d A - \lambda B}$$
(4.4)

Substitution of the values of A and B from Eq.(4.3) into Eq.(4.4) gives:

$$\tan \omega_{d} t = \frac{\lambda x_{10} - x_{20} - \zeta \omega_{n} x_{10} + \zeta \omega_{n} x_{10}}{-\frac{\zeta x_{20} + \zeta^{2} \omega_{n} x_{10}}{\sqrt{1 - \zeta^{2}}} - \frac{\omega_{n} (1 - \zeta^{2}) x_{10}}{\sqrt{1 - \zeta^{2}}} - \lambda \left(\frac{x_{20} + \zeta \omega_{n} x_{10}}{\omega_{n} \sqrt{1 - \zeta^{2}}}\right)}$$

$$\Rightarrow t = \frac{1}{\omega_{d}} \tan^{-1} \left[ \frac{(\lambda x_{10} - x_{20}) \sqrt{1 - \zeta^{2}}}{-\zeta x_{20} - \omega_{n} x_{10} - \lambda \left(\frac{x_{20} + \zeta \omega_{n} x_{10}}{\omega_{n}}\right)} \right]$$
(4.5)

This expression implies that all trajectories in  $Z_1$  reach  $L_3$  at finite time.

The boundaries of  $Z_2$  are  $L_2$  and  $L_3$ . Furthermore, the trajectories in  $Z_2$  cannot cross  $L_2$  since  $L_2$  represents a trajectory itself, and trajectories cannot cross each other. We now show all trajectories in  $Z_2$  reach  $L_3$  in finite time. To show this we consider the equation of motion of the system for  $\alpha = -1$ , given by Eq.(2.28)

$$\dot{x}_2 = \ddot{x}_1 = 2\zeta \omega_n \dot{x}_1 + \omega_n^2 x_1$$

The general form of the solution of this differential equation is

$$x_1(t) = D e^{\omega_n t(\zeta - \sqrt{1 + \zeta^2})} + E e^{\omega_n t(\zeta + \sqrt{1 + \zeta^2})}$$
(4.6)

and

$$x_2(t) = \omega_n \left( \zeta - \sqrt{1 + \zeta^2} \right) \, D \, e^{\omega_n t \left( \zeta - \sqrt{1 + \zeta^2} \right)}$$

$$+\omega_n \left(\zeta + \sqrt{1+\zeta^2}\right) E \, e^{\omega_n t (\zeta + \sqrt{1+\zeta^2})} \tag{4.7}$$

Substitution of the initial conditions  $x_1(0) = x_{10}$ , and  $x_2(0) = x_{20}$  into Eqs.(4.6) and (4.7), where  $(x_{10}, x_{20})$  lies in  $Z_2$  we get:

$$D = x_{10} - \frac{x_{20} - \omega_n x_{10} (\zeta - \sqrt{1 + \zeta^2})}{2\omega_n \sqrt{1 + \zeta^2}}, \qquad E = \frac{x_{20} - \omega_n x_{10} (\zeta - \sqrt{1 + \zeta^2})}{2\omega_n \sqrt{1 + \zeta^2}}$$
(4.8)

To find the time when trajectory in  $Z_2$  reaches  $L_3$ , we substitute Eqs.(4.6), and (4.7) into the equation of  $L_3$ , namely:

$$x_2(t) = \lambda x_1(t)$$

This gives:

$$\omega_{n}\left(\zeta - \sqrt{1 + \zeta^{2}}\right) D e^{\omega_{n}t\left(\zeta - \sqrt{1 + \zeta^{2}}\right)} + \omega_{n}\left(\zeta + \sqrt{1 + \zeta^{2}}\right) E e^{\omega_{n}t\left(\zeta + \sqrt{1 + \zeta^{2}}\right)}$$

$$= \lambda \left(D e^{\omega_{n}t\left(\zeta - \sqrt{1 + \zeta^{2}}\right)} + E e^{\omega_{n}t\left(\zeta + \sqrt{1 + \zeta^{2}}\right)}\right)$$

$$e^{\omega_{n}t(2\sqrt{1 + \zeta^{2}})} = \frac{D\left[\lambda - \omega_{n}\left(\zeta - \sqrt{1 + \zeta^{2}}\right)\right]}{E\left[\omega_{n}\left(\zeta + \sqrt{1 + \zeta^{2}}\right) - \lambda\right]}$$

$$(4.9)$$

Substitution of the values of D and E from Eq.(4.8) into Eq.(4.9) gives:

$$e^{\omega_n t (2\sqrt{1+\zeta^2})} = \frac{Q_1}{Q_2}$$

$$\Rightarrow t = \frac{1}{2\omega_n \sqrt{1+\zeta^2}} \ln \left[ \frac{Q_1}{Q_2} \right]$$
(4.10)

where  $Q_1$  and  $Q_2$ , which necessarily have the same sign, are:

$$Q_{1} = -\left(x_{20} - \omega_{n}x_{10}\left(\zeta + \sqrt{1 + \zeta^{2}}\right)\right)\left[\lambda - \omega_{n}\left(\zeta - \sqrt{1 + \zeta^{2}}\right)\right]$$

$$Q_{2} = \left(x_{20} - \omega_{n}x_{10}\left(\zeta - \sqrt{1 + \zeta^{2}}\right)\right)\left[\omega_{n}\left(\zeta + \sqrt{1 + \zeta^{2}}\right) - \lambda\right]$$

This expression implies that all trajectories in  $\mathbb{Z}_2$  reach  $\mathbb{L}_3$  at finite time.

The line L<sub>3</sub> is a sliding surface since all trajectories in  $Z_1$  and  $Z_2$  approach L<sub>3</sub> – see Fig.4.3. On L<sub>3</sub> we have  $x_2 = \dot{x}_1 = \lambda x_1 \rightarrow x_1(t) = x_1(0) e^{\lambda t}$ . Therefore, all trajectories on L<sub>3</sub> converge to the origin.

The boundaries of  $Z_3$  are  $L_1$  and  $L_2$ . Furthermore, the trajectories in  $Z_3$  cannot cross  $L_2$  since  $L_2$  represent a trajectory itself and trajectories cannot cross each other. Moreover, the trajectories on  $L_1$  enter  $Z_1$ . We now show all trajectories in  $Z_3$  reach  $L_1$  in finite time. The general form of the solution of the differential equation is described by Eqs.(4.6), and (4.7). To find the time when trajectory in  $Z_3$  reaches  $L_1$ , we substitute Eq. (4.6) into the equation of  $L_1$ , namely:

$$x_1 = 0$$

This gives:

$$D e^{\omega_n t(\zeta - \sqrt{1 + \zeta^2})} + E e^{\omega_n t(\zeta + \sqrt{1 + \zeta^2})} = 0$$

$$e^{\omega_n t(2\sqrt{1 + \zeta^2})} = -\frac{D}{F}$$
(4.11)

Substitution of the values of D and E from Eq.(4.8) into Eq.(4.11) gives:

$$e^{\omega_n t(2\sqrt{1+\zeta^2})} = \frac{Q_3}{Q_4}$$

$$\Rightarrow t = \frac{1}{2\omega_n \sqrt{1+\zeta^2}} \ln\left[\frac{Q_3}{Q_4}\right]$$
(4.12)

where  $Q_3$  and  $Q_4$ , which necessarily have the same sign, are:

$$Q_3 = [x_{20} - \omega_n x_{10} \left( \zeta + \sqrt{1 + \zeta^2} \right)]$$

$$Q_4 = [x_{20} - \omega_n x_{10} \left( \zeta - \sqrt{1 + \zeta^2} \right)]$$

This expression implies that the trajectories in  $Z_3$  reach  $L_1$  at finite time.

The VSS is a hybrid system that switches between an asymptotically stable system and unstable system. However, from the above discussion it is clear that the origin of the VSS is asymptotically stable. The trajectories of the VSS converge to the origin through  $L_2$  or  $L_3$  – see Fig.4.4.

### **4.2.2.** Performance – Response to Step Input

To investigate the performance of the VSS, we will study the response of the VSS to a step input and compare its performance with that of the original system for the same step input.

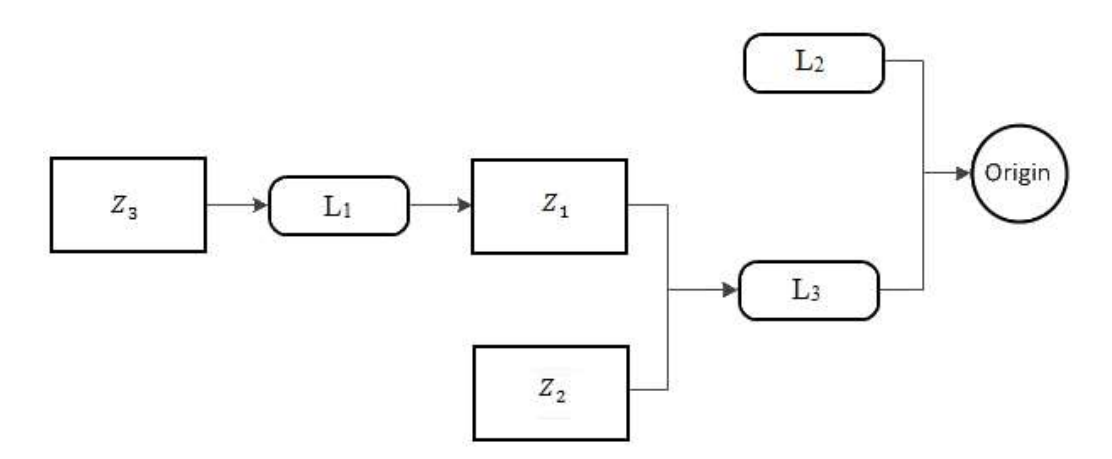


Figure 4.4. Convergence of VSS trajectories to the origin for  $\zeta < 1$  and  $\mu_1 < \lambda < 0$ 

For the original system, the response to a step input has been studied in section 3.2.1, and was described in Eq.(3.14). For convenience, it is provided below:

$$\ddot{y} = -\frac{c}{m}\dot{y} - \frac{k}{m}y, \quad y(0) = -1, \quad \dot{y}(0) = 0$$
 (4.13)

To obtain the same VSS as in Eqs.(2.21) and (2.25), we redefine F in Eq.(2.24) as follows:

$$F = k + \begin{cases} 0 & \text{if } (S > 0 \text{ and } x \ge 1) \text{ or } (S < 0 \text{ and } x \le 1) \\ 2k(x-1) + 2c\dot{x} & \text{if } S(x-1) < 0 \end{cases}$$
(4.14)

Substitution of the values of Eq.(4.14) into Eq.(2.23) and change of variables y = (x - 1) and  $\dot{y} = \dot{x}$ , we get:

$$\ddot{y} = -\alpha \frac{c}{m} \dot{y} - \alpha \frac{k}{m} y, \quad y(0) = -1, \quad \dot{y}(0) = 0$$
 (4.15)

where  $\alpha = \begin{cases} +1 & \text{if } (S > 0 \text{ and } y \ge 0) \text{ or } (S < 0 \text{ and } y \le 0) \\ -1 & \text{if } Sy < 0 \end{cases}$ 

Note that Eqs.(4.13) and (4.15) are very similar and have the same initial conditions. Also, note that Eq.(4.15) is identical to Eq.(2.25); therefore, the analysis presented in the section 4.2.1 is applicable.

The phase portrait of the VSS in Eq.(4.15) has already been studied in section 4.2.1. From this study we know that no trajectories of the system will undergo a phase change of more than  $2\pi$ , and therefore, the VSS will not exhibit oscillations for a step input. Consequently, the rise time and percentage overshoot of the system are not relevant. In the absence of oscillations, we investigate the performance of the VSS using the metric of settling time. To this end, we first consider the time needed by the VSS to reach the sliding surface L<sub>3</sub>, given by Eq.(4.5), which is now rewritten using variables y and  $\dot{y}$ . If  $y_0$  and  $\dot{y}_0$  donate the values of y(0) and  $\dot{y}(0)$  respectively, the time needed to reach L<sub>3</sub> is given by:

$$t = \frac{1}{\omega_d} \tan^{-1} \left[ \frac{(\lambda y_0 - \dot{y}_0) \sqrt{1 - \zeta^2}}{-\zeta \dot{y}_0 - \omega_n y_0 - \lambda \left( \frac{\dot{y}_0 + \zeta \omega_n y_0}{\omega_n} \right)} \right]$$

Substitution of the values of  $y_0 = -1$  and  $\dot{y}_0 = 0$  , gives

$$t_1 = \frac{1}{\omega_d} \tan^{-1} \left[ \frac{-\lambda \sqrt{1 - \zeta^2}}{\omega_n + \lambda \zeta} \right]$$
 (4.16)

we substitute the values of  $y_0 = -1$ ,  $\dot{y}_0 = 0$ , and  $t_1$  described by Eq.(4.16) into Eqs.(4.1) and (4.2), with variables  $x_1$  and  $x_2$  replaced by y and  $\dot{y}$  respectively. This gives the values of y and  $\dot{y}$  when the VSS reaches the sliding surface L<sub>3</sub>:

$$y_s = e^{-\zeta \omega_n t_1} \left[ -\cos \omega_d t_1 - \frac{\zeta}{\sqrt{1 - \zeta^2}} \sin \omega_d t_1 \right]$$
 (4.17)

$$\dot{y}_s = -\zeta \omega_n e^{-\zeta \omega_n t_1} \left[ -\cos \omega_d t_1 - \frac{\zeta}{\sqrt{1 - \zeta^2}} \sin \omega_d t_1 \right]$$

$$+e^{-\zeta\omega_n t_1} \left[ \omega_d \sin \omega_d t_1 - \frac{\zeta}{\sqrt{1-\zeta^2}} \omega_d \cos \omega_d t_1 \right]$$
 (4.18)

where

$$\omega_d = \omega_n \sqrt{1 - \zeta^2}$$

To find the time needed for the trajectories on  $L_3$  to enter the region  $|y| \le 0.02$ , we consider the dynamics on  $L_3$ , namely:

$$y(t) = y_s e^{\lambda t}, \qquad \lambda < 0 \tag{4.19}$$

Substitution of y(t) = -0.02 yields:

$$e^{\lambda t} = \frac{-0.02}{y_s} \quad \Rightarrow t_2 = \frac{1}{\lambda} \ln \left( \frac{-0.02}{y_s} \right) \tag{4.20}$$

The settling time of the VSS is given by:

$$t_s = t_1 + t_2 = \frac{1}{\omega_d} \tan^{-1} \left[ \frac{-\lambda \sqrt{1 - \zeta^2}}{\omega_n + \lambda \zeta} \right] + \frac{1}{\lambda} \ln \left( \frac{-0.02}{y_s} \right)$$
(4.21)

where  $y_s$  is defined by Eq.(4.17). For proper comparison of the performance, we nondimensionalize time using the variable  $\tau = \omega_n t$ . Concurrently, we define  $\lambda = \kappa \mu_1$  where  $\kappa$ ,  $0 < \kappa < 1$ , is a constant. The nondimensional settling time is now given by the following equation:

$$\tau_S = \tau_1 + \tau_2 \tag{4.22}$$

where

$$\tau_1 = \frac{1}{\sqrt{1 - \zeta^2}} \tan^{-1} \frac{\kappa \left[ -\zeta + \sqrt{\zeta^2 + 1} \right] \sqrt{1 - \zeta^2}}{1 + \zeta \kappa \left[ \zeta - \sqrt{\zeta^2 + 1} \right]}$$
(4.23)

$$\tau_2 = \frac{1}{\kappa \left[\zeta - \sqrt{\zeta^2 + 1}\right]} \ln\left(\frac{-0.02}{y_s}\right) \tag{4.24}$$

and where

$$y_{s} = e^{-\zeta \tau_{1}} \left[ -\cos \tau_{1} \sqrt{1 - \zeta^{2}} - \frac{\zeta}{\sqrt{1 - \zeta^{2}}} \sin \tau_{1} \sqrt{1 - \zeta^{2}} \right]$$
 (4.25)

Figure 4.5 shows a comparison of the settling time of the VSS for different value of  $\kappa$  ( $\kappa=0.3, \kappa=0.5, \kappa=0.7, \kappa=0.9$ ) and the original system. The settling time for the original system shows several discontinuities in the settling time. For  $\kappa=0.3$ , the VSS has better performance than that of the original system only when  $\zeta<0.24$ . For  $\kappa=0.5$ , the performance is better for a larger range of  $\zeta$ , namely  $\zeta<0.34$ . As we increase  $\kappa$ , the performance is better for a larger range of  $\zeta$ : for  $\kappa=0.7$  and 0.9 the performance is better for  $\zeta<0.39$  and  $\zeta<0.52$  respectively. The settling time of the original system can be reduced by increasing the value of  $\zeta$  but for most  $\zeta$  values, a VSS can be found ( $\kappa$  can be chosen) that has better performance in terms of the settling time. For example, for  $\zeta=0.2$ , the settling time for the original system is  $\tau_s=19.55$ , whereas it is equal to 16.03, 9.75, 7.11, and 5.67 for VSS with  $\kappa=0.3, 0.5, 0.7$ , and 0.9 respectively. It is clear that the VSS improves the settling time for  $\zeta=0.2$  by 18.18% when  $\kappa=0.3$ , by 50,2% when

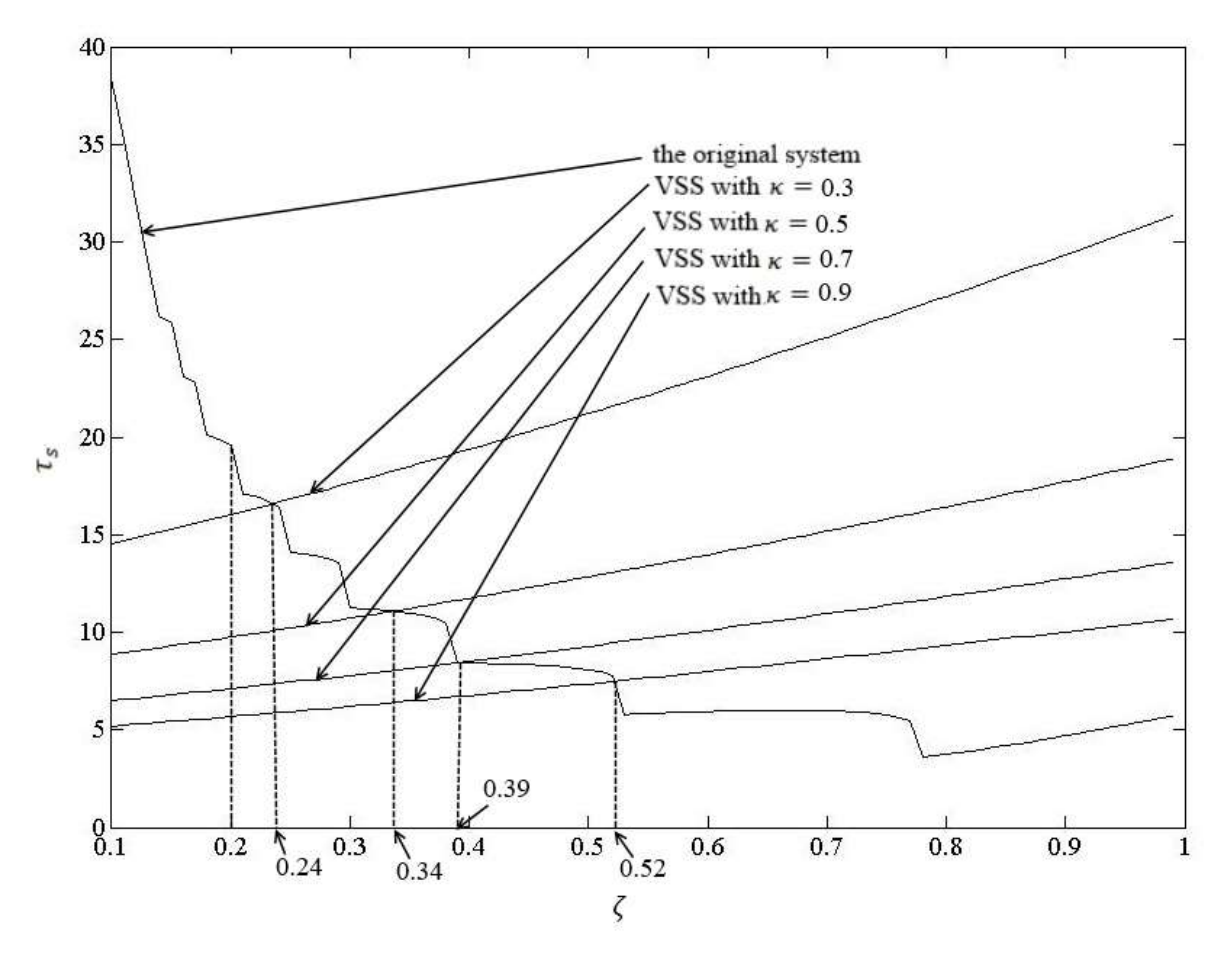


Figure 4.5. Comparison of the settling times of the VSS and the original system.

 $\kappa=0.5$ , by 63.71% when  $\kappa=0.7$ , and by 71.04% when  $\kappa=0.9$ . The best performance is achieved by the VSS when  $\kappa\to 1$  or  $\lambda\to \mu_1$ . However, the maximum value of  $\kappa$  can be chosen is less than unity (0.95, for example) because of the finite time needed to switching of  $\alpha$  from +1 to -1. If  $\kappa\approx 1$  the area of  $Z_2$  in Fig.4.3 is almost zero and there will be no switching in this zone and the switching will be in  $Z_3$ .

In this section, we investigated the performance of the VSS with switched stiffness and damping for a step input for different values of  $\lambda$ . The VSS has a smaller settling time than that of the original mass-spring-damper system for a range of  $\zeta$  values. As we increase

 $\lambda$ , the settling time of the VSS is smaller for a larger range of  $\zeta$  values, and the best performance achieved when  $\lambda \rightarrow \mu_1$ .

#### **4.2.3.** Performance – Speed of Convergence

In last section, we investigated the performance of the VSS for a step input. This problem was recast as an initial value problem with the initial conditions at (-1,0) in the phase plane. Since (-1,0) lies in  $Z_1$ , we now compare the performance of the VSS with switched stiffness and the original system for arbitrary initial conditions in Z2 and Z3. For an initial conditions in  $Z_2$  (see Fig.4.3), the time needed by the VSS to reaches the sliding surface  $L_3$  ( $x_2 = \lambda x_1$ ) has been studied in section 4.2.1, and was described by Eq.(4.10). The values of  $x_1$  and  $x_2$  when the VSS reaches the sliding surface L<sub>3</sub> has been studied in section 4.2.1, and was described by Eq.(4.6), and (4.7). The time needed for the trajectories on L<sub>3</sub> to enter the region  $|x_1| \le 0.02$  has been studied in section 4.2.1, and was described by Eq.(4.20). Using these relations, the settling time of the VSS can be shown to be:

$$\tau_s = \tau_1 + \tau_2 \tag{4.26}$$

where 
$$au_1 = \omega_n t_1 = \frac{1}{2\sqrt{1-\zeta^2}}$$

$$\ln \left[ \frac{\left[ -x_{20} + x_{10} \left( \zeta + \sqrt{1 + \zeta^2} \right) \right] \left[ \kappa \left( \zeta - \sqrt{1 + \zeta^2} \right) - \left( \zeta - \sqrt{1 + \zeta^2} \right) \right]}{\left[ x_{20} - x_{10} \left( \zeta - \sqrt{1 + \zeta^2} \right) \right] \left[ \left( \zeta + \sqrt{1 + \zeta^2} \right) - \kappa \left( \zeta - \sqrt{1 + \zeta^2} \right) \right]} \right]$$
(4.27)

$$\tau_2 = \omega_n t_2 = \frac{-1}{\left[\zeta + \sqrt{\zeta^2 + 1}\right]} \ln\left(\frac{-0.02}{x_{1s}}\right)$$
 (4.28)

where 
$$x_{1s} = D e^{\tau_1(\zeta - \sqrt{1 + \zeta^2})} + E e^{\tau_1(\zeta + \sqrt{1 + \zeta^2})}$$
 (4.29)

and 
$$D = x_{10} - \frac{x_{20} - \omega_n x_{10} (\zeta - \sqrt{1 + \zeta^2})}{2\omega_n \sqrt{1 + \zeta^2}}, \quad E = \frac{x_{20} - \omega_n x_{10} (\zeta - \sqrt{1 + \zeta^2})}{2\omega_n \sqrt{1 + \zeta^2}}$$

where  $x_{10}$  and  $x_{20}$  are the initials conditions in  $Z_2$ . Figure 4.6 shows a comparison of the settling time of the VSS for different value of  $\kappa$  ( $\kappa=0.3, \kappa=0.5, \kappa=0.9$ ) and the original system for initial conditions in  $Z_2$ . The initial conditions were arbitrarily chosen as  $x_{10}=-1$ , and  $x_{20}=-0.95~\mu_1$ . For  $\kappa=0.3$ , the VSS has better performance than that of the original system only when  $\zeta<0.25$ . For  $\kappa=0.5$ , the performance is better for a larger range of  $\zeta$ , namely  $\zeta<0.36$ . As we increase  $\kappa$ , the performance is better for a larger range of  $\zeta$ : for  $\kappa=0.9$ , the performance is better for  $\zeta<0.54$ . The settling time of the original system can be reduced by increasing the value of  $\zeta$  but for most  $\zeta$  values, a VSS can be found ( $\kappa$  can be chosen) that has better performance in terms of the settling time. For example, for  $\zeta=0.2$ , the settling time for the original system is  $\tau_s=19.31$ , whereas it is equal to 13.8, 8.81, and 5.29 for VSS

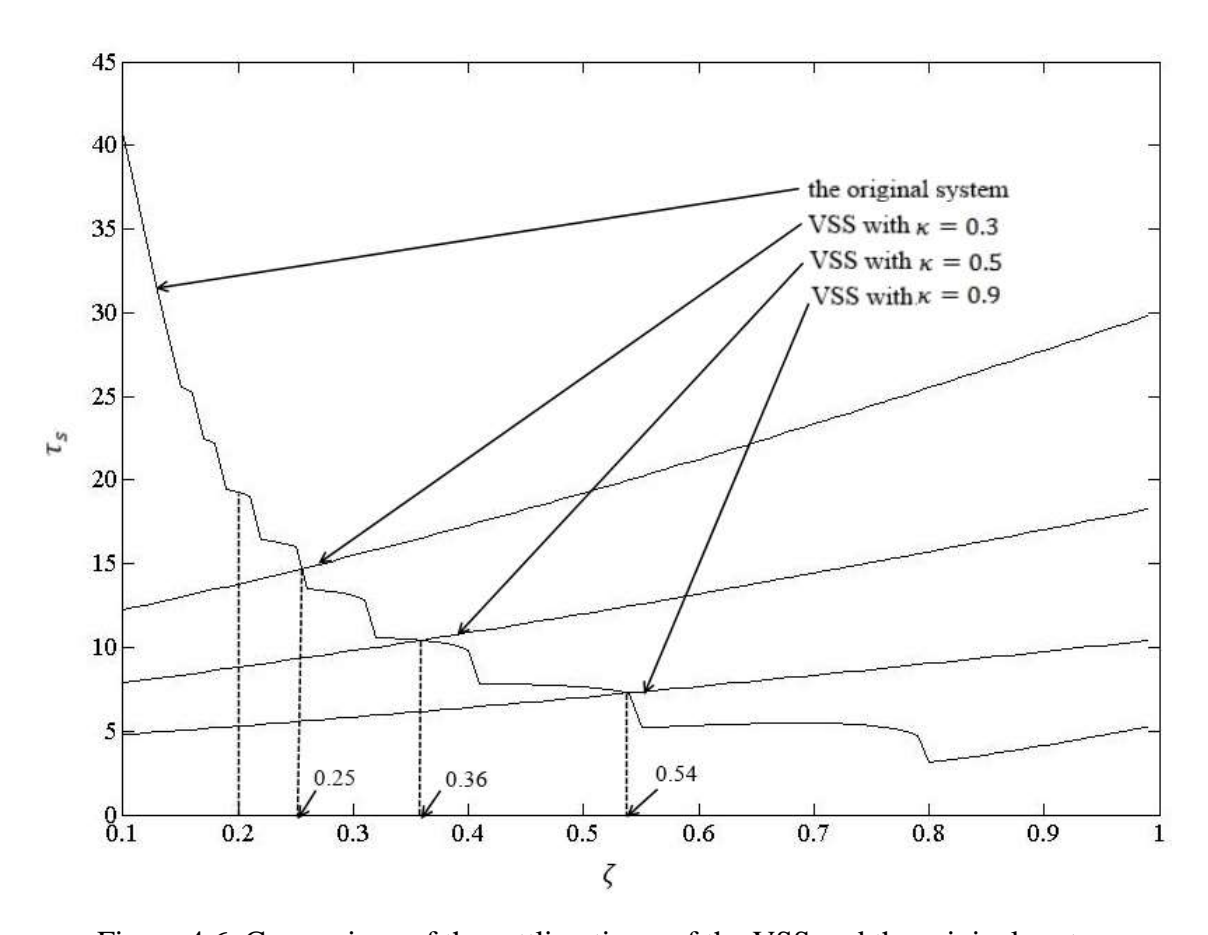


Figure 4.6. Comparison of the settling times of the VSS and the original system

with  $\kappa=0.3,0.5$ , and 0.9 respectively. It is clear that the VSS improves the settling time for  $\zeta=0.2$  by 28.58% when  $\kappa=0.3$ , by 54.37% when  $\kappa=0.5$ , and by 72.6% when  $\kappa=0.9$ . The best performance is achieved by the VSS when  $\kappa\to 1$  or  $\lambda\to\mu_1$ .

For an initial conditions in  $Z_3$  (see Fig.4.3), the time needed by the VSS to reaches  $L_1$  has been studied in section 4.2.1, and was described by Eq.(4.12). The values of  $x_1$  and  $x_2$  when the VSS reach the sliding surface  $L_1$  ( $x_1 = 0$ ) has been studied in section 4.2.1, and was described by Eq.(4.6), and (4.7). The time needed by the VSS to reaches the sliding surface  $L_3$  ( $x_2 = \lambda x_1$ ) has been studied in section 4.2.1, and was described by Eq.(4.5). The values of  $x_1$  and  $x_2$  when the VSS reach the sliding surface  $L_3$  has been studied in section 4.2.1, and was described by Eq.(4.1) and (4.2). The time needed for the trajectories on  $L_3$  to enter the region  $|x_1| \le 0.02$  has been studied in section 4.2.1, and was described by Eq.(4.20). Using these relations, the settling time of the VSS can be shown to be:

$$\tau_s = \tau_1 + \tau_2 + \tau_3 \tag{4.30}$$

where

$$\tau_1 = \omega_n t_1 = \frac{1}{2\sqrt{1+\zeta^2}} \ln \left[ \frac{\left[ x_{20} - \omega_n x_{10} \left( \zeta + \sqrt{1+\zeta^2} \right) \right]}{\left[ x_{20} - \omega_n x_{10} \left( \zeta - \sqrt{1+\zeta^2} \right) \right]} \right]$$
(4.31)

$$\tau_2 = \omega_n t_2 = \frac{1}{\sqrt{1 - \zeta^2}} \tan^{-1} \left[ \frac{\sqrt{1 - \zeta^2}}{\zeta + \kappa (\zeta - \sqrt{1 + \zeta^2})} \right]$$
(4.32)

$$\tau_3 = \omega_n t_3 = \frac{1}{\kappa \left[\zeta - \sqrt{\zeta^2 + 1}\right]} \ln\left(\frac{0.02}{x_{1s}}\right) \tag{4.33}$$

and

$$x_{1s} = e^{-\zeta \omega_n \tau_2} \left[ \frac{x_{2l1}}{\sqrt{1 - \zeta^2}} \sin \sqrt{1 - \zeta^2} \tau_2 \right]$$
 (4.34)

where 
$$x_{2l1} = \left(\zeta - \sqrt{1 + \zeta^2}\right) D e^{\tau_1 \left(\zeta - \sqrt{1 + \zeta^2}\right)} + \left(\zeta + \sqrt{1 + \zeta^2}\right) E e^{\tau_1 \left(\zeta + \sqrt{1 + \zeta^2}\right)}$$
 (4.35)

where 
$$D = x_{10} - \frac{x_{20} - \omega_n x_{10} \left(\zeta - \sqrt{1 + \zeta^2}\right)}{2\omega_n \sqrt{1 + \zeta^2}}, \quad E = \frac{x_{20} - \omega_n x_{10} \left(\zeta - \sqrt{1 + \zeta^2}\right)}{2\omega_n \sqrt{1 + \zeta^2}}$$

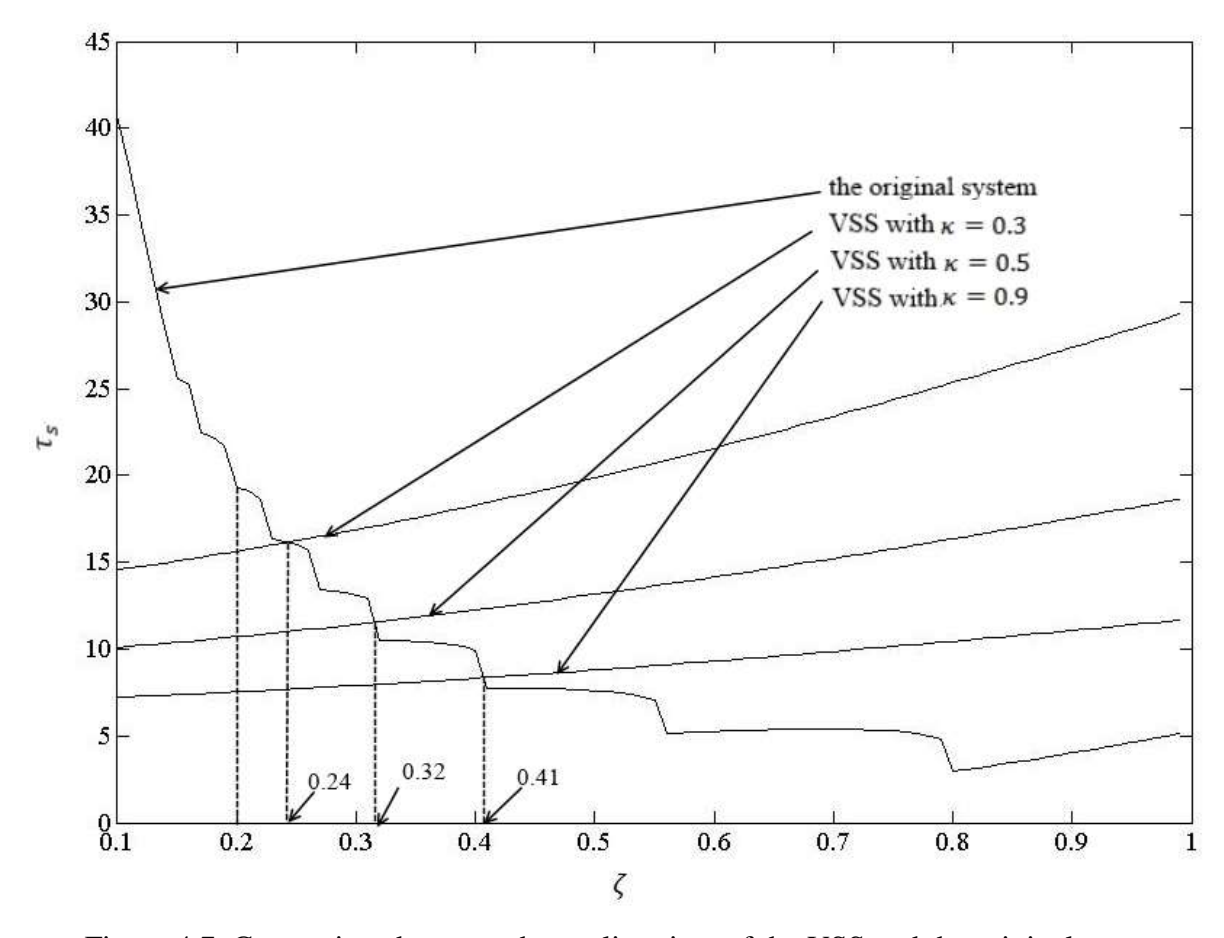


Figure 4.7. Comparison between the settling time of the VSS and the original system where  $x_{10}$  and  $x_{20}$  are the initials conditions in  $Z_3$ . Fig.4.7 shows a comparison of the settling time of the VSS for different value of  $\kappa$  ( $\kappa=0.3, \kappa=0.5, \kappa=0.9$ ) and the original system for initial conditions in  $Z_3$ . The initial conditions were arbitrarily chosen as  $x_{10}=-1$ , and  $x_{20}=-1.1\,\mu_1$ . For  $\kappa=0.3$ , the VSS has better performance than that of the original system only when  $\zeta<0.24$ . For  $\kappa=0.5$ , the performance is better for a larger range of  $\zeta$ , namely  $\zeta<0.32$ . As we increase  $\kappa$ , the performance is better for a larger range of  $\zeta$ : for  $\kappa=0.9$ , the performance is better for  $\zeta<0.41$ . The settling time of the original system can be reduced by increasing the value of  $\zeta$  but for most  $\zeta$  values, a VSS can be found ( $\kappa$  can be chosen) that has better performance in terms of the settling time. For example, for  $\zeta=0.2$ , the settling time for the original system is  $\tau_s=19.3$ , whereas it is equal to 15.62, 10.71, and 7.53 for

VSS with  $\kappa=0.3$ , 0.5, and 0.9 respectively. It is clear that the VSS improves the settling time for  $\zeta=0.2$  by 19.04% when  $\kappa=0.3$ , by 44.5% when  $\kappa=0.5$ , and by 60.9% when  $\kappa=0.9$ . The best performance is achieved by the VSS when  $\kappa\to 1$  or  $\lambda\to\mu_1$ .

In this section, we investigated the performance of the VSS with switched stiffness and damping for arbitrary initial conditions in  $Z_2$  and  $Z_3$ , and for different values of  $\lambda$ . The VSS has a smaller settling time than that of the original mass-spring-damper system. As we increase  $\lambda$  the settling time of the VSS is smaller for a larger range of  $\zeta$  values, and the best performance achieved when  $\lambda \to \mu_1$ .

### 4.3. Case B: $\lambda < \mu_1 < 0$

#### **4.3.1.** Stability

The VSS is a hybrid system that switches between an asymptotically stable system, the phase portrait of which is shown in Fig.4.8, and an unstable system whose phase portrait is shown in Fig.4.9. The union of these phase portraits is shown in Fig.4.10. To investigate the stability of the equilibrium of the VSS, the phase plane is divided into two zones, namely:

$$Z_1 = \{x \in R^2 | Sx_1 > 0\}$$

$$Z_2 = \{x \in R^2 | x_1(x_2 - \lambda \; x_1) < 0\}$$

The two zones are separated by the following two lines:

$$L_1: x_1 = 0$$

$$L_2: x_2 = \lambda x_1$$

We investigate the system trajectories in these zones and on these lines next.

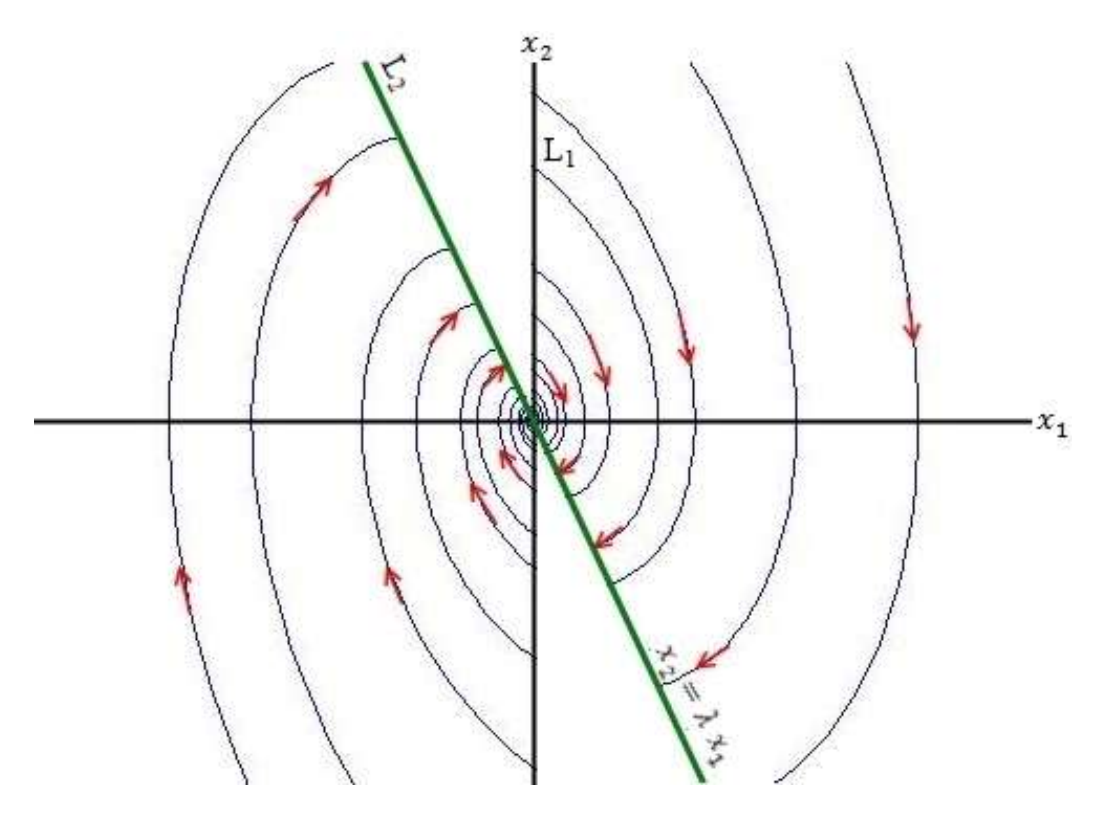


Figure 4.8. Phase portrait of the Variable Structure System (VSS) for  $\alpha = +1$ 

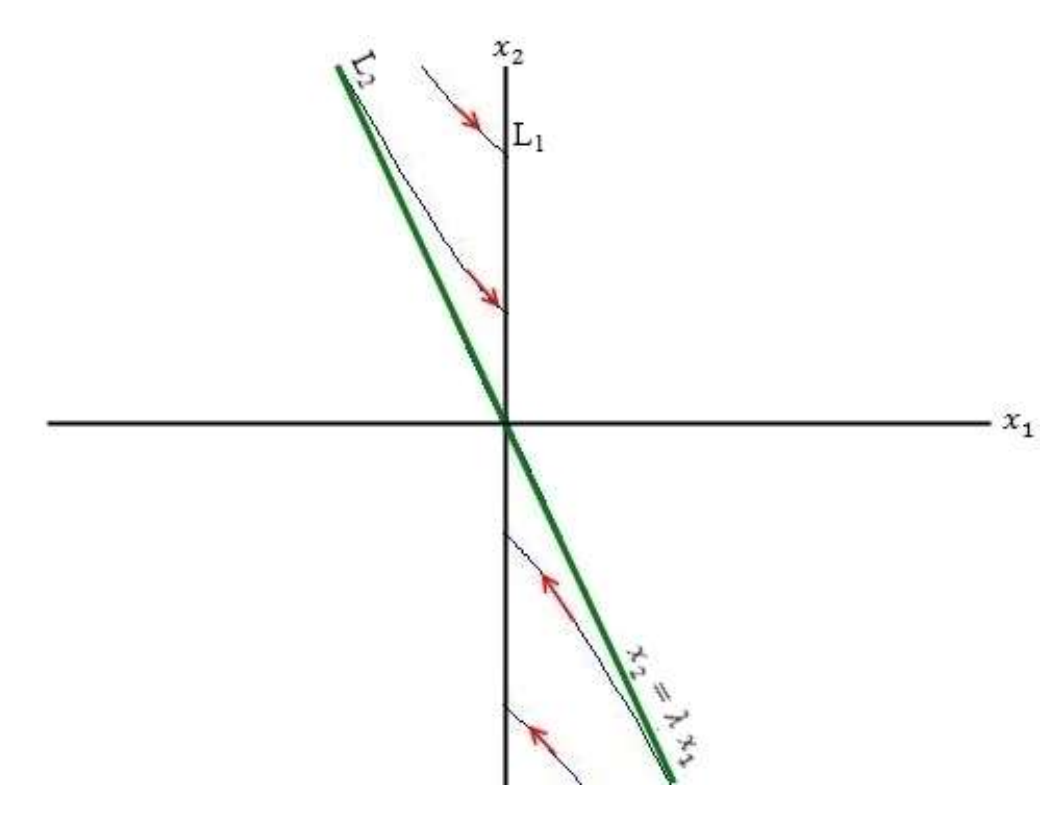


Figure 4.9. Phase portrait of the Variable Structure System (VSS) for  $\alpha=-1$ 

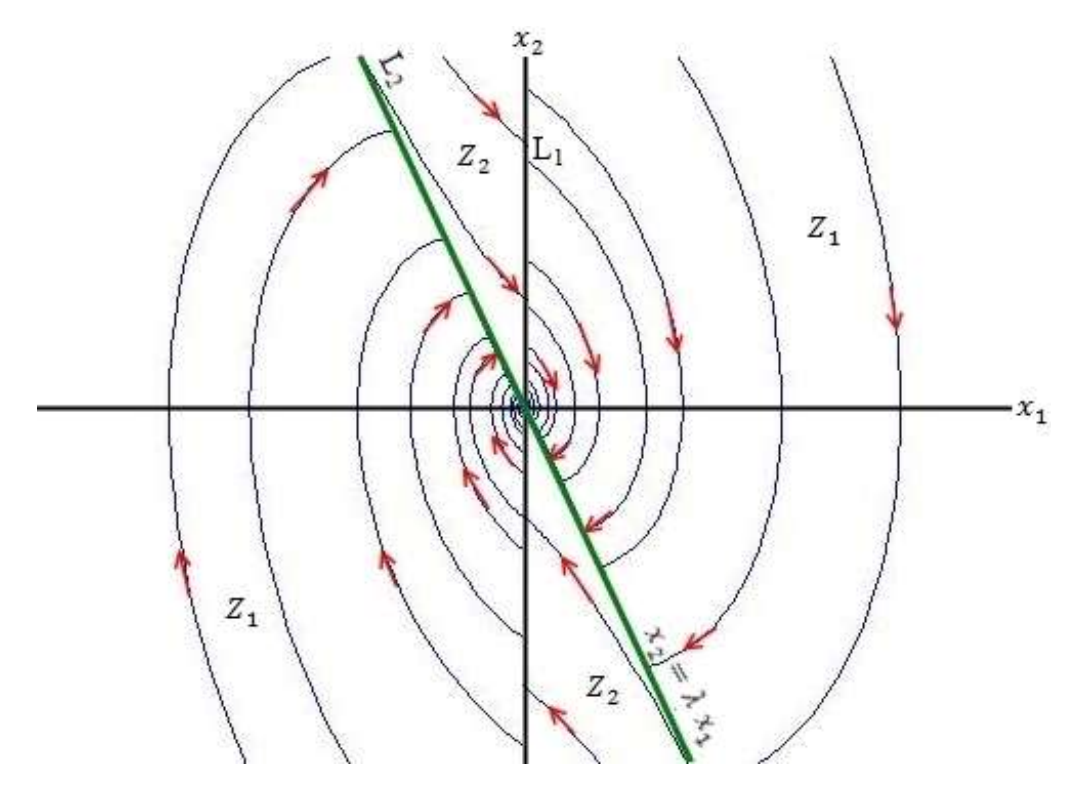


Figure 4.10. Phase portrait of the Variable Structure System (VSS) for  $~\lambda > \mu_1$ 

To study the behavior of the trajectories on  $L_1$ , we investigate the direction of the vector field on  $L_1$ . For  $x_2 > 0$  (and  $x_1 = 0$ ), we have the following equations and vector field:

$$\dot{x}_1 = x_2 > 0$$

$$\dot{x}_2 = -\frac{c}{m}x_2 < 0$$

Therefore, the trajectories enter  $Z_1$ . For  $x_2 < 0$  (and  $x_1 = 0$ ), we have the following equations and vector field:

$$\dot{x}_1 = x_2 < 0$$

$$\dot{x}_2 = -\frac{c}{m}x_2 > 0$$

Therefore, all trajectories on  $L_1$  will enter  $Z_1$ .

The boundaries of  $Z_1$  are  $L_1$  and  $L_2$ . We have already shown that trajectories on  $L_1$  enter  $Z_1$ . We now show all trajectories in  $Z_1$  reaches  $L_2$  in finite time. The time when the

trajectory in  $Z_1$  reaches  $L_2$  has been studied in section 4.2.1, and was described by Eq.(4.5). For convenience, it is provided below:

$$t = \frac{1}{\omega_d} \tan^{-1} \left[ \frac{(\lambda x_{10} - x_{20}) \sqrt{1 - \zeta^2}}{-\zeta x_{20} - \omega_n x_{10} - \lambda \left( \frac{x_{20} + \zeta \omega_n x_{10}}{\omega_n} \right)} \right]$$

This expression implies that all trajectories in  $Z_1$  reaches  $L_2$  at finite time.

The boundaries of  $Z_2$  are  $L_2$  and  $L_1$ . We have already shown that the trajectories on  $L_1$  enter  $Z_1$ . We now show that all trajectories in  $Z_2$  reaches  $L_1$  in finite time. The time when a trajectory in  $Z_2$  reaches  $L_1$  has been studied in section 4.2.1, and was described by Eq.(4.12). For convenience, it is provided below:

$$t = \frac{1}{2\omega_n \sqrt{1+\zeta^2}} \ln \left[ \frac{\left[ x_{20} - \omega_n x_{10} \left( \zeta + \sqrt{1+\zeta^2} \right) \right]}{\left[ x_{20} - \omega_n x_{10} \left( \zeta - \sqrt{1+\zeta^2} \right) \right]} \right]$$

This expression implies that all trajectories in  $\mathbb{Z}_2$  reaches  $\mathbb{L}_1$  at finite time.

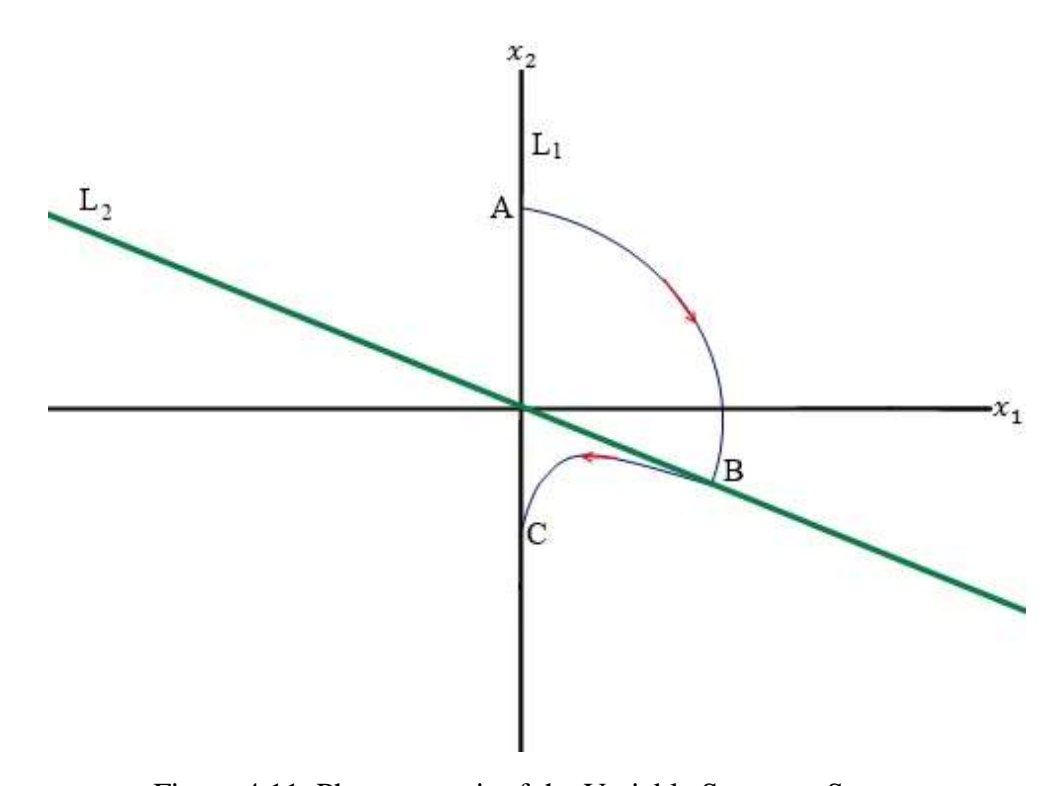


Figure 4.11. Phase portrait of the Variable Structure System

From the above discussion it is clear that the trajectories of the VSS move alternately between zones  $Z_1$  and  $Z_2$  by crossing lines  $L_2$  and  $L_1$ . Since the phase plane is symmetric about the  $x_2$  axis (see Fig. 4.10), we now investigate if there will be a contraction or an expansion in the total energy of the system when the VSS undergoes a phase change equal to  $\pi$ . Fig.4.11 shows the phase portrait of the VSS undergoing a phase change of  $\pi$  between points A and C. The values of  $x_1$  and  $x_2$  when the VSS is at point A are:

$$x_{1A} = 0 (4.36)$$

$$x_{2A} = x_{20} (4.37)$$

where  $x_{20}$  is some positive number. The time needed by the VSS to move from point A to point C been studied in section 4.2.1, and was described by Eq.(4.5). For convenience, it is provided below:

$$t_{AB} = \frac{1}{\omega_n \sqrt{1 - \zeta^2}} \tan^{-1} \left[ \frac{\sqrt{1 - \zeta^2}}{\zeta + \lambda \left( \frac{1}{\omega_n} \right)} \right]$$
(4.38)

The values of  $x_1$  and  $x_2$  when the VSS reach point B has been studied in section 4.2.1, and was described by Eq.(4.1), and (4.2). For convenience, it is provided below:

$$x_{1B} = e^{-\zeta \omega_n t} \left( \frac{x_{2A}}{\omega_n} \right) \sin \omega_n \sqrt{1 - \zeta^2} t_{AB}$$
 (4.39)

$$x_{2B} = \lambda x_{1B} = \lambda e^{-\zeta \omega_n t} \left(\frac{x_{2A}}{\omega_n}\right) \sin \omega_n \sqrt{1 - \zeta^2} t_{AB}$$
(4.40)

The time needed for the VSS to move from point B to point C was studied in section 4.2.1, and was described by Eq.(4.12). For convenience, it is provided below:

$$t_{BC} = \frac{1}{2\omega_n \sqrt{1+\zeta^2}} \ln \left[ \frac{\left(\lambda - \omega_n \left(\zeta + \sqrt{1+\zeta^2}\right)\right)}{\left(\lambda - \omega_n \left(\zeta - \sqrt{1+\zeta^2}\right)\right)} \right]$$
(4.41)

The values of  $x_1$  and  $x_2$  when the VSS reaches point C has been studied in section 4.2.1, and was described by Eq.(4.6), and (4.7). For convenience, it is provided below:

$$x_{1C} = 0 ag{4.42}$$

$$x_{2C} = \omega_n \left( \zeta - \sqrt{1 + \zeta^2} \right) D e^{\omega_n t_{BC} \left( \zeta - \sqrt{1 + \zeta^2} \right)}$$

$$+\omega_n \left(\zeta + \sqrt{1+\zeta^2}\right) E e^{\omega_n t_{BC}(\zeta + \sqrt{1+\zeta^2})} \tag{4.43}$$

where

$$D = x_{1B} \left[ \frac{-\lambda + \omega_n \left(\zeta + \sqrt{1 + \zeta^2}\right)}{2\omega_n \sqrt{1 + \zeta^2}} \right], \qquad E = x_{1B} \left[ \frac{\lambda - \omega_n \left(\zeta - \sqrt{1 + \zeta^2}\right)}{2\omega_n \sqrt{1 + \zeta^2}} \right]$$
(4.44)

The total energy of the mass-spring-damper at point A is:

$$T_A = \frac{1}{2} m x_{2A}^2 \tag{4.45}$$

The total energy of the mass-spring-damper at point C is:

$$T_A = \frac{1}{2} m x_{2C}^2 \tag{4.46}$$

The contraction in the total energy of the VSS between points A and C is:

$$T_A - T_C = \frac{1}{2} m x_{2A}^2 - \frac{1}{2} m x_{2C}^2$$
 (4.47)

The percentage of the contraction in the total energy of the VSS between points A and C can be shown to be:

$$\frac{T_A - T_C}{T_A} \times 100 = \frac{\frac{1}{2} m x_{2A}^2 - \frac{1}{2} m x_{2C}^2}{\frac{1}{2} m x_{2A}^2} \times 100 = \frac{x_{2A}^2 - x_{2C}^2}{x_{2A}^2} \times 100$$
(4.48)

For proper comparison of the contraction in the total energy, we nondimensionalize the time using the variable  $\tau = \omega_n t$ . Concurrently, we define  $\lambda = \rho \mu_1$  where  $\rho \ge 1$  is a constant. The

percentage of the contraction in the total energy of the VSS between points A and C given by the following equation:

$$E_p = (1 - x_c^2) \times 100 \tag{4.49}$$

where

$$x_{c} = \frac{x_{2C}}{x_{2A}} = \left(\zeta - \sqrt{1 + \zeta^{2}}\right) D e^{\tau_{BC}\left(\zeta - \sqrt{1 + \zeta^{2}}\right)} + \left(\zeta + \sqrt{1 + \zeta^{2}}\right) E e^{\tau_{BC}\left(\zeta + \sqrt{1 + \zeta^{2}}\right)}$$
(4.50)

where

$$\tau_{BC} = t_{BC}\omega_n = \frac{1}{2\sqrt{1+\zeta^2}} \ln \left[ \frac{\left(\rho[\zeta - \sqrt{\zeta^2 + 1}] - [\zeta + \sqrt{1+\zeta^2}]\right)}{\left(\rho[\zeta - \sqrt{\zeta^2 + 1}] - [\zeta - \sqrt{1+\zeta^2}]\right)} \right]$$
(4.51)

$$D = x_B \left( \frac{-\rho \left[ \zeta - \sqrt{\zeta^2 + 1} \right] + \left( \zeta + \sqrt{1 + \zeta^2} \right)}{2\sqrt{1 + \zeta^2}} \right)$$
 (4.52)

$$E = x_B \left( \frac{\rho \left[ \zeta - \sqrt{\zeta^2 + 1} \right] - \left( \zeta - \sqrt{1 + \zeta^2} \right)}{2\sqrt{1 + \zeta^2}} \right)$$
 (4.53)

$$x_B = \frac{x_{1B}}{x_{2A}} = e^{-\zeta \omega_n t} \sin \sqrt{1 - \zeta^2} \tau_{AB}$$
 (4.54)

$$\tau_{AB} = t_{AB}\omega_n = \frac{1}{\sqrt{1-\zeta^2}} \tan^{-1} \left[ \frac{\sqrt{1-\zeta^2}}{\zeta + \rho[\zeta - \sqrt{\zeta^2 + 1}]} \right]$$
(4.55)

The VSS will be an asymptotically stable if there is a contraction in total energy between point A and point C ( $E_p > 0$ ), stable if the total energy remains constant between point A and point C ( $E_p = 0$ ), and an unstable if there is an increasing in total energy between point A and point C ( $E_p < 0$ ). Fig.4.12 shows the percentage of the contraction in total energy of the VSS between point A and point C for different value of  $\rho$  ( $\rho = 1.1, \rho = 1.2, \rho = 1.3, \rho = 1.4, \rho = 1.5$ ). For  $\rho = 1.1$ , the VSS is asymptotically stable only when  $\zeta < 0.7$ , stable for  $\zeta = 0.7$ , and unstable for  $\zeta > 0.7$ . For  $\rho = 1.2$ , the VSS is asymptotically stable only when  $\zeta < 0.74$ , a stable for  $\zeta = 0.74$ , and unstable for  $\zeta > 0.74$ . For  $\rho = 1.3$ , the VSS is asymptotically stable

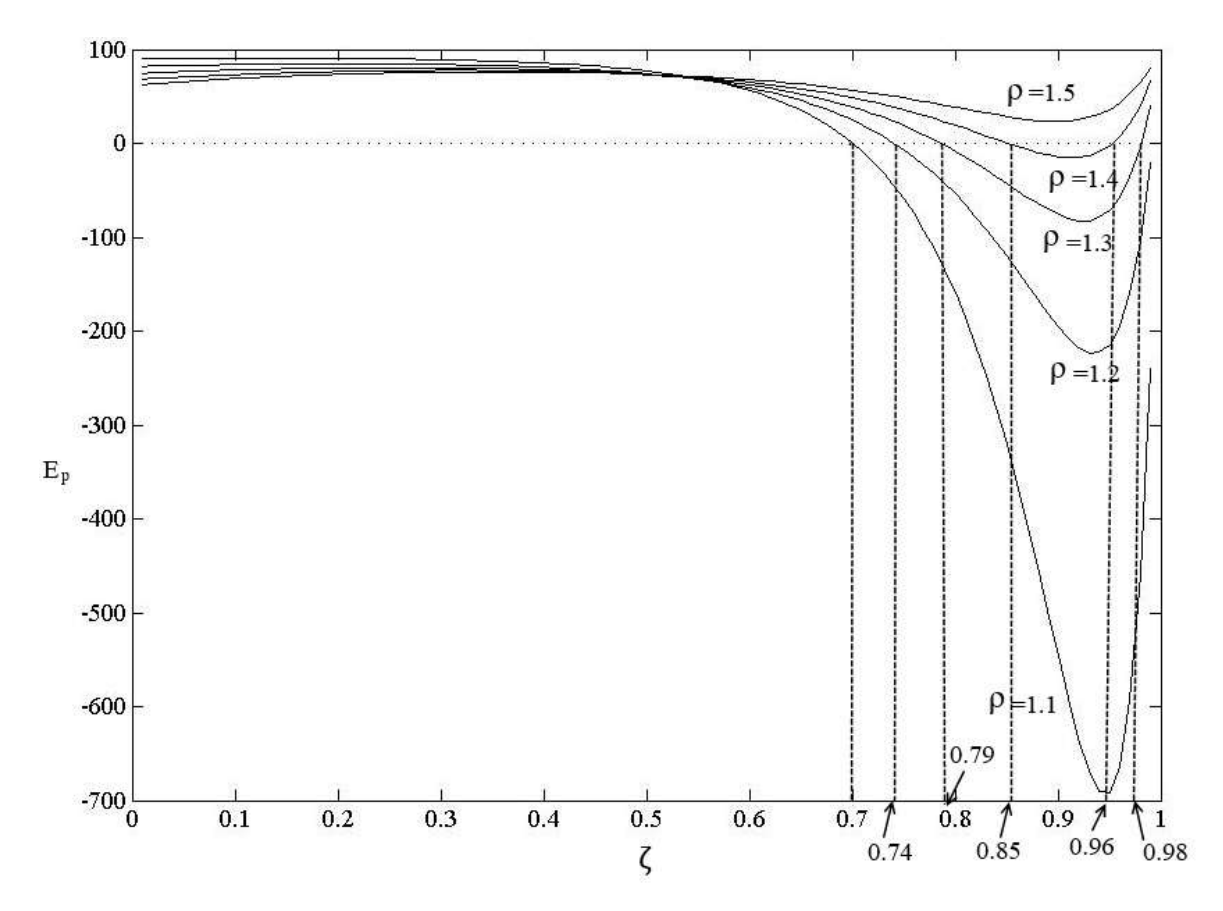


Figure 4.12. The percentage of the contraction in energy of the VSS between points A and C when  $\zeta < 0.79$  or  $\zeta > 0.98$ , stable for  $\zeta = 0.79$  or  $\zeta = 0.98$ , and unstable for  $0.78 < \zeta < 0.98$ . As we increase  $\rho$ , the VSS is unstable for a smaller range of  $\zeta$  values: for  $\rho = 1.4$ , the VSS is an asymptotically stable when  $\zeta < 0.85$  or  $\zeta > 0.96$ , stable when  $\zeta = 0.85$  or  $\zeta < 0.96$ , and unstable when  $0.85 < \zeta < 0.96$ . For  $\rho = 1.5$ , the VSS is an asymptotically stable for all values of  $\zeta$ . By trial and error, it was determined that the VSS is an asymptotically stable for all values of  $\zeta$  for  $\rho > 1.44$ .

## **4.3.2.** Performance – Response to Step Input

To investigate the performance of the VSS, we will study the response of the VSS to a step input and compare its performance with that of the original system for the same step input.

For the original system, the response to a step input has been studied in section 4.2.1, and was described in Eq.(3.14). For convenience, it is provided below:

$$\ddot{y} = -\frac{c}{m}\dot{y} - \frac{k}{m}y, \quad y(0) = -1, \quad \dot{y}(0) = 0$$
 (4.56)

The response of the VSS to the same step input was described in Eq.(130). For convenience, it is provided below:

$$\ddot{y} = -\alpha \frac{c}{m} \dot{y} - \alpha \frac{k}{m} y, \quad y(0) = -1, \quad \dot{y}(0) = 0$$
 (4.57)

where 
$$\alpha = \begin{cases} +1 & \text{if } (S > 0 \text{ and } y \ge 0) \text{ or } (S < 0 \text{ and } y \le 0) \\ -1 & \text{if } Sy < 0 \end{cases}$$

Note that Eqs.(4.56) and (4.57) are very similar and have the same initial conditions. Also, note that Eq.(4.57) is identical to Eq.(2.25); therefore, all the analysis presented in section 4.3.1 will be applicable.

The phase portrait of the VSS in Eq.(4.57) has already been studied in section 4.3.1. From this study we know that the trajectories of the system will spiral to the origin and the system will be asymptotically stable for  $\rho > 1.44$ . Unlike the previous case, it is not possible to claim that the phase change of the trajectories will be less than  $2\pi$ . In other words, a step input will result in oscillations, similar to the original system. Therefore, the performance of the original system and the VSS can be compared by on the basis of

- (a) the rise time  $t_r$ ,
- (b) the maximum percentage of overshoot  $M_p$ , and
- (c) the settling time.

The rise time and the maximum percentage of overshoot can be calculated analytically but the same is not true for the settling time. To calculate the rise time and the maximum percentage of overshoot, we define three points A, B, and C on the phase portrait of the VSS, shown in Fig

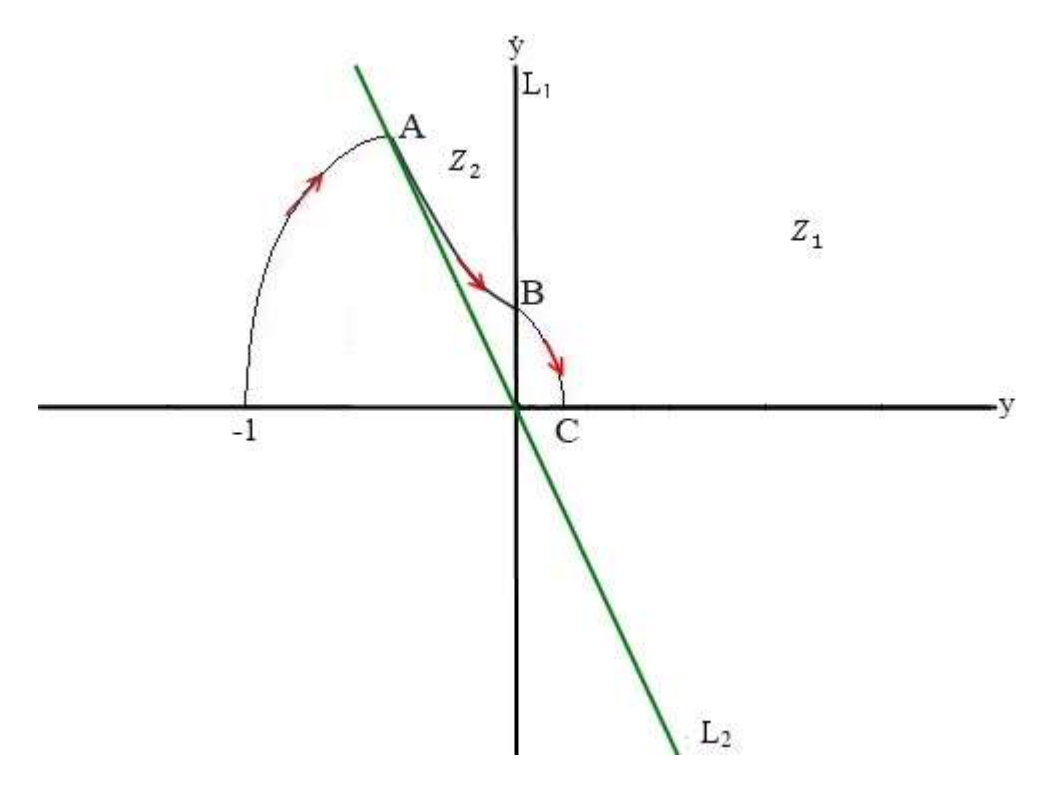


Figure 4.13. Step response in the phase plane of the Variable Structure System (VSS) for  $\lambda < \mu_1$ 

4.13. These points are also shown in Fig.4.14, which is a plot of the time response of the VSS to the step input. Consider the time needed by the VSS to reach point A; this has been studied in section 4.2.1, and was described by Eq.(120). Using variables y and  $\dot{y}$  we can write it as follows:

$$t_A = \frac{1}{\omega_d} \tan^{-1} \left[ \frac{(\lambda y_0 - \dot{y}_0) \sqrt{1 - \zeta^2}}{-\zeta \dot{y}_0 - \omega_n y_0 - \lambda \left( \frac{\dot{y}_0 + \zeta \omega_n y_0}{\omega_n} \right)} \right] = \frac{1}{\omega_d} \tan^{-1} \left[ \frac{-\lambda \sqrt{1 - \zeta^2}}{\omega_n + \lambda \zeta} \right]$$
(4.58)

where  $y_0 = -1$  and  $\dot{y}_0 = 0$  are the initial conditions. The values of y and  $\dot{y}$  at A has been studied in section 4.2.1, and was described by Eq.(116), and (117). For convenience, it is provided below:

$$y_A = e^{-\zeta \omega_n t_A} [A \cos \omega_d t_A + B \sin \omega_d t_A]$$
 (4.59)

$$\dot{y}_A = -\zeta \omega_n e^{-\zeta \omega_n t_A} [A \cos \omega_d t_A + B \sin \omega_d t_A]$$

$$+e^{-\zeta\omega_n t_A} \left[ -A \,\omega_d \sin \omega_d t_A + B \,\omega_d \cos \omega_d t_A \right] \tag{4.60}$$

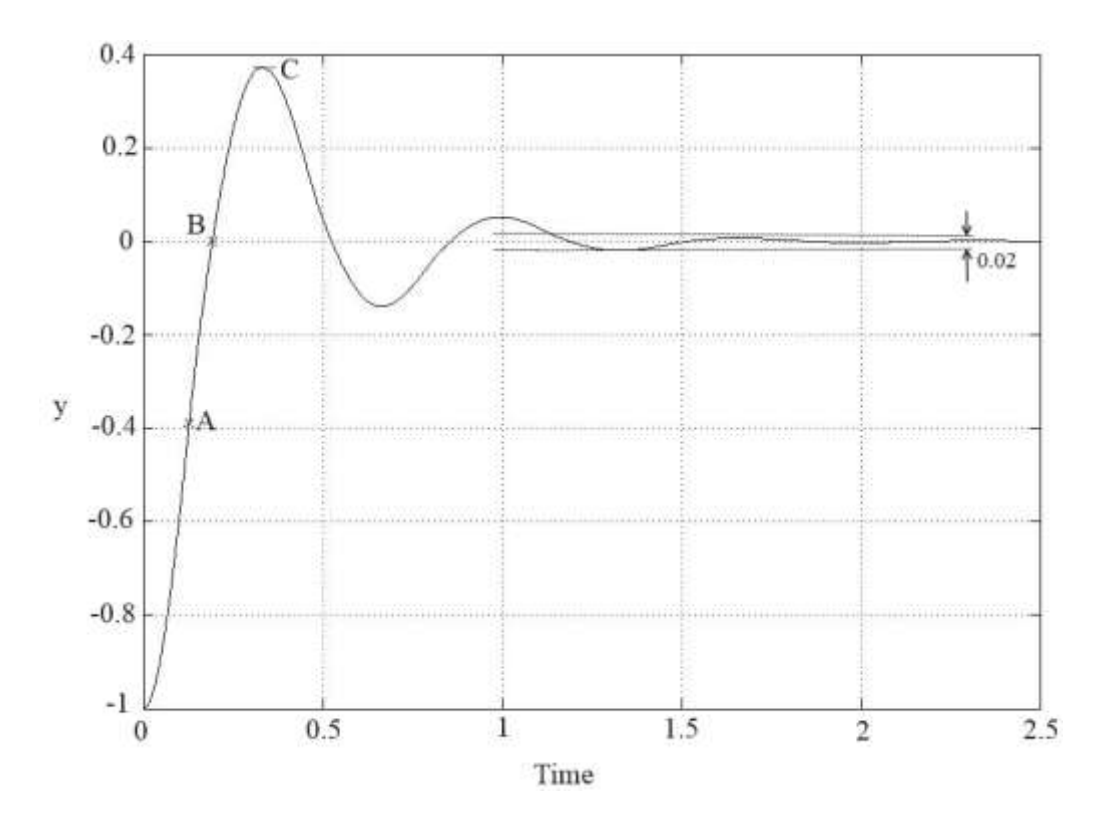


Figure 4.14. Step response of the Variable Structure System (VSS) for  $~\lambda < \mu_{\,1}$ 

where  $\omega_d = \omega_n \sqrt{1-\zeta^2}$ , A = -1,  $B = -\frac{\zeta}{\sqrt{1-\zeta^2}}$ 

The time needed for the VSS to move from point A to point B has been studied in section 4.2.1, and was described by Eq.(4.12), For convenience, it is provided below:

$$t_{AB} = \frac{1}{2\omega_n \sqrt{1+\zeta^2}} \ln \left[ \frac{\left[ \dot{y}_A - \omega_n y_A \left( \zeta + \sqrt{1+\zeta^2} \right) \right]}{\left[ \dot{y}_A - \omega_n y_A \left( \zeta - \sqrt{1+\zeta^2} \right) \right]} \right]$$
(4.61)

where  $y_A$ , and  $\dot{y}_A$  are the initial conditions and given by Eqs.(4.58) and (4.60). The values of y and  $\dot{y}$  at B has been studied in section 4.2.1, and was described by Eq.(121) and (122). For convenience, it is provided below:

$$y_B = 0 (4.62)$$

$$\dot{y}_B = \omega_n \left( \zeta - \sqrt{1 + \zeta^2} \right) D e^{\omega_n t_{AB} \left( \zeta - \sqrt{1 + \zeta^2} \right)}$$

$$+\omega_n \left(\zeta + \sqrt{1 + \zeta^2}\right) E e^{\omega_n t_{AB}(\zeta + \sqrt{1 + \zeta^2})} \tag{4.63}$$

where

$$D = y_A - \frac{\dot{y}_A - \omega_n y_A \left(\zeta - \sqrt{1 + \zeta^2}\right)}{2\omega_n \sqrt{1 + \zeta^2}}, \qquad E = \frac{\dot{y}_A - \omega_n y_A \left(\zeta - \sqrt{1 + \zeta^2}\right)}{2\omega_n \sqrt{1 + \zeta^2}}$$

To find the time needed for the VSS to move from point B to point C, we substitute Eq.(4.2) into the equation of y-axis where point C lie on this axis, namely:

$$\dot{v} = 0$$

This gives

$$-\zeta \omega_n e^{-\zeta \omega_n t} [A \cos \omega_d t + B \sin \omega_d t]$$

$$+ e^{-\zeta \omega_n t} [-A \omega_d \sin \omega_d t + B \omega_d \cos \omega_d t] = 0$$

$$\Rightarrow \tan \omega_d t = \frac{-\zeta \omega_n A + B \omega_d}{\zeta \omega_n B + \omega_d A}$$
(4.64)

Substitution of the values of A and B from Eq.(4.3) into Eq.(4.64) gives

$$\Rightarrow \tan \omega_d t = \frac{\sqrt{1 - \zeta^2}}{\zeta}$$

$$\Rightarrow t_{BC} = \frac{1}{\omega_d} \tan^{-1} \left[ \frac{\sqrt{1 - \zeta^2}}{\zeta} \right]$$
(4.65)

Substitution of the value of  $t_{BC}$  from Eq.(4.64) into Eqs.(4.1) and (4.2) gives the values of y and  $\dot{y}$  at C, namely:

$$y_C = e^{-\zeta \omega_n t_{BC}} \left[ \frac{\dot{y}_B}{\omega_n \sqrt{1 - \zeta^2}} \sin \omega_n \sqrt{1 - \zeta^2} t_{BC} \right]$$
 (4.66)

$$\dot{y}_C = 0 \tag{4.67}$$

The rise time of the VSS can now be calculated as follows:

$$t_r = t_A + t_{AB}$$

$$= \frac{1}{\omega_d} \tan^{-1} \left[ \frac{-\lambda \sqrt{1 - \zeta^2}}{\omega_n + \lambda \zeta} \right]$$

$$+\frac{1}{2\omega_n\sqrt{1+\zeta^2}}\ln\left[\frac{\left[\dot{y}_A-\omega_ny_A\left(\zeta+\sqrt{1+\zeta^2}\right)\right]}{\left[\dot{y}_A-\omega_ny_A\left(\zeta-\sqrt{1+\zeta^2}\right)\right]}\right] \tag{4.68}$$

where  $y_A$ , and  $\dot{y}_A$  are defined by Eqs.(4.59) and (4.60) respectively. The maximum percent overshoot of the VSS depend on  $t_{BC}$  and is given by:

$$M_p = e^{-\zeta \omega_n t_{BC}} \left[ \frac{\dot{y}_B}{\omega_n \sqrt{1 - \zeta^2}} \sin \omega_n \sqrt{1 - \zeta^2} t_{BC} \right] \times 100$$

$$= e^{\left(\frac{-\zeta}{\sqrt{1 - \zeta^2}} \tan^{-1} \left[\frac{\sqrt{1 - \zeta^2}}{\zeta}\right]\right)} \left[\frac{\dot{y}_B}{\omega_n}\right] \times 100$$
(4.69)

where  $\dot{y}_B$  is defined by Eq.(178). For proper comparison of the performance, we nondimensionalize the time using the variable  $\tau = \omega_n t$ . Concurrently, we define  $\lambda = \rho \mu_1$  where  $\rho \geq 1$  is a constant. The nondimensional rise time and the maximum percentage overshoot are given by the following equations respectively:

$$\tau_{r} = \omega_{n} t_{r} = \frac{1}{\sqrt{1 - \zeta^{2}}} \tan^{-1} \left[ \frac{\rho \left[ -\zeta + \sqrt{\zeta^{2} + 1} \right] \sqrt{1 - \zeta^{2}}}{1 + \zeta \rho \left[ \zeta - \sqrt{\zeta^{2} + 1} \right]} \right] + \frac{1}{2\sqrt{1 + \zeta^{2}}} \ln \left[ \frac{\left[ \dot{y}_{A} - y_{A} \left( \zeta + \sqrt{1 + \zeta^{2}} \right) \right]}{\left[ \dot{y}_{A} - y_{A} \left( \zeta - \sqrt{1 + \zeta^{2}} \right) \right]} \right]$$
(4.70)

$$M_p = e^{\frac{-\zeta}{\sqrt{1-\zeta^2}} \tan^{-1} \frac{\sqrt{1-\zeta^2}}{\zeta}} \dot{y}_B \times 100$$
 (4.71)

where  $y_A = e^{-\zeta \tau_A} \left[ A \cos \sqrt{1 - \zeta^2} \tau_A + B \sin \sqrt{1 - \zeta^2} \tau_A \right]$  (4.72)

$$\dot{y}_A = -\zeta e^{-\zeta \tau_A} \left[ A \cos \sqrt{1 - \zeta^2} \tau_A + B \sin \sqrt{1 - \zeta^2}_d \tau_A \right]$$

$$+ \sqrt{1 - \zeta^2} e^{-\zeta \tau_A} \left[ -A \sin \sqrt{1 - \zeta^2} \tau_A + B \cos \sqrt{1 - \zeta^2} \tau_A \right]$$
(4.73)

$$\dot{y}_B = \left(\zeta - \sqrt{1 + \zeta^2}\right) D e^{\tau_{AB}\left(\zeta - \sqrt{1 + \zeta^2}\right)} + \left(\zeta + \sqrt{1 + \zeta^2}\right) E e^{\tau_{AB}\left(\zeta + \sqrt{1 + \zeta^2}\right)} \tag{4.74}$$

$$\tau_A = \frac{1}{\sqrt{1 - \zeta^2}} \tan^{-1} \left[ \frac{\rho \left[ -\zeta + \sqrt{\zeta^2 + 1} \right] \sqrt{1 - \zeta^2}}{1 + \zeta \rho \left[ \zeta - \sqrt{\zeta^2 + 1} \right]} \right] \tag{4.75}$$

$$\tau_{AB} = \frac{1}{2\sqrt{1+\zeta^2}} \ln \left[ \frac{\left[ \dot{y}_A - y_A \left( \zeta + \sqrt{1+\zeta^2} \right) \right]}{\left[ \dot{y}_A - y_A \left( \zeta - \sqrt{1+\zeta^2} \right) \right]} \right]$$
(4.76)

$$A = -1, \qquad B = -\frac{\zeta}{\sqrt{1 - \zeta^2}}$$

$$D = y_A - \frac{\dot{y}_A - y_A(\zeta - \sqrt{1 + \zeta^2})}{2\sqrt{1 + \zeta^2}}, \qquad E = \frac{\dot{y}_A - y_A(\zeta - \sqrt{1 + \zeta^2})}{2\sqrt{1 + \zeta^2}}$$

The settling time for the VSS is the time needed for the VSS trajectory to enter the region  $|y| \le 0.02$ . This cannot be calculate analytically because the VSS may enter the region  $|y| \le 0.02$  in  $Z_1$  or in  $Z_2$ . Therefore, we calculate the settling time numerically.

Figure 4.15 shows a comparison of the rise times of the VSS for different values of  $\rho$ 

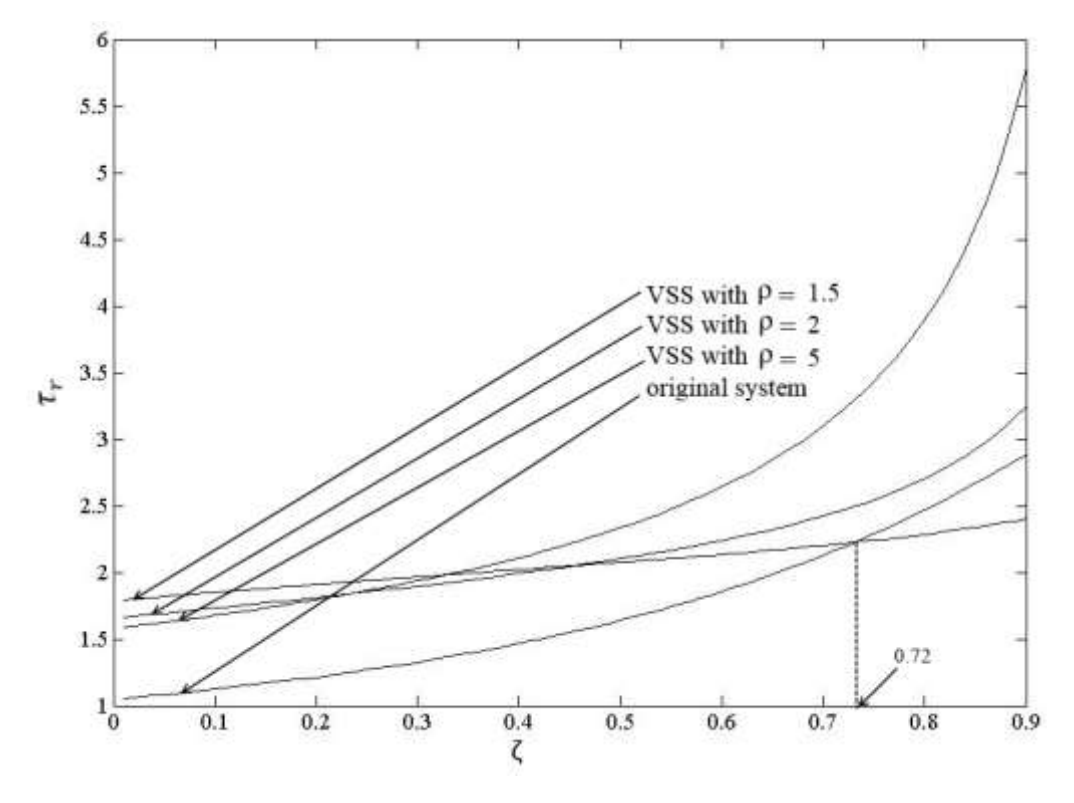


Figure 4.15. Comparison of the rise times of the VSS and original system

( $\rho=1.5$ ,  $\rho=2$ ,  $\rho=5$ ) and the original system.  $\rho$  has been chosen to be greater than 1.44 to make sure that the VSS will be asymptotically stable. For  $\rho=1.5$ , the VSS has better performance than that the original system only when  $\zeta>0.72$ . It is clear that the original system has better rise time than the VSS for  $\rho=2$  and 5.

Figure 4.16 shows a comparison of the maximum percentage of overshoots of the VSS for different values of  $(\rho=1.5, \rho=2, \rho=5)$  and the original system. Once again,  $\rho$  has been chosen to be greater than 1.44 to make sure that the VSS will be asymptotically stable. For  $\rho=5$ , the VSS has lower maximum percentage of overshoot than that of the original system only when  $\zeta<0.06$ . For  $\rho=2$ , the maximum percentage of overshoot is lower for a larger range of  $\zeta$ , namely  $\zeta<0.15$ . As we decreases  $\rho$ , the maximum percentage of overshoot is lower for a larger range of  $\zeta$ : for  $\rho=1.5$ , the maximum percentage of overshoot is lower for  $\zeta<0.21$ .

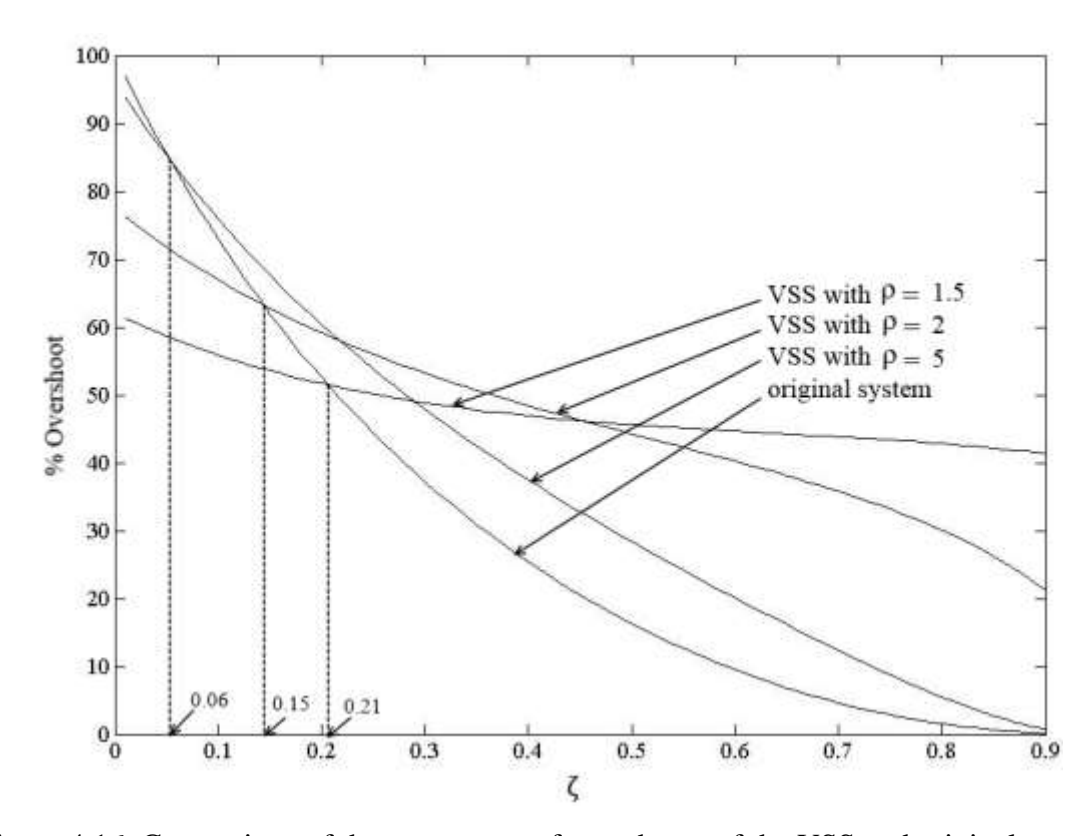


Figure 4.16. Comparison of the percentage of overshoots of the VSS and original system

Figure 4.17 shows a comparison of the settling time of the VSS for different value of  $\rho$  ( $\rho$  = 1.5,  $\rho$  = 2,  $\rho$  = 5) and the original system.  $\rho$  has been chosen to be greater than 1.44 to make sure that the VSS will be asymptotically stable. For  $\rho$  = 5, the VSS has larger settling time that that of the original system for all values of  $\zeta$ . For  $\rho$  = 2, the VSS has lower settling time than that of the original system only when  $\zeta$  < 0.15 As we decrease  $\rho$ , the settling time is lower for a larger range of  $\zeta$ : for  $\rho$  = 1.5, the settling time is lower for  $\zeta$  < 0.18.

In this section, we investigated the performance of the VSS with switched stiffness and damping for a step input for different values of  $\rho$ . The value of  $\rho$  was chosen to be greater than 1.44 to make sure that the VSS will be asymptotically stable. The VSS has a smaller settling time than that of the original mass-spring-damper system for a small range of  $\zeta$  values. As we decrease  $\lambda$ , the settling time of the VSS is smaller for a larger range of  $\zeta$  values,

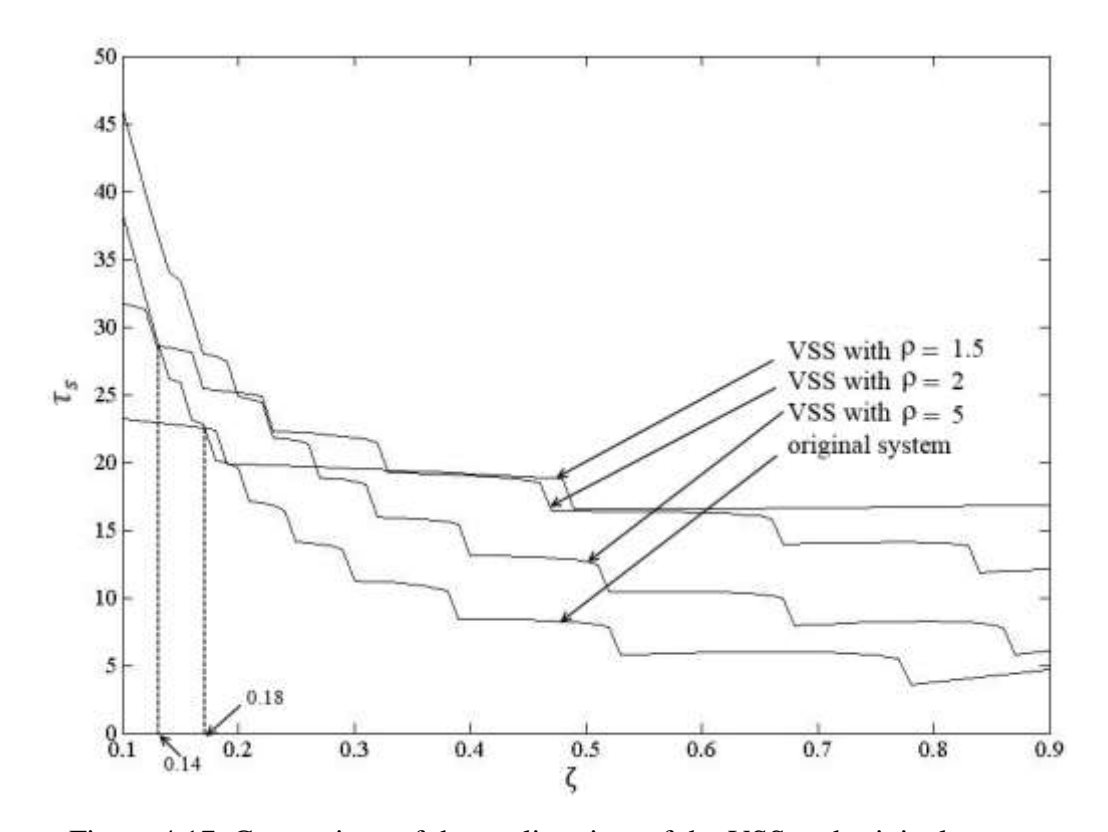


Figure 4.17. Comparison of the settling time of the VSS and original system

and the best performance is achieved by the VSS when  $\rho \rightarrow 1.44$ .

### **4.3.3.** Performance – Speed of Convergence

In last section, we investigated the performance of the VSS for a step input. This problem was recast as an initial value problem with the initial conditions at (-1,0) in the phase plane. Since (-1,0) lies in  $Z_1$ , we now compare the performance of the VSS with switched stiffness and the original system for arbitrary initial conditions in  $Z_2$ . For initial conditions in  $Z_2$  (see Fig.4.10), the performance of the original system and the VSS can be compared by computing:

- (a) the rise time  $t_r$ ,
- (b) the maximum percentage of overshoot  $M_p$ , and
- (c) the settling time.

The rise time and the maximum percentage of overshoot can be calculated analytically but the same is not true for the settling time. To calculate the rise time and maximum percentage of overshoot, we define two points A and B on the phase portrait of the VSS, shown in Fig.4.18. These points are also shown in Fig.4.19, which is a plot of the time response of the VSS to the step input. Consider the time needed by the VSS to reach point B; this has been studied in section 4.2.1, and was described by Eq.(4.12). The values of  $x_1$  and  $x_2$  at A has been studied in section 4.2.1, and was described by Eq.(4.6) and (4.7). To find the time needed for the VSS to move from point A to point B, we substitute Eq.(4.2) into the equation of y-axis where point B lies on this axis, namely:

$$x_2 = 0$$

This gives:

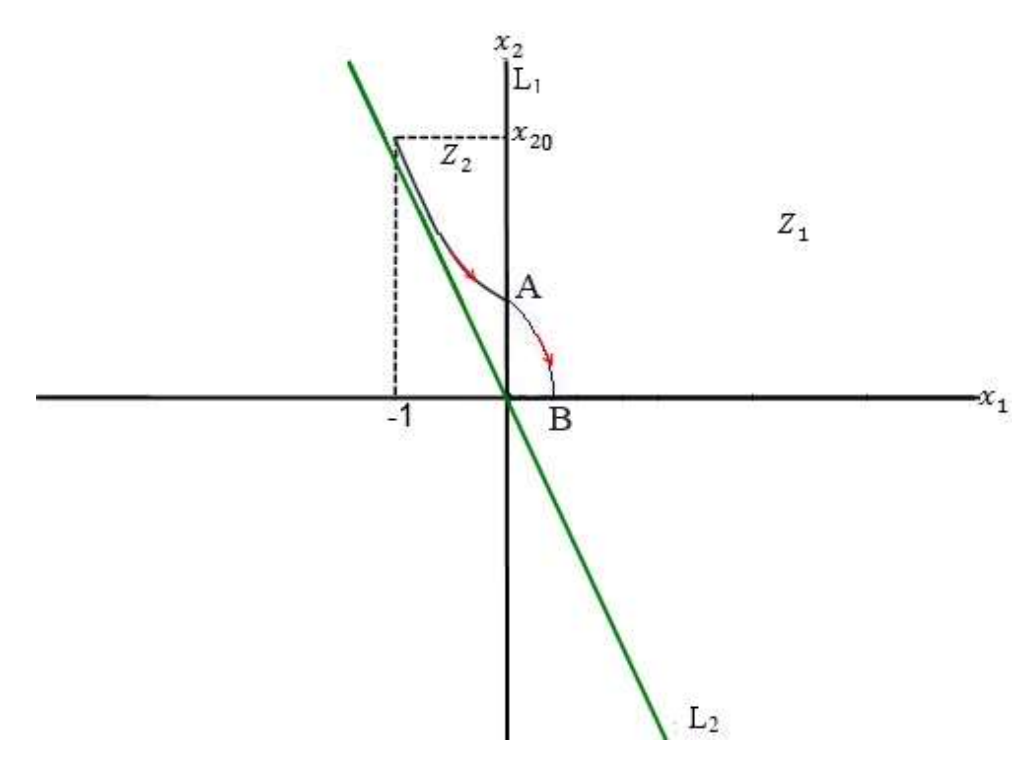


Figure 4.18. Step response in the Phase plane for the Variable Structure System (VSS) for  $~\lambda < \mu_{\,1}$ 

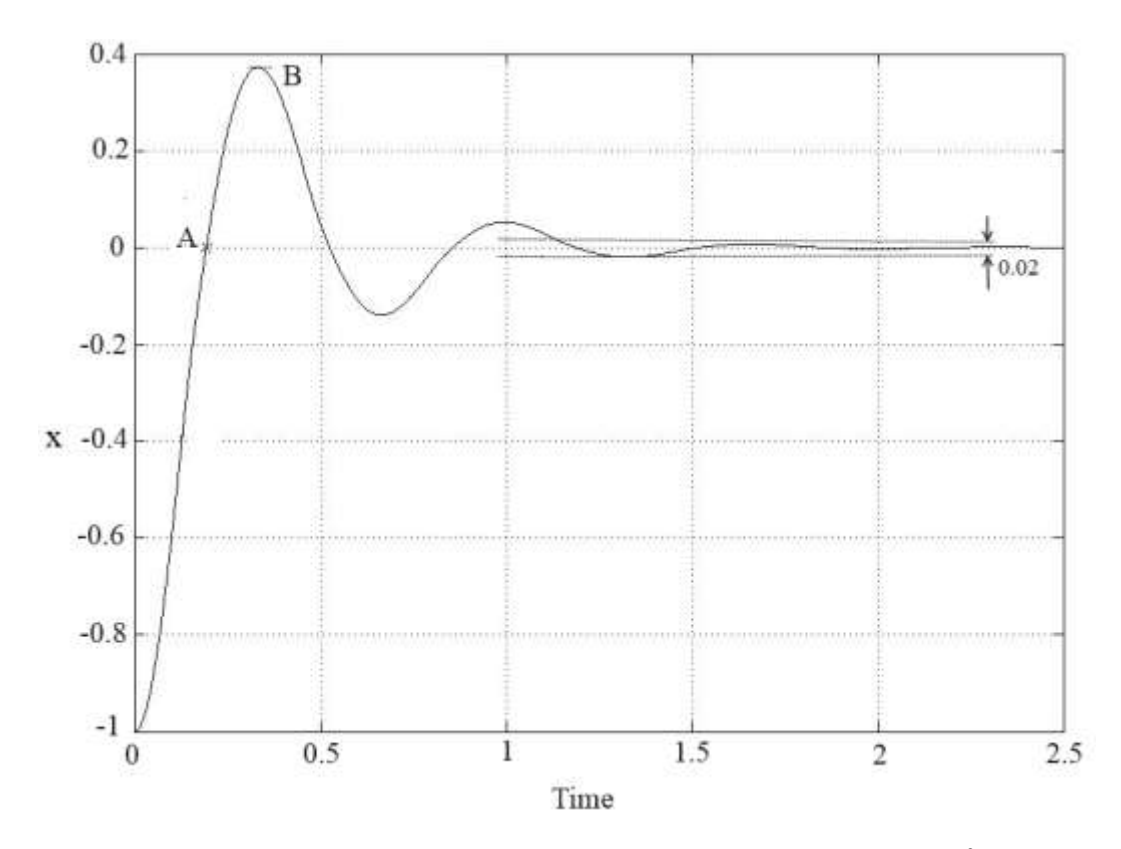


Figure 4.19. Step response for the Variable Structure System (VSS) for  $~\lambda < \mu_{\,1}$ 

$$-\zeta \omega_n e^{-\zeta \omega_n t} [A \cos \omega_d t + B \sin \omega_d t]$$

$$+ e^{-\zeta \omega_n t} [-A \omega_d \sin \omega_d t + B \omega_d \cos \omega_d t] = 0$$

$$\Rightarrow \tan \omega_d t = \frac{-\zeta \omega_n A + B \omega_d}{\zeta \omega_n B + \omega_d A}$$
(4.77)

Substitution of the values of A and B from Eq.(4.3) into Eq.(4.77) gives:

$$\Rightarrow \tan \omega_d t = \frac{\sqrt{1 - \zeta^2}}{\zeta}$$

$$\Rightarrow t_{AB} = \frac{1}{\omega_d} \tan^{-1} \left[ \frac{\sqrt{1 - \zeta^2}}{\zeta} \right]$$
(4.78)

Substitution of the value of  $t_{AB}$  into Eqs.(4.2), and (4.3) gives the values of  $x_1$  and  $x_2$  at B, namely:

$$x_{1B} = e^{-\zeta \omega_n t_{AB}} \left[ \frac{x_{2A}}{\omega_n \sqrt{1 - \zeta^2}} \sin \omega_n \sqrt{1 - \zeta^2} t_{AB} \right]$$
(4.79)

$$\chi_{2B} = 0 \tag{4.80}$$

The rise time of the VSS can now be calculated as follows:

$$t_r = t_A = \frac{1}{2\omega_n \sqrt{1+\zeta^2}} \ln \left[ \frac{\left[ x_{20} - \omega_n x_{10} \left( \zeta + \sqrt{1+\zeta^2} \right) \right]}{\left[ x_{20} - \omega_n x_{10} \left( \zeta - \sqrt{1+\zeta^2} \right) \right]} \right]$$
(4.81)

where  $x_{10}$ , and  $x_{20}$  are the initial conditions. The maximum percent overshoot of the VSS depend on  $t_{BC}$  and is given by:

$$M_p = e^{-\zeta \omega_n t_{AB}} \left[ \frac{x_{2A}}{\omega_n \sqrt{1 - \zeta^2}} \sin \omega_n \sqrt{1 - \zeta^2} t_{AB} \right] \times 100$$

$$= e^{\left(\frac{-\zeta}{\sqrt{1 - \zeta^2}} \tan^{-1} \left[\frac{\sqrt{1 - \zeta^2}}{\zeta}\right]\right)} \left[ \frac{x_{2A}}{\omega_n} \right] \times 100$$
(4.82)

where  $x_{2A}$  is defined by Eq.(4.7). For proper comparison of the performance, we nondimensionalize the time using the variable  $\tau = \omega_n t$ . Concurrently, we define  $\lambda = \rho \mu_1$  where

 $\rho \ge 1$  is a constant. The nondimensional rise time and the maximum percent overshoot are given by the following equations respectively:

$$\tau_r = \omega_n t_r = \frac{1}{2\sqrt{1+\zeta^2}} \ln \left[ \frac{\left[ x_{20} - x_{10} \left( \zeta + \sqrt{1+\zeta^2} \right) \right]}{\left[ x_{20} - x_{10} \left( \zeta - \sqrt{1+\zeta^2} \right) \right]} \right]$$
(4.83)

$$M_{v} = e^{\frac{-\zeta}{\sqrt{1-\zeta^{2}}} \tan^{-1} \frac{\sqrt{1-\zeta^{2}}}{\zeta}} x_{2A} \times 100$$
 (4.84)

where 
$$x_{2A} = \left(\zeta - \sqrt{1+\zeta^2}\right) D e^{\tau_A \left(\zeta - \sqrt{1+\zeta^2}\right)} + \left(\zeta + \sqrt{1+\zeta^2}\right) E e^{\tau_A \left(\zeta + \sqrt{1+\zeta^2}\right)}$$
 (4.85)

$$\tau_A = \frac{1}{2\sqrt{1+\zeta^2}} \ln \left[ \frac{\left[ x_{20} - x_{10} \left( \zeta + \sqrt{1+\zeta^2} \right) \right]}{\left[ x_{20} - x_{10} \left( \zeta - \sqrt{1+\zeta^2} \right) \right]} \right]$$
(4.86)

$$D = x_{10} - \frac{x_{20} - x_{10}(\zeta - \sqrt{1 + \zeta^2})}{2\sqrt{1 + \zeta^2}}, \qquad E = \frac{x_{20} - x_{10}(\zeta - \sqrt{1 + \zeta^2})}{2\sqrt{1 + \zeta^2}}$$

where  $x_{10}$  and  $x_{20}$  are the initials conditions in  $Z_2$ . The settling time of the VSS is the time needed for the VSS to enter the region  $|x_1| \le 0.02$ . There is no way to calculate the settling time analytically, because the VSS may enter the region  $|x_1| \le 0.02$  in  $Z_1$  or  $Z_2$ . Therefore we calculate the settling time numerically.

Figure 4.20 shows a comparison between the rise time of the VSS with  $\rho = 1.5$  and the original system for initial conditions in  $\mathbb{Z}_2$ .  $\rho$  has been chosen to be greater than 1.44 to make sure that the VSS will be asymptotically stable. The initial conditions were arbitrarily chosen as  $x_{10} = -1$ , and  $x_{20} = 2.88$ . The VSS has lower rise time than that of the original system only when  $\zeta$  < 0.12. Therefore, the VSS may have a lower rise time than that of the original system if the initial conditions are in  $\mathbb{Z}_2$ .

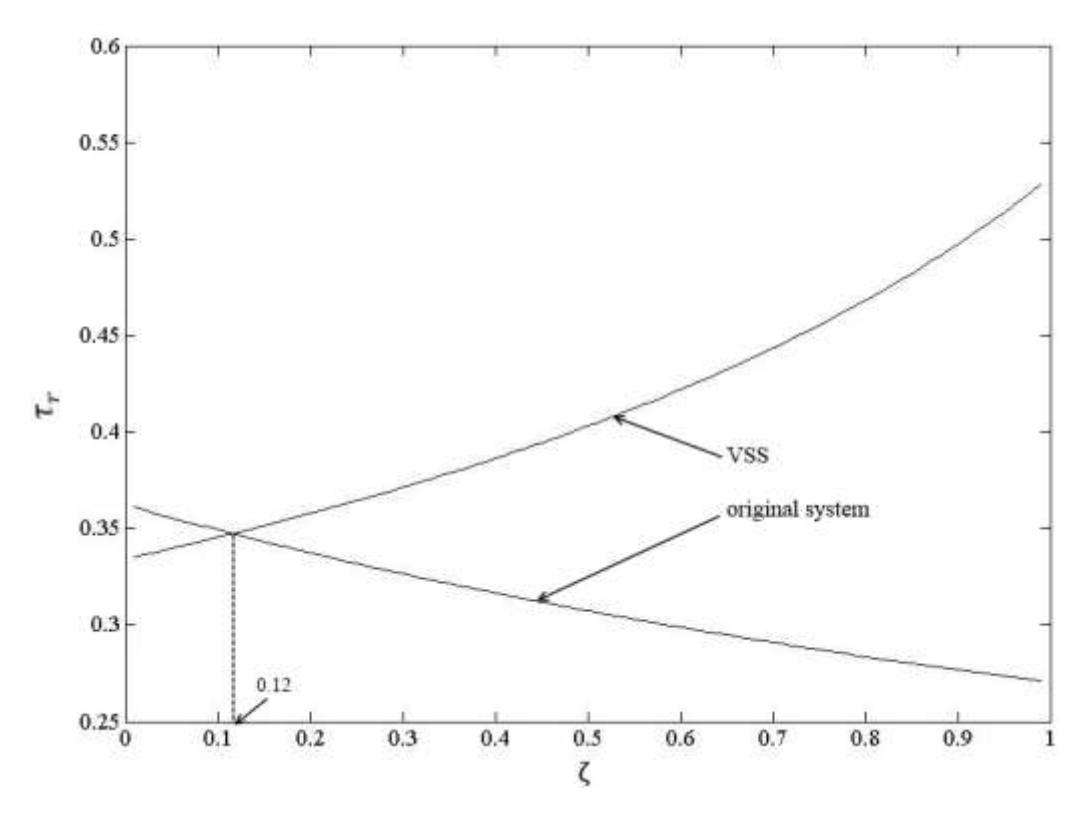


Figure 4.20. The rise time for VSS and original system

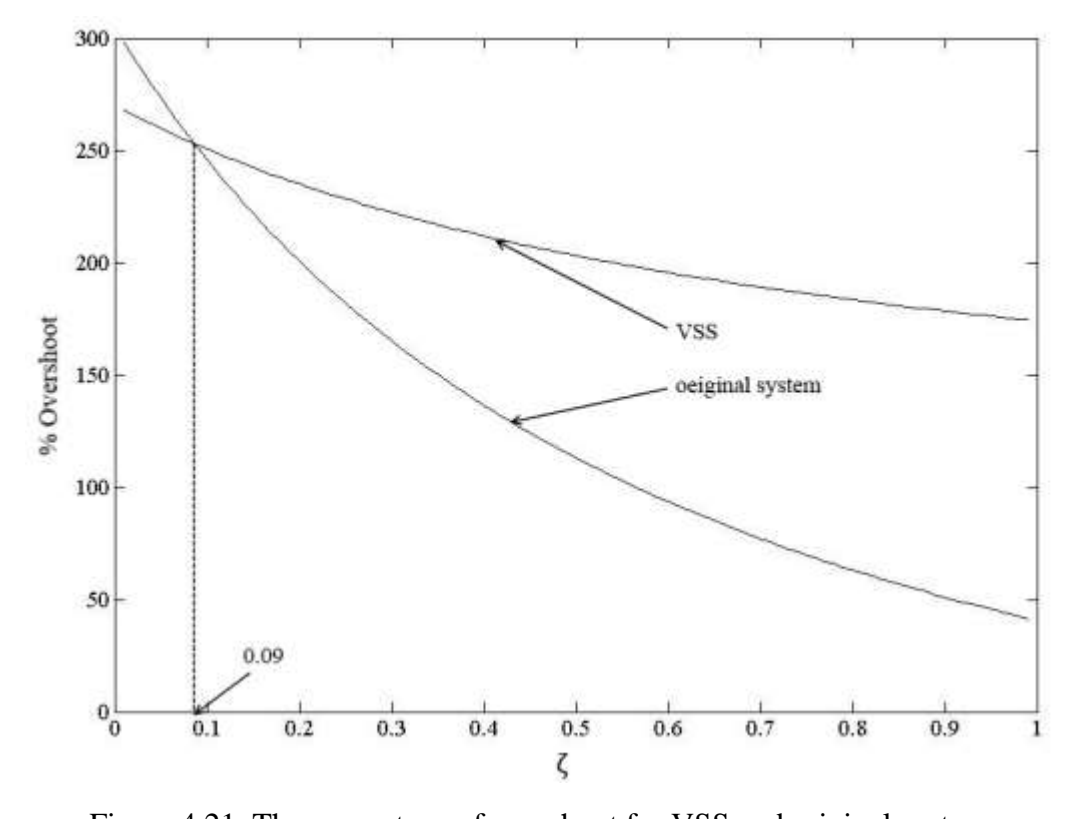


Figure 4.21. The percentage of overshoot for VSS and original system

Figure 4.21 shows a comparison between the percentage of overshoot of the VSS with  $\rho=1.5$  and the original system for initial conditions in  $Z_2$ . The initial conditions were arbitrarily chosen as  $x_{10}=-1$ , and  $x_{20}=2.88$ . The VSS has lower maximum percentage of overshoot than that of the original system only when  $\zeta<0.09$ . Therefore, the VSS may have a lower maximum percentage of overshoot than that of the original system if the initial conditions are in  $Z_2$ .

Figure 4.22 shows a comparison between the settling time of the VSS with  $\rho=1.5$  and the original system for initial conditions in  $Z_2$ .  $\rho$  has been chosen to be greater than 1.44 to make sure that the VSS will be asymptotically stable. The initial conditions were arbitrarily chosen as  $x_{10}=-1$ , and  $x_{20}=2.88$ . The VSS has lower settling time than that of the original system only when  $\zeta < 0.19$ . Therefore, the VSS may have a lower rise time than that of the original

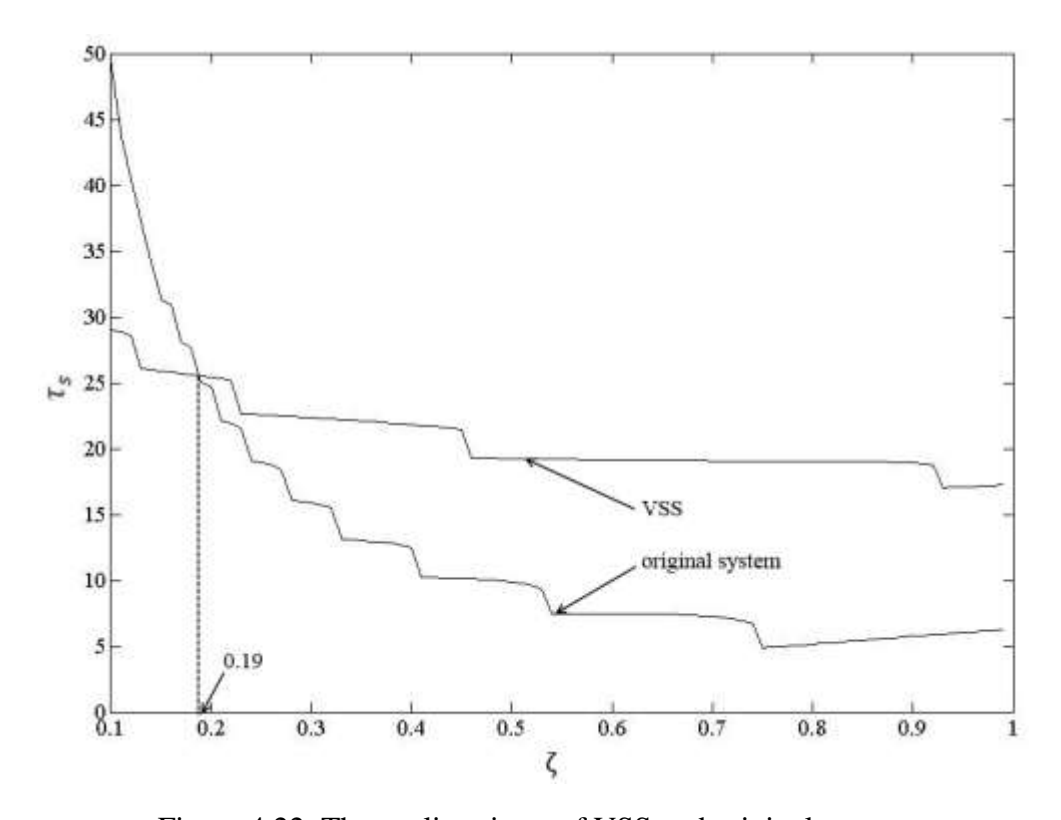


Figure 4.22. The settling times of VSS and original system

system if the initial conditions are in Z<sub>2</sub>.

In this section, we investigated the performance of the VSS with switched stiffness and damping for a step input. The value of  $\rho$  was chosen to be greater than 1.44 to make sure that the VSS will be asymptotically stable. The VSS has a smaller settling time than that of the original mass-spring-damper system for a small range of  $\zeta$ . As we decrease  $\lambda$ , the settling time of the VSS is smaller for a larger range of  $\zeta$  values, and the best performance is achieved by the VSS when  $\rho \to 1.44$ .

#### 4.4. Conclusion

In this Chapter, we investigated the behavior of the VSS with switched stiffness and damping. For Case A ( $\mu_1 < \lambda < 0$ ), the VSS is asymptotically stable and no trajectories of the VSS undergo a phase change of more than  $2\pi$ ; therefore, the VSS does not exhibit oscillations. Also, the VSS has a smaller settling time than that of the original system for a range of  $\zeta$  values. As we increase  $\lambda$ , the settling time of the VSS is smaller for a larger range of  $\zeta$  values. The best performance is achieved by the VSS when  $\lambda \to \mu_1$ . Therefore, the VSS improves the performance for the mass-spring-damper system. For Case B ( $\lambda \le \mu_1 < 0$ ), the VSS may be asymptotically stable, stable, or unstable. However, if we chose  $\rho > 1.44$ , the VSS will be asymptotically stable. For  $\rho > 1.44$  the trajectories of the VSS will undergo a phase change of more than  $2\pi$ ; therefore, the VSS will exhibit oscillations. The VSS improves the performance of the mass-spring-damper system for a small range of  $\zeta$  values. As we decrease  $\lambda$  the settling time of the VSS is smaller for a larger range of  $\zeta$  values, and the best performance is achieved by the VSS when  $\rho \to 1.44$ .

# Chapter 5

## Conclusion

We investigated the behavior of two hybrid mass-spring-damper (MSD) systems. The first system uses switched stiffness, where the stiffness in the model switches between its nominal value and its negative value. The second system uses switched stiffness and damping, where both the stiffness and damping coefficients in the model are switched between their nominal values and their negative values. Both hybrid MSD systems are switched based on the location of the system in its configuration space. Each hybrid system is asymptotically stable even though they are individually comprised of an asymptotically stable and an unstable sub-system. Through proper design of the switching logic, the hybrid systems can have significantly better performance than the nominal system in terms of rise time, settling time, and overshoot.

Based on the design of the switching logic, the MSD system with switched stiffness has two behaviors. In the first case, all trajectories in the phase plane asymptotically converge to the origin, but more importantly, no trajectory is capable of undergoing a phase change of more than  $2\pi$  rad. This establishes the fact that the hybrid system will not exhibit oscillations, even if the original system is underdamped. Additionally, the hybrid system has a rise time comparable to that of the original system but a significantly lower settling time. In the second case, all trajectories in the phase plane asymptotically converge to the origin, but the hybrid system exhibits oscillations.

The original system has a smaller rise time than the hybrid system but the hybrid system has a smaller maximum percentage of overshoot and a smaller settling time. The hybrid system therefore improves the performance of the nominal system if the nominal system is underdamped. The analysis presented in this work provides clues on how the switching logic can be designed to achieve the best performance improvement for a given value of damping ratio.

Similar to the hybrid system with switched stiffness, the hybrid system with switched stiffness and damping has two behaviors depending on the design of the switching logic. In the first case, the origin is asymptotically stable since and all trajectories in the phase plane converge to origin. Also, the hybrid system does not exhibit oscillations due to the fact that no trajectory is capable of undergoing a phase change of more than  $2\pi$  rad. Additionally, the hybrid system has a rise time comparable to that of the original system but a lower settling time for a small range of damping ratios ( $\zeta < 0.5$ , for example). For the second case, the hybrid system can be asymptotically stable, stable, or unstable based on the design of the switching logic. For the asymptotically stable case, the hybrid system does exhibit oscillations but it has better performance than the nominal system (in terms of what) for a small range of damping ratios ( $\zeta < 0.2$ , for example). The analysis presented in this work provides clues on how the switching logic can be designed to guarantee asymptotic stability for the hybrid system and achieve the best performance improvement for a given value of damping ratio.

**REFERENCES** 

#### REFERENCES

- [1] Ogata, Katsuhiko. "Modern Control Engineering, PHI Learning Pvt." Ltd., New Delhi, India (2009).
- [2] VADIM, I. UTKIN. "Survey paper variable structure systems with sliding modes." IEEE Transactions on Automatic control 22.2 (1977).
- [3] Sabanovic, Asif, Leonid M. Fridman, and Sarah K. Spurgeon, eds. Variable structure systems: from principles to implementation. Vol. 66. IET, 2004.
- [4] Hung, John Y., Weibing Gao, and James C. Hung. "Variable structure control: a survey." Industrial Electronics, IEEE Transactions on 40.1 (1993): 2-22.
- [5] Yu, Xing Huo, and Jian-Xin Xu. Advances in Variable Structure Systems: Analysis, Integration and Applications: Proceedings of the 6th IEEE International Workshop on Variable Structure Systems: Gold Coast, Queensland, Australia, 7-9 December 2000. World Scientific Pub Co Inc, 2001.
- [6] Ramaratnam, Arun, and Nader Jalili. "A switched stiffness approach for structural vibration control: theory and real-time implementation." Journal of Sound and Vibration 291.1 (2006): 258-274.
- [7] Ramaratnam, Arun, Nader Jalili, and Darren M. Dawson. "Semi-active vibration control using piezoelectric-based switched stiffness." American Control Conference, 2004. Proceedings of the 2004. Vol. 6. IEEE, 2004.
- [8] Yang, J. N., J. C. Wu, and Z. Li. "Control of seismic-excited buildings using active variable stiffness systems." Engineering Structures 18.8 (1996): 589-596.
- [9] Garabini, Manolo, et al. "Optimality principles in variable stiffness control: The VSA hammer." Intelligent Robots and Systems (IROS), 2011 IEEE/RSJ International Conference on. IEEE, 2011.
- [10] Mizuno, Takeshi, Takefumi Toumiya, and Masaya Takasaki. "Vibration isolation system using negative stiffness." JSME International Journal Series C 46.3 (2003): 807-812.
- [11] Le, Thanh Danh, and Kyoung Kwan Ahn. "A vibration isolation system in low frequency excitation region using negative stiffness structure for vehicle seat." Journal of Sound and Vibration 330.26 (2011): 6311-6335.

- [12] Lee, C-M., V. N. Goverdovskiy, and A. I. Temnikov. "Design of springs with "negative" stiffness to improve vehicle driver vibration isolation." Journal of Sound and Vibration 302.4 (2007): 865-874.
- [13] Khalil, Hassan K., and J. W. Grizzle. Nonlinear systems. Vol. 3. Upper Saddle River: Prentice hall, 2002.
- [14] Hu, Qinglei, and Guangfu Ma. "Variable structure control and active vibration suppression of flexible spacecraft during attitude maneuver." *Aerospace Science and Technology* 9.4 (2005): 307-317.
- [15] Chen, Runlin, et al. "Modeling and applications of variable structure damper." Assembly and Manufacturing (ISAM), 2013 IEEE International Symposium on. IEEE, 2013.